The effect of isothiocyanates on heat shock protein, heme oxygenase-1 and α-tubulin levels and localization in *Xenopus* A6 kidney cells

by

Imran Khamis

A thesis
presented to the University of Waterloo
in fulfillment of the
thesis requirement for the degree of
Doctor of Philosophy
in
Biology

Waterloo, Ontario, Canada, 2017

Examining Committee Membership
The following served on the Examining Committee for this thesis. The decision of the Examining Committee is by majority vote.

External Examiner	Dr. Richard D. Mosser Associate Professor University of Guelph, Ontario, Canada
Supervisor(s)	Dr. John J. Heikkila Professor
Internal Member	Dr. Bernard P. Duncker Professor
Internal Member	Dr. Brian Dixon Professor
Internal-external Member	Dr. A. Russell Tupling Professor

Author's Declaration

I hereby declare that I am the sole author of this thesis. This is a true copy of my thesis, including any required final revisions, as accepted by my examiners.

I understand that my thesis may be made electronically available to the public.

Abstract

Numerous studies have elucidated the health promoting properties of organosulfur compounds derived from cruciferous vegetables known as isothiocyanates (ITCs). As electrophiles, the impact of ITCs at the molecular level is profound, with the ability to directly bind and modify thiol-containing compounds such as glutathione and cellular protein, including tubulin. While the biochemical effects of ITCs have been well characterized, less information is available regarding their effects on the accumulation of stress-inducible heme oxygenase-1 (HO-1) and heat shock proteins (HSPs) as well as the possible formation of aggregated protein due to thiol modification. In the present study, I examined the effect of benzyl isothiocyanate (BITC), phenethyl isothiocyanate (PEITC), and sulforaphane (SFN) on the accumulation of HO-1, HSP70, HSP30 and HSPB6 in A6 kidney epithelial cells derived from the frog, *Xenopus laevis*. Immunoblot analysis revealed that treatment of cells with each of the ITCs induced the accumulation of HO-1 and HSP70 while HSP30 levels were only enhanced in cells treated with BITC at 30 °C. In contrast, HSPB6 levels were not affected by ITCs. Pretreatment with transcriptional (actinomycin D), translational (cycloheximide) or HSF1 (KNK437) inhibitors prevented the ITC-induced accumulation of HO-1, HSP70 and HSP30. Immunocytochemical studies determined that ITC treatment also resulted in F-actin disorganization and membrane ruffling. Furthermore, the addition of BITC or PEITC to A6 cells enhanced the presence of ubiquitinated protein and induced the accumulation of aggregated protein. In an examination of the effect of BITC or PEITC on microtubule filament protein, immunoblot analysis revealed significant decreases in the relative levels of α-tubulin. Immunocytochemical analysis revealed that BITC induced the collapse and fragmenting of the microtubule filaments while PEITC had a lesser effect. However, treatment of cells with BITC or PEITC at 30 °C greatly enhanced

microtubule fragmentation. Normally, the accumulation of aggregated protein results in their coalescence forming large aggresomes, which move along microtubules to the perinuclear region. However, this phenomenon was not readily observed with BITC or PEITC possibly due to microtubule fragmentation. This possibility was supported by the finding that BITC pretreatment reduced the formation of aggresome-like structures induced by the proteasomal inhibitor, MG132. The final chapter of this thesis investigated characteristics of the *Xenopus* small heat shock protein HSPB6, a HSP whose levels were not affected by ITC treatment of A6 cells. HSPB6 was determined to be an ortholog of mammalian HSPB6 and encoded a 168 amino acid protein that contained an α-crystallin domain, a polar C-terminal extension and possible phosphorylation sites. It shared 94% identity with *X. tropicalis* HSPB6 but only 49% and 59% with zebrafish and human proteins, respectively. Phylogenetic analysis revealed that *X. laevis* HSPB6 grouped more closely with mammalian and reptilian HSPB6s than with fish HSPB6. Western blot analysis determined that HSPB6 was present constitutively in A6 cells, induced by MG132 and slightly by cadmium chloride treatment but not by heat shock. Immunocytochemistry revealed that HSPB6 was present in the perinuclear region of the cytoplasm with some in the nucleus.

The research detailed in this thesis examined the effect of BITC, PEITC and SFN on the accumulation of HO-1 and HSPs and documented the impact of BITC and PEITC on aggregated protein in a kidney epithelial cell line. Since a great deal of the molecular and cellular research with *Xenopus* is applicable to humans, an increase in our knowledge of the effects of ITCs is of importance given their potential role as therapeutic compounds in the treatment of cancer, neurodegenerative diseases and bacterial and viral infections.

Acknowledgements

First and foremost, I would like to begin by thanking God for granting me the strength, perseverance and ability to successfully complete this degree, while showering countless blessings upon my family.

Next, I would like to extend a big thank you to Dr. John J. Heikkila. You gave me the opportunity I needed to start my graduate school career in your lab, and I am eternally grateful for that. At the time, I didn't realize how lucky I was having you as my supervisor. Taking the time to mentor and guide me in the right direction, you helped me grow both as a scientist and as a person. In addition, I would like to acknowledge and thank my committee members, Dr. Bernard Duncker and Dr. Brian Dixon for reading my work and providing helpful feedback. I would also like to thank my external examiners Dr. Richard D. Mosser and Dr. Russell Tupling for examining my thesis, being part of my defense and providing excellent advice. Thanks to my lab mates past and present who filled my experience in the lab with some great memories: Jara, AJ, Charles, Ena, Saad, Cody and James. A special mention to both Saad and James for reading my thesis and preparing me for my defense. James, you are one of the most hilarious people I know, providing many laughs during some stressful moments which helped keep me composed and sane; I don't think I will ever forget all of the fun, crazy moments in the lab. I would also like to thank the administrative staff, research technicians and laboratory assistants within the Department of Biology for their help and pleasant conversations.

To my entire Kincardine Bad Boyz crew, I couldn't have asked for a better group of friends. It's always fun getting together, and fantasy football is guaranteed to bring out the best (and worst) in all of us. Bring on the new NFL season.

I also owe a huge debt of gratitude to Safiyya. The time I spent completing my PhD was extra special because during it, I met you. Nothing makes me happier than knowing I found someone who I can always count on and trust. The support you have given me throughout my PhD was never taken for granted, and it helped me get through some tough hurdles and challenges that came with academic life. This includes my defense; your smile from the back of the room kept me calm and grounded. I know how lucky and blessed I am to find someone who cares and supports me so much. I'd like to also extend a thank you to your entire family for always sending positive vibes, well wishes and leftovers.

Finally, and most importantly, I would like to thank my family. To my brother, Riyad, thanks for always being there for me, and also introducing me to the world of fantasy football (shoutout to DWarNation). To my parents – both of you found success through hard work, respect and kindness towards others. You instilled these values in both Riyad and I, always teaching us to strive to do and be our best. I have no doubt this contributed to the successful completion of my doctoral degree. It is as a result of your unrelenting support, prayers and continuous love which has given me strength and endurance to achieve this significant milestone in my life.

Table of Contents

List of Figures

List of Tables

List of Abbreviations

ActD	actinomycin D
ANOVA	analysis of variance
APS	ammonium persulfate
ARE	antioxidant response element
As	sodium arsenite
ATP	adenosine triphosphate
Bach1	bric-a-brac and cap'n'collar homology
BCA	bicinchoninic acid
BSA	bovine serum albumin
BCIP	5-bromo-4-chloro-3-indolyl phosphate
BITC	benzyl isothiocyanate
BSA	bovine serum albumin
C	control
CdRE	cadmium response element
CHX	cycloheximide
CO	carbon monoxide
CuO	copper oxide
DAPI	4,6-diamidino-2-phenylindole
DBD	DNA binding domain
DMSO	dimethylsulphoxide
E protein	ubiquitin activating enzyme
EDTA	ethylene-diamine-tetraacetic acid
EGTA	ethylene glycol tetraacetic acid
ER	endoplasmic reticulum
GTP	guanosine triphosphate
HBSS	Hank's balanced salt solution
HDAC6	histone deacetylase 6
HeLa	*Homo sapiens* cervix adenocarcinoma
HEPES	4-(2-hydroxyethyl)-1-piperazineethanesulfonic acid
HO	heme oxygenase
HR	hydrophobic repeat
HSC	heat shock cognate
HSE	heat shock element
HSF	heat shock factor
HSP	heat shock protein
Hsp	heat shock protein gene or mRNA
HSR	heat shock response
Keap1	kelch-like erythroid-cell derived protein with cap'n'collar homology-associated protein1
KCl	potassium chloride
L-15	Leibovitz-15
LSCM	laser scanning confocal microscopy
MAPK	mitogen activated protein kinase

MARE	musculoaponeurotic fibrosarcoma recognition element
MG	MG132
MM	multiple myeloma
NaCl	sodium chloride
NADPH	nicotinamide adenine dinucleotide phosphate
NBT	4-nitro blue tetrazolium
Nrf2	NF-E2-related factor 2
NF-κB	nuclear factor-κB
NO	nitric oxide
PBS	phosphate buffered saline
PEITC	phenethyl isothiocyanate
PFAs	perfluoroalkylated substances
Rec	recovery
ROS	reactive oxygen species
SDS	sodium dodecyl sulfate
SDS-PAGE	sodium dodecyl sulfate-polyacrylamide gel electrophoresis
SHSP	small heat shock protein
SFN	sulforaphane
TBS-T	tris buffered saline solution – Tween20
TEMED	tetra-methyl-ethylene-diamine
TRITC	rhodamine-tetramethylrhodamine-5-isothiocyanate phalloidin
UPS	ubiquitin proteasome system
UV	ultraviolet light

Chapter 1: Introduction

During evolution, the survival of organisms in harsh environments required the development of intracellular stress networks to counteract various stressors (Morimoto, 1998). At the molecular level, environmental and physiological stressors can disrupt protein function and stability causing proteins to unfold or fold into non-native conformations (Morimoto, 1998; Balch et al., 2008). Abnormally folded polypeptides are prone to cytotoxic aggregation which can result in aberrant cellular processes and/or disease (Morimoto, 2008, Valastyan and Lindquist, 2014). The accumulation of stress-induced unfolded protein can trigger the tr

anscription of heat shock protein (*hsp*) genes to produce a class of molecular chaperones called heat shock proteins (HSPs), which serve a protective mechanism to maintain normal cellular function and to prevent proteotoxicity (Oksala et al., 2014).

1.1. Heat shock proteins

HSPs are involved in many cellular processes during normal and stressful conditions including protein synthesis, folding/assembly, translocation, degradation as well as protein re-folding during recovery from stress (Katschinski, 2004; Khan et al., 2014). Although HSPs were originally identified as a response to heat shock, a wide variety of stresses including chemical, ultraviolet (UV) light or wound healing were shown to induce their accumulation (Ritossa, 1962; Bellaye, 2014). HSPs are highly conserved and have been well documented in a wide variety of organisms ranging from bacteria to humans (Kregel, 2002; Katschinski, 2004; Daugaard et al., 2007). There are at least 6 different HSP families that have been classified primarily by size including small HSPs (sHSPs), HSP40, HSP60, HSP70, HSP90 and HSP100 (Backthisaran et al., 2015). *Hsp* gene expression patterns were shown to vary between organisms, tissue types and

developmental stages (Lindquist, 1986; Katschinski, 2004; Heikkila, 2010).

1.1.1. Heat shock protein 70 (HSP70) family

The HSP70 family of molecular chaperones is evolutionarily conserved, being found in every organism and containing multiple family members (Murphy, 2013). Constitutive or stress-inducible members function in regulating protein folding by identifying exposed hydrophobic surfaces and refolding them in an ATP-dependent manner (Katschinski, 2004). In eukaryotic cells, the HSP70 family members include cytoplasmic stress-inducible HSP70 (HSPA1A), cytoplasmic constitutively expressed heat shock cognate 70 (HSC70; HSPA8), mitochondrial HSP70 (HSPA9) and immunoglobulin binding protein (also known as glucose regulated protein 78; HSPA5), found in the endoplasmic reticulum (ER).

1.1.1.1. Stress-inducible HSP70

The functional components of the cytoplasmic stress-inducible HSP70 include an N-terminal ATPase domain, a peptide-binding domain, and a C-terminal region required for binding with other co-chaperones (Beere et al., 2000; Daugarud et al., 2007; Murphy, 2013). The peptide binding domain plays a role in attachment and release of non-native proteins, while the 25 kDa C-terminal region contains a Glu-Glu-Val-Asp (EEVD) motif enabling HSP70 to interact with other HSPs and various co-chaperones. (Katschinski, 2004; Daugaard et al., 2007; Giuseppina et al., 2011). This interaction with co-chaperones such as HSP40/DNAJ and carboxy terminus of HSC70-interacting protein is possible due to the 10 kDa α-helical C-terminal domain, which forms a lid mediating the binding (Murphy, 2013). HSP70 is involved in the ATP-dependent folding of nascent proteins, signal transduction, protein translocation and the inhibition of stress-induced protein aggregation.

Stressors known to induce HSP70 accumulation include heat shock, UV irradiation,

proteasomal inhibition and exposure to some heavy metals (Yu et al., 2015). HSP70 was found to be an inhibitor of apoptosis as it repressed both caspase-dependent and independent cell death (Sevin et al., 2015). Interestingly, high levels of HSP70 are a key marker for certain cancers. Furthermore, its overexpression was associated with resistance to certain chemopreventive drugs used to treat breast, endometrial or gastric cancers, among others (Murphy, 2013; Sevin et al., 2015).

1.1.2. Small heat shock proteins

SHSPs, which range in size from 12 to 43 kDa, are not highly conserved except for an 80-100 amino acid long α-crystallin domain, which is also found in the lens proteins αA-crystallin and αB-crystallin (Katschinski, 2004; Bakthisaran et al., 2015). Despite their lack of conservation, most sHSPs usually have three functional domains that include an α-crystallin domain, an amino-terminal region and a carboxy-terminal extension. The secondary structure of the α-crystallin domain contains β-strands organized into β-sheets that are vital for the formation of dimers, the basic functional units of sHSP complexes (MacRae, 2000, Basha et al., 2012). The N-terminal region of the sHSP may play a role in oligomer formation (Lambert et al., 1999; Ganea, 2001). The C-terminal extension which is poorly conserved and variable in length, is essential for self and client protein solubility (due to the high proportion of polar amino acids) and stabilization of sHSP structure, both of which are required for optimal chaperone activity (MacRae, 2000; Fernando and Heikkila, 2000; Morris et al., 2008; Heikkila, 2017). Upon stressful conditions that result in unfolded protein, the cellular pools of sHSPs bind and stabilize unfolded protein substrate (Haslbeck and Vierling, 2015; Treweek et al., 2015). Subsequently, dimers can assemble into larger oligomeric forms (Heikkila, 2017). SHSP oligomeric structures aid in ameliorating the formation of toxic protein aggregates in the cell caused by environmental

stress or disease states by maintaining protein solubility and then transferring them to ATP-dependent chaperones for refolding or degradation. (MacRae, 2000; Heikkila, 2010; Mymrikov et al., 2011; Bakthisaran et al., 2015; Heikkila, 2017).

Research suggests that sHSPs are involved in a number of cellular functions including resistance against apoptosis, acquisition of thermotolerance, actin capping/decapping activity and cellular differentiation (MacRae, 2000; Van Montfort et al., 2001; Heikkila, 2004; 2010; Mymrikiv, et al., 2011; Acunzo et al., 2012; Garrido et al., 2012; Treweek et al., 2015; Heikkila, 2017). Furthermore, the accumulation of sHSPs or their mutants have been associated with a number of medical conditions such as diabetes, multiple sclerosis, oncogenesis, cardiovascular, inflammatory and neurodegenerative diseases (Westerheide and Morimoto, 2005; Ghayour-Mobarhan et al., 2012; Vidyasagar et al., 2012; Mymrikov and Haslbeck, 2015).

1.1.2.1. HSPB6

HSPB6, also known as HSP20, was originally discovered in 1994 as part of a complex with HSPB1 (also termed HSP27) and HSPB5 (also known as αB-crystallin) isolated from mammalian muscle (Kato et al., 1994). Various studies reported that HSPB6 was not upregulated by heat shock although enhanced levels of this sHSP were detected in cells or tissues subjected to various stressors that function via other signalling pathways (Kato et al., 1994; Marvin et al., 2008; Edwards et al., 2011; Kirbach and Golenhofen, 2011; Mymrikov et al., 2011). HSPB6 was shown to function as an ATP-independent molecular chaperone since it inhibited either heat- or chemical-induced aggregation of various client proteins (Van de Klundert et al., 1998; Bukach et al., 2004; Heirbaut et al., 2014; Nahomi et al., 2015). Furthermore, the interaction of HSPB6 with various protein kinases and its phosphorylation appears to be important for its roles in muscle contraction, cardioprotection and insulin resistance (Fan et al., 2005; Dreiza et al., 2010;

Edwards et al., 2011; Mymrikov et al., 2011). Other functions proposed for HSPB6 include the regulation of platelet function as well as the acquisition of thermotolerance and anti-apoptotic activity (Myrmikov et al., 2011; Nagasawa et al., 2014; Nahomi et al., 2015).

1.1.2.2. HSP30

Stress-inducible HSP30, part of the sHSP superfamily, has been found in amphibian, fish, reptilian and avian species but not mammals (Heikkila, 2017). The initial isolation of the *hsp30C* and *D* genes in *Xenopus laevis* by Krone et al. (1992) paved the way for the discovery of *hsp30* genes in various species (additional information about *X. laevis* HSP30 will be covered in section 1.8.2.). Interestingly, there is a high degree of divergence within the non-mammalian vertebrate HSP30s, possibly due to the rapid evolution of *hsp30* genes relative to other genes within the sHSP family (Norris and Hightower, 2002). Phylogenetic analysis revealed that HSP25/HSP30 proteins within birds, fish, amphibians and reptiles grouped together and were distinct from their HSPB1/HSP27 counterparts (Heikkila, 2017). Additionally, the number of *hsp30* genes can vary between species of non-mammalian vertebrates (Bienz, 1984; Krone et al., 1992; Norris et al., 1997; Helbing et al., 1996; Franck et al., 2004; Katoh et al., 2004; Elicker and Hutson, 2007).

Although an examination of *hsp30* gene expression during embryogenesis in non-mammalian vertebrates has been investigated, a number of studies have shown heat stress induced *hsp30* mRNA and protein accumulation in adults and tissue culture cells of fish, amphibians and birds (Zarate and Bradley, 2003; Kondo et al., 2004; Mulligan-Tuttle and Heikkila, 2007; Heikkila, 2017). Studies utilizing amphibian, fish and avian systems have examined the effect of chemical stressors on the induction of *hsp25/hsp30* gene expression (Heikkila, 2017). For example, Katoh et al. (2004) demonstrated an increase in HSP25/HSP30 accumulation in quail and chicken embryo fibroblast cells when treated with a proteasomal

inhibitor. HSP25/HSP30 accumulation was observed in the perinuclear regions of the cell and was associated with perinuclear inclusions or aggresomes. Enhanced *hsp30* gene expression in fish has also been documented in response to various pollutants and pesticides as well as during feeding states following amino acid starvation (Wang et al., 2007; Miller at al., 2009; Garcia de la serrana and Johnston, 2013; Shahid et al., 2016).

1.2. Heat shock response

The heat shock response (HSR) is a universal cellular cytoprotective mechanism that confers resistance against various stressors (Verghese et al., 2012). In the presence of stressful stimuli such as elevated temperatures, heavy metals, oxidants or disease states, an accumulation of unfolded protein results in proteotoxic stress leading to the activation of the HSR (Morimoto, 2008). The accumulation of unfolded protein was shown to trigger the binding of the transcription factor heat shock factor (HSF1) to the heat shock element (HSE), an enhancer situated in the upstream promoter region of *hsp* genes (Morimoto, 1998; 2008, Xie et al., 2014).

1.2.1. Heat shock factor 1

To date, there have been 4 HSFs (HSF1-4) identified in vertebrates. HSF1 is the master regulator involved in the expression of stress-induced *hsp* genes (Jaegar et al., 2014; Xie et al., 2014). HSF1 is composed of an amino-terminal looped helix-turn-helix DNA binding domain (DBD), an oligomerization domain and a C-terminal transcriptional transactivation domain (Figure 1; Anckar and Sistonen, 2011; Jaegar et al., 2014). The well-conserved DBD is responsible for interaction with the HSE, while the hydrophobic repeat domains located within the oligomerization domain (HR-A/B) or adjacent to the transcriptional activation domain (HR-C), control trimerization through intermolecular interactions (Anckar and Sistonen, 2011). During normal conditions, the HR-C domain is believed to fold back and interact with the HR-

Figure 1. HSF1 structure. Schematic representation of the HSF1 structural motifs that correspond to the amino-terminal looped helix-turn-helix DNA binding domain (DBD), hydrophobic repeat sequences HR-A/B contained within the oligomerization domain (OD) and hydrophobic repeat sequence HR-C adjacent to the carboxy-terminal transcriptional transactivation domain. During normal conditions, interactions between HR-C and HR-A/B prevent HSF1 trimer formation (adapted from Anckar and Sistonen, 2011).

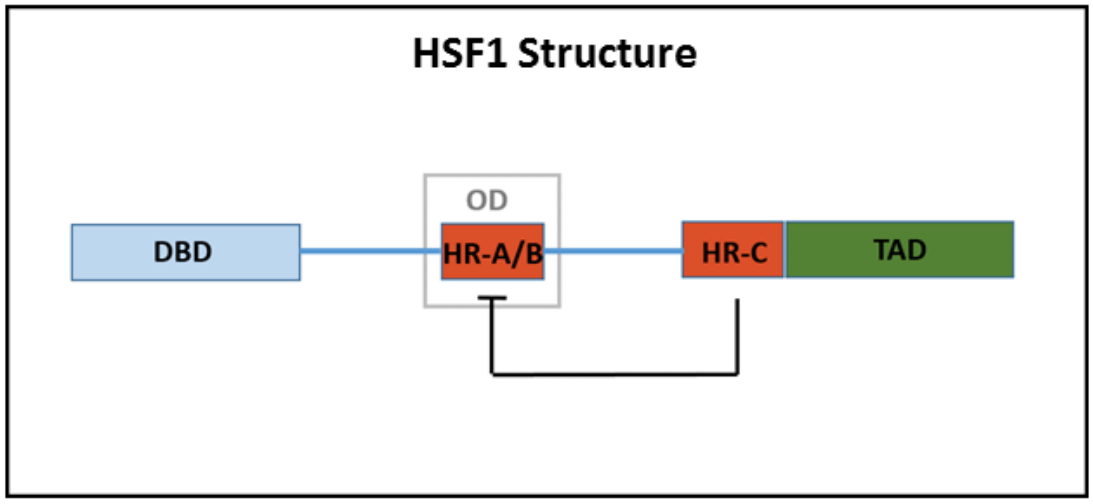
HSF1 Structure
OD
DBD
HR-A/B
HR-C
TAD

A/B domains preventing the possibility of trimerization, keeping HSF1 in an inactive, monomeric state (Anckar and Sistonen, 2011). During this time, HSF1 is bound to HSP90 and possibly histone deacetylase 6 (HDAC6; Hentze et al., 2016). Several studies determined that under proteotoxic stress conditions which may overwhelm, compromise or inhibit the proteasome, polyubiquitinated protein binds HDAC6 resulting in the disassociation from the HSF1-HSP90 complex (Pernet et al., 2014). Meanwhile, HSP90 is recruited to bind unfolded protein and prevent its aggregation. This permits HSF1 to trimerize into its active form before moving into the nucleus, becoming hyperphosphorylated at serine residues and binding to the HSE to initiate transcription of *hsp* genes (Figure 2; Sakurai and Enoki, 2010; Hentze et al., 2016).

HSF1 was found to undergo post-translational modifications which can regulate HSF1 transcriptional ability (Dinkova-Kostova, 2012; Hentze et al., 2016). As mentioned above, phosphorylation can enhance HSF1's ability to initiate transcription. However, acetylation and sumoylation can function to repress the ability of HSF1 to induce the expression of *hsp* genes (Anckar and Sistonen, 2011; Hentze et al., 2016).

1.3. Heme oxygenase-1

Heme oxygenase-1 (HO-1; also known as HSP32), first identified by Tenhunen et al. (1968), catalyzes the catabolism of heme to iron, carbon monoxide and biliverdin, requiring the presence of NADPH and oxygen. Biliverdin is then converted to bilirubin (Araujo et al., 2012). When not bound to hemoproteins, heme causes deleterious effects at the cellular level leading to reactive oxygen species (ROS) formation and membrane lipid peroxidation (Choi et al., 2014). HO-1, unlike HO-2 and HO-3 isoforms, is the stress-inducible isozyme (Ryter et al., 1999). The 32 kDa HO-1 protein is detectable in all cells including kidney and liver with a high amount

Figure 2. Stress-induced activation of the heat shock response. 1) External stressful stimuli (indicated by the lightning bolt) can result in the unfolding of native protein within the cell. 2) HSP90 is bound to HSF1 under normal conditions in the cell. 3) HSP90 is recruited to prevent aggregation of unfolded proteins. 4) This allows HSF1 monomers to trimerize and translocate to the nucleus. 5) The HSF1 trimer is hyperphosphorylated and binds to the HSE at the 5' promoter of *hsp* genes. 6) HSF1 binding to the HSE results in the initiation of transcription by RNA Polymerase II resulting in the accumulation of stress-induced HSPs.

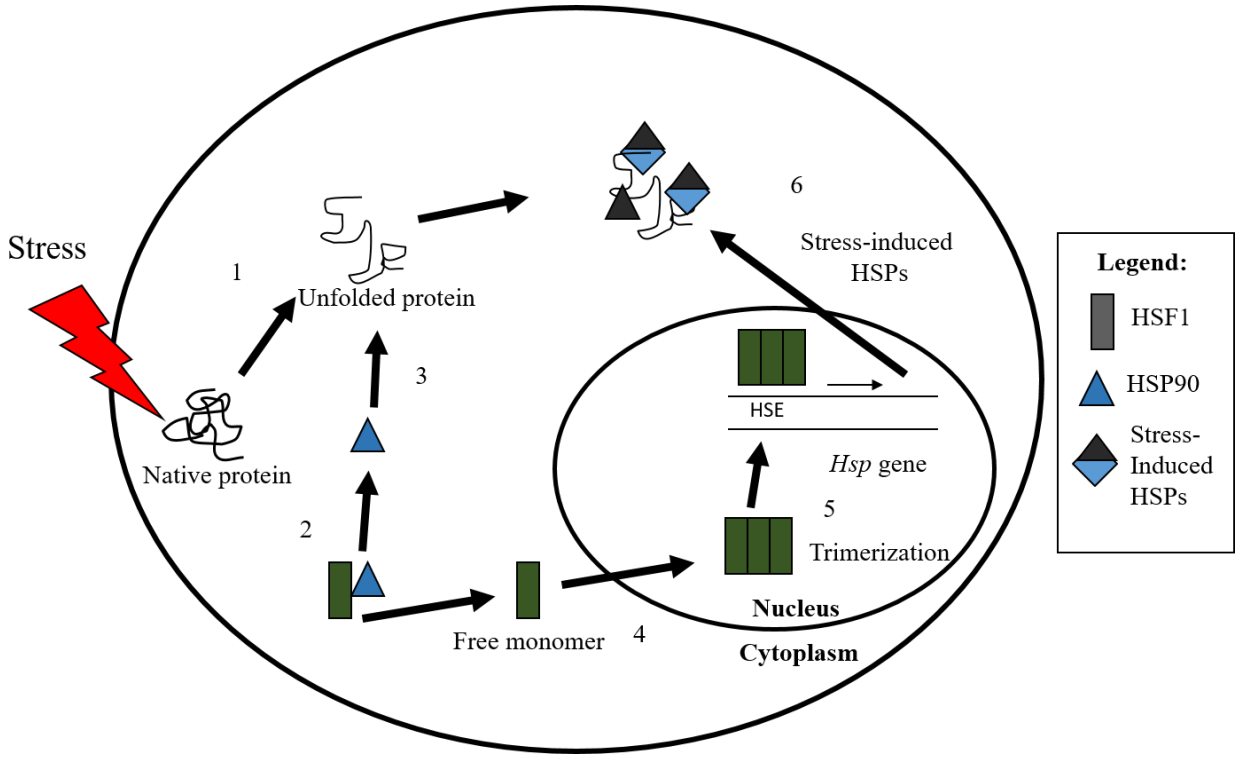
Stress
1
Unfolded protein
6
Stress-induced HSPs
Native protein
3
HSE
Hsp gene
2
5
Trimerization
Nucleus
Free monomer
4
Cytoplasm
Legend:
HSF1
HSP90
Stress-Induced HSPs

in spleen, which is involved in the sequestration of senescent erythrocytes and the location where hemoglobin is degraded (Chau, 2015). It has been suggested that HO-1 is anchored into the ER membrane post-translationally (Chau, 2015).

The cytoprotective role of HO-1 involves its aforementioned catalytic by-products. For example, bilirubin has strong antioxidant capabilities such as decreasing lipid peroxidation. Lipid peroxidation due to cadmium toxicity for instance has been attributed to alterations in expression of enzymes involved in the cellular antioxidant defense system. Therefore, the reduction of this toxic process by means of bilirubin is beneficial to the cell (Patra et al., 2011). Carbon monoxide (CO) in low concentrations can have a positive impact at the cellular level through various mechanisms. Supressing pro-inflammatory cytokines such as tumour necrosis factor alpha, interleukin-1β and macrophage inflammatory protein-1 highlights its ability to act as an anti-inflammatory agent (Pae and Chung, 2009; Araujo et al., 2012). Furthermore, CO can prevent apoptosis through the inhibition of mitochondrial cytochrome c release as well as its interaction with p38 mitogen-activated kinase (MAPK; Queiroga et al., 2012).

HO-1 is essential for human health since its deficiency has been characterized by growth retardation, hemolytic anemia, endothelial damage, iron deposition as well as increased vulnerability to oxidative stress-related injury (Yachie et al., 1999; Chang et al., 2015). In mammalian systems, a variety of inducers including curcumin, MG132, sodium arsenite and cadmium were shown to induce *ho-1* gene expression (Alam et al., 2000; Wu et al., 2004; Yamamoto et al., 2010; Wang et al., 2013). Protein deposition disorders including Alzheimer's and Parkinson's disease are usually accompanied by a significant increase in HO-1 levels to help combat the oxidative stress caused by the disease. Therefore, the use of HO-1 as a biomarker for neurological diseases has become extremely useful in therapeutics approaches (Abraham and

Kappas, 2008).

1.3.1. *Heme oxygenase-1* gene regulation

Ho-1 gene expression is controlled primarily at the transcriptional level (Ryter et al., 2006). In response to stressful stimuli, transcription factors bind to certain *cis*-acting elements found within the 5' region of the *ho-1* gene. This includes the musculoaponeurotic fibrosarcoma (MAF) recognition antioxidant response element (MARE; also called the stress response element), cadmium response element (CdRE) and the HSE (Choi and Alam, 1996; Lee et al., 1996, Alam et al., 2000; Alam and Cook, 2007). The primary transcription factor responsible for *ho-1* gene expression is the nuclear factor erythroid 2 (NFE2)-related factor 2 (Nrf2; Choi et al., 2014). Regarded as a member of the leucine zipper transcription factors, Nrf2 is supressed under basal conditions as it is bound to Kelch-like ECH-associated protein 1 (Keap1). Upon stress, modification of cysteine residues within Keap1 results in the dissociation of Nrf2, giving Nrf2 the opportunity to translocate into the nucleus. Subsequently, Nrf2 forms a heterodimer with Maf protein before binding to the ARE to induce *ho-1* gene expression (Figure 3; Choi et al., 2014). Under normal conditions, Bric-a-brac and Cap-n-Collar homology (Bach1) prevents *ho-1* gene induction by associating with Maf proteins and binding to DNA at ARE-like enhancers (Perez-De-Puig et al., 2013). Pro-oxidants as well as heme are known to inactivate Bach1 (Ogawa et al., 2001). Aside from Nrf2, several protein families were implicated in *ho-1* gene activation including nuclear factor-κB (NF-κB), activator protein-1 and HSF (Alam & Cook, 2007).

Although HO-1 is generally not heat shock inducible, HSF1 has been found to interact with pescadillo, a transcription factor known to bind to the CdRE (Sikorski et al., 2006). Furthermore, HSF1 overexpression has been shown to enhance *ho-1* gene transcription while HSF1 knockout in mouse embryonic fibroblast cells resulted in decreased *ho-1* gene expression

Figure 3. *Ho-1* gene regulation. Under normal conditions, Nrf2, the transcription factor responsible for the induction of the *ho-1* gene, is bound to Kelch-like ECH-associated protein 1 (Keap1), sequestering it in the cytoplasm. Meanwhile, in the nucleus, the repressor Bric-a-brac and Cap-n-Collar homology (Bach1) forms a heterodimer with Maf transcription factor and the complex binds to Maf recognition elements (MARE; an antioxidant response element or ARE) to prevent transcription of the gene. Upon cellular stress, Bach1 is exported from the nucleus, while Nrf2 dissociates from Keap1 and is imported into the nucleus. Here, it binds the MARE within the *ho-1* gene and initiates transcription (adapted from Naito et al., 2011).

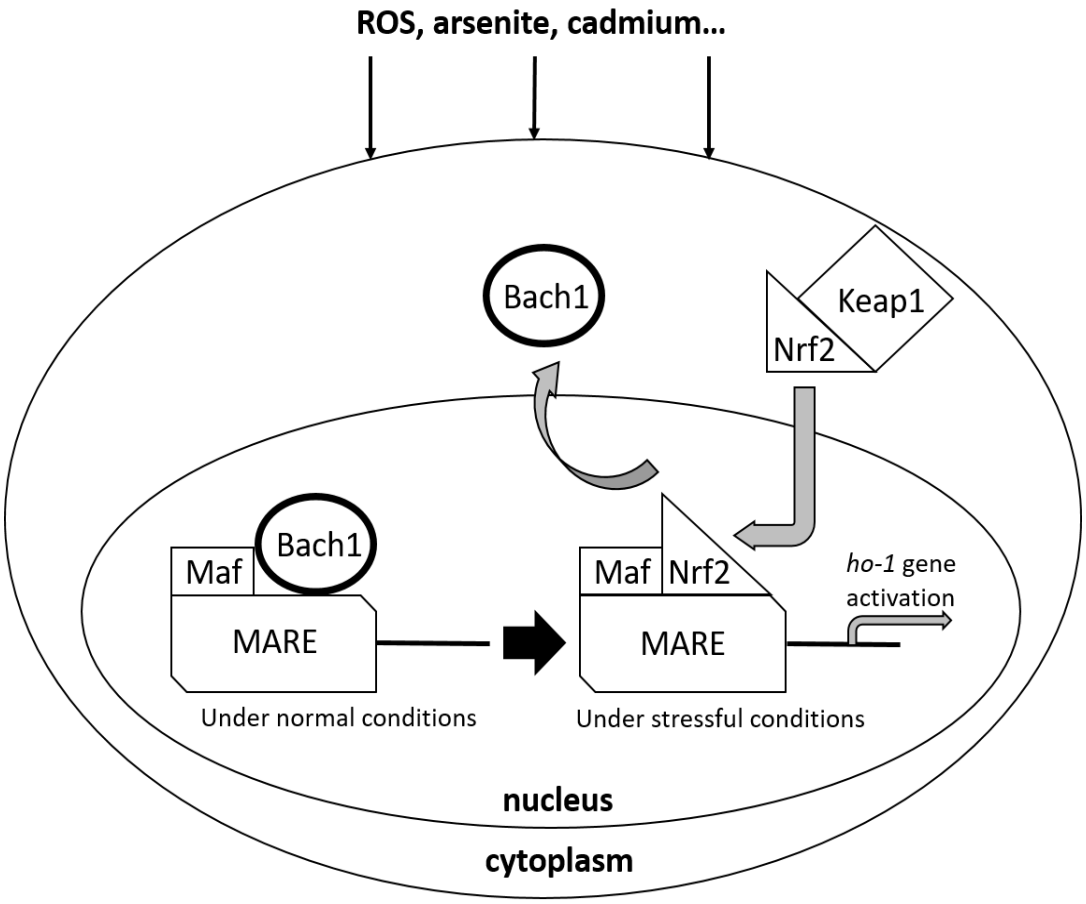
ROS, arsenite, cadmium…
Bach1
Keap1
Nrf2
Maf
Bach1
MARE
Maf
Nrf2
MARE
ho-1 gene
activation
Under normal conditions
Under stressful conditions
nucleus
cytoplasm

(Alam & Cook, 2007; Koizumi et al., 2007). These findings suggested that HSF1 may have a potential involvement in *ho-1* gene expression. Recently it was determined that treatment with SB2023580, a p38 MAPK inhibitor, significantly reduced *ho-1* gene induction giving insight into yet another protein which induces *ho-1* expression by mediating Nrf2 translocation (Park et al., 2013).

1.4. Ubiquitin-proteasome system

The ubiquitin-proteasome system (UPS), a tightly regulated mechanism responsible for the degradation of 70-80% of cellular protein, is essential for regulation of protein homeostasis (Tramutola et al., 2016). Mediating and targeting selective proteins for degradation affects fundamental biological processes such as signal transduction, cell cycle arrest as well as apoptosis (Bassermann et al., 2014; Tramutola et al., 2016). Several studies have revealed that cancer progression was dependent on elaborate cellular system regulators which maintained proteostasis, like the UPS. Therefore, certain proteasomal inhibitors including bortezomib and isothiocyanates are currently being used in various clinical trials to treat cancers such as multiple myeloma and mantle cell lymphoma (Deshaies, 2014). The UPS degradation pathway functions in an ATP-dependent manner and uses ubiquitin molecules to target proteins for degradation by the 26S proteasome (Tramutola et al., 2016).

1.4.1. Protein ubiquitination

Ubiquitin, a highly stable 8.5 kDa protein, is conserved through evolution and functions to tag and target proteins destined for degradation by the UPS (Komander and Rape, 2012; Tramutola et al., 2016). The process of ubiquitination involves various ubiquitinating enyzmes denoted E1 to E4. First, E1 activates the ubiquitin molecule in an ATP-dependent manner through adenylation, resulting in a high-energy thioester bond. This bond exists between E1's

active site cysteine residue and the carboxy terminus of the ubiquitin protein. The ubiquitin-conjugating enzyme E2 subsequently receives and forms a similar thioester bond with the activated ubiquitin protein. E3, an ubiquitin ligase, plays a crucial step in transferring one ubiquitin to a lysine residue of a substrate protein resulting in monoubiquitination (Deshaies, 2014; Weathington and Mallampalli, 2014; Tramutola et al., 2016). A protein destined for degradation requires at least 4 ubiquitin molecules (facilitated by E4, a ubiquitin chain elongation factor) for efficient translocation to the proteasome and its subsequent degradation (Micel et al., 2013). Since E3 ligases essentially select which proteins become targeted for degradation, certain therapeutic approaches have targeted the functioning of these enzymes. More specifically, inactivation of E3's active site or compromising the enzyme's ability to form protein-protein interactions could be of value in the treatment of cancer and other diseases (Bassermann et al., 2014).

1.4.2. Proteasome

The highly specific and efficient 26S proteasome, approximately 2.5 MDa in size, contains two 19S regulatory particles which serve to cap either end of the multi-subunit holoenzyme as well as a 20S catalytic core (Ross et al., 2015). Each 900 kDa 19S regulatory unit has two very important catalytic functions: deubiquitination of the protein though proteolytic cleavage as well as ATP hydrolysis allowing the protein to be unfolded and passed on to the 20S catalytic core (Bhattacharyya et al., 2014; Dou, 2014). The 20S core is comprised of four stacked rings in an αββα conformation (Figure 4). The α subunits allow the entrance of the protein into the core from the 19S regulatory regions, while the β subunits contain chymotrypsin-like, trypsin-like and caspase-like catalytic activity (Dou, 2014; Ross et al., 2015). Following degradation, exopeptidases break down the peptides further into amino acids while other

Figure 4. Ubiquitin-proteasome system. 1) Ubiquitinating enzymes E1-E3 activate and transfer a ubiquitin molecule to a protein targeted for degradation. 2) E4 assists in the polyubiquitination of the protein. 3) The polyubiquitinated protein enters the 26S proteasome complex and is degraded. 4) The resulting peptides are further broken down into amino acids or displayed on the surface of the cell, while the ubiquitin molecules are recycled. (Adapted from Lee and Goldberg, 1998).

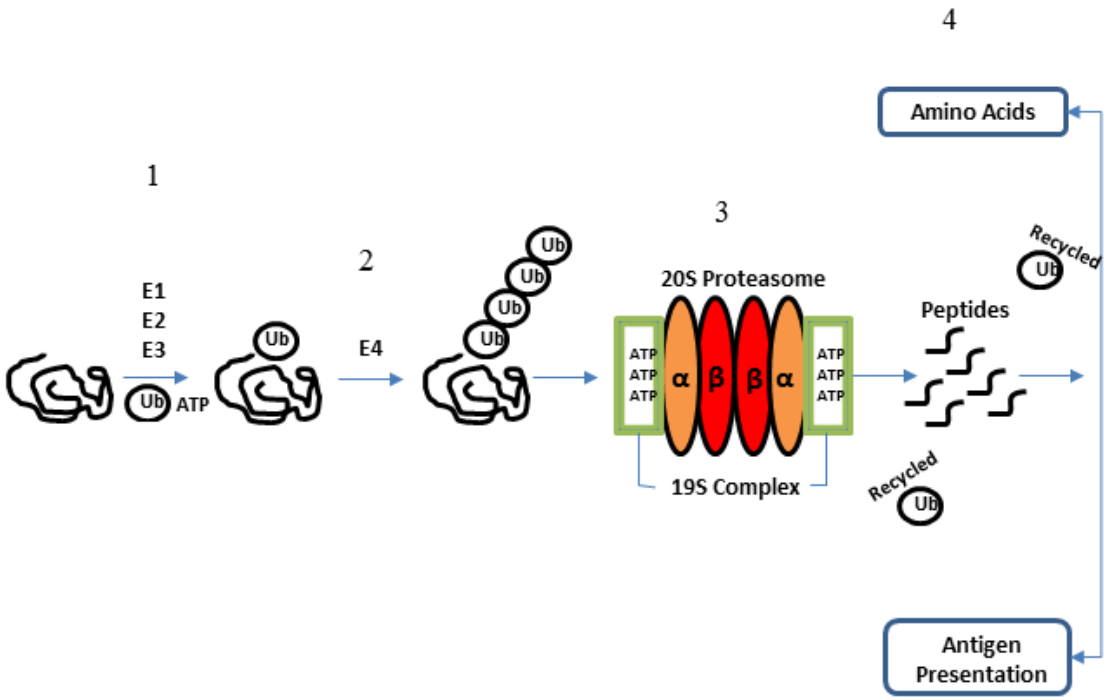
4
Amino Acids
1
3
2
Recycled
Ub
E1
E2
E3
Ub
Ub
Ub
Ub
Ub
20S Proteasome
Peptides
Ub
ATP
E4
ATP
ATP
ATP
α
β
β
α
ATP
ATP
ATP
19S Complex
Recycled
Ub
Antigen
Presentation

peptides bind to major histocompatibility complex class 1 molecules in the ER, ultimately appearing on the cell surface for antigen presentation.

1.5. Aggresomes

Different stressors have the ability to greatly increase the number of unfolded or misfolded proteins within a cell. Exceeding or impairing the ability of the proteasome to hydrolyze ubiquitinated protein destined for degradation leads to the formation of aggresomes (An and Statsyuk, 2015). This is the cell's cytoprotective solution to minimizing and isolating toxic protein aggregates, which might otherwise be dispersed leading to deleterious effects on various cellular processes.

The formation and growth of aggresomes occurs through a microtubule-dependent process which involves the transport of aggregated protein along microtubule networks using dynein motors (Uversky and Fink, 2007). The first step of this process is anchoring the protein destined for the aggresome to the dynein motor responsible for shuttling along the microtubule. HDAC6 anchors ubiquitinated protein cargo while Bcl-2-associated athanogene 3 protein anchors non-ubiquitinated protein cargo (Munoz-Moreno et al., 2015). Studies have shown that drugs such as nocodazole, a microtubule depolymerizing agent, inhibits the formation of aggresomes indicating the importance of microtubule networks for this shuttling process (Garcia-Mata et al., 1999; Kopito, 2000). The aggregated protein is ultimately shipped to the microtubule organizing centre located in the perinuclear region of the cell, where it becomes part of the larger aggresome containing γ-tubulin, vimentin and aggregated protein (Shen et al., 2011; Nakajima and Suzuki, 2013; Munoz-Moreno et al., 2015).

Vimentin, a type III intermediate filament, makes up a crucial part of the external structure of the aggresome, forming a cage-like framework that encapsulates the mass of

aggregated protein (Figure 5; Pérez-Sala et al., 2015). The purpose of the cage-like intermediate filament structure is still unknown although it could serve to stabilize the aggresome or prevent non-specific interactions (Olzmann et al., 2008). The association of certain molecular chaperones within aggresomes have been described in various studies including avian HSP25, mammalian HSP27 and/or αB-crystallin, as well as amphibian HSP30 (Katoh et al., 2004; Ito et al., 2005; Bauer and Richter-Landsberg, 2006; Goldbaum et al., 2009; Bolhuis and Richter-Landsberg, 2010; Khan et al., 2015). The presence of soluble toxic protein aggregates have been shown to underlie various neurodegenerative diseases such as Alzheimer's disease, Huntington's disease, Parkinson's disease and oculopharyngeal muscular dystrophy (Olzmann et al., 2008).

1.6. Actin and microtubule filament structure and function

Actin and microtubules along with intermediate filaments make up the three important components of the cellular cytoskeleton. Actin, found in the monomeric G-form or filamentous F-form, plays important physiological roles in the cell including the maintenance of cell shape as well as executing morphogenesis to cytokinesis (Dominguez and Holmes, 2011). Various stressors including cadmium, sodium arsenite and elevated temperatures have been shown to disrupt the F-actin cytoskeleton in mammalian and amphibian systems (Li and Chou, 1992; Young and Heikkila, 2009; Khamis and Heikkila, 2013; Khamis et al., 2016).

Microtubules play a vital role in a variety of cellular processes including intracellular trafficking as well as motility and cell division (Kononova et al., 2014). Polymerization and depolymerization of α- and β-tubulin heterodimers are required for the biological functions of microtubules in cell growth as well the formation of mitotic spindles in order to segregate replicated chromosomes into two daughter cells (Mi et al., 2008). The αβ heterodimer is the basic structural subunit of a microtubule protofilament, with the α and β globular proteins held

Figure 5. Aggresome formation. 1) Proteins in their native conformation become misfolded upon the presence of a stressful stimuli. 2) During conditions where the UPS is overwhelmed or inhibited, Bcl-2-associated athanogene 3 (BAG3) bridges non-ubiquitinated protein onto dynein-bound microtubule tracks, while histone deacetylase 6 (HDAC6) performs a similar role with polyubiquitinated protein. 3) After the protein cargo has been shuttled to the aggresome, it is encapsulated and held within a vimentin cage-like structure (Adapted from Olzmann et al., 2008).

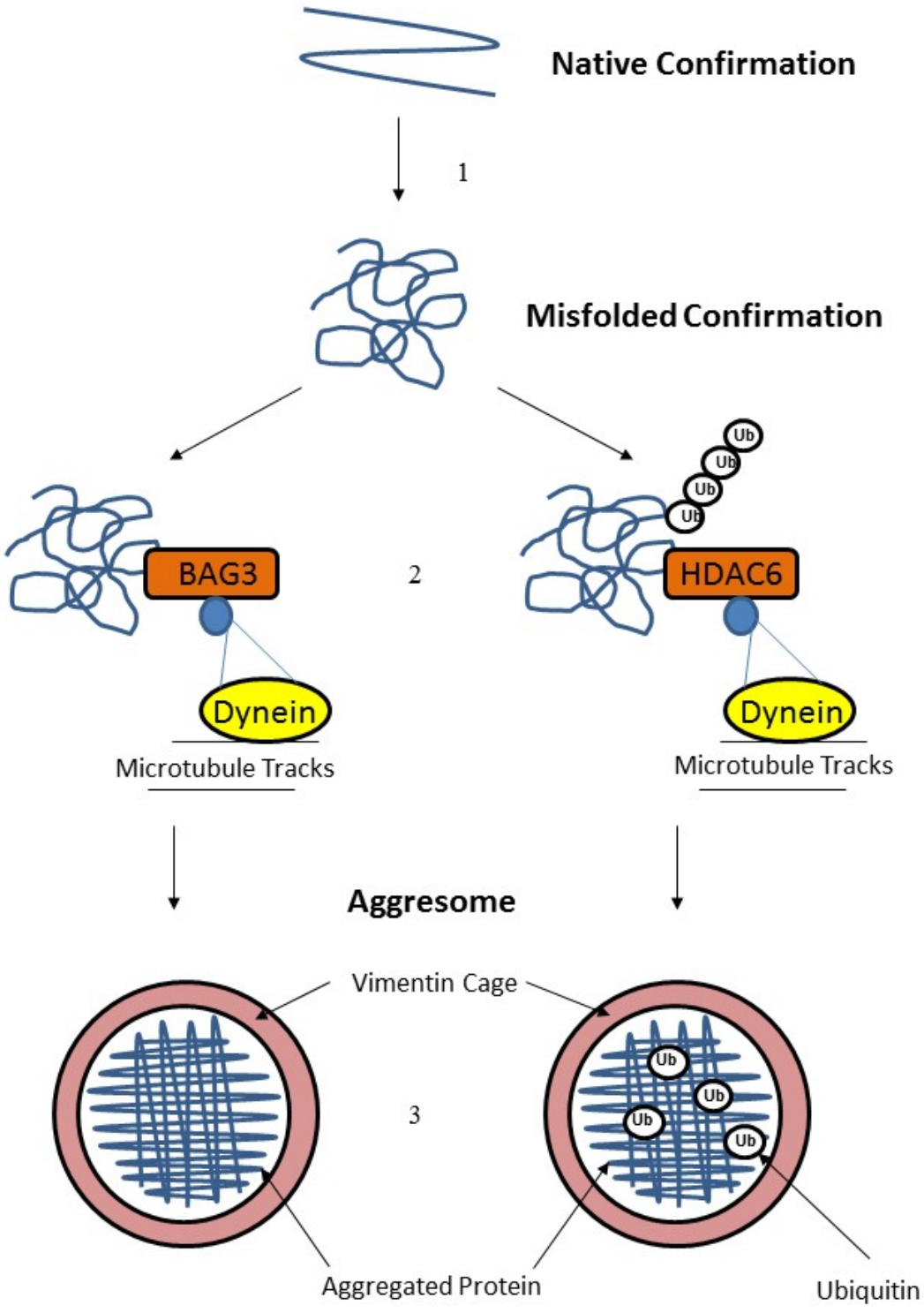
Native Confirmation
1
Misfolded Confirmation
Ub
Ub
Ub
Ub
BAG3
2
HDAC6
Dynein
Dynein
Microtubule Tracks
Microtubule Tracks
Aggresome
Vimentin Cage
Ub
Ub
Ub
Ub
3
Aggregated Protein
Ubiquitin

together by non-covalent bonds (Alberts, 2002). A long, cylindrical 25 nm microtubule is formed from 13 protofilaments, with each protofilament containing numerous α- and β-tubulin heterodimer subunits joined end to end (Goyal et al., 2010). The nucleotide binding site of α-tubulin contains a GTP which is trapped at the dimer interface and therefore cannot be hydrolyzed, unlike the GTP in β-tubulin. The rate of hydrolysis of β-tubulin GTP to GDP after addition of the heterodimer to the microtubule plus end influences the dynamic instability of the protofilament, resulting in either rapid growth (rescue) or shrinkage (catastrophe; Piedra et al., 2016). These changes in microtubule length result in the ability to completely reorganize within a short amount of time (Parker et al., 2014). This is of utmost significance in maintaining cellular health and function not only in interphase cells, but mitotic cells undergoing chromosomal segregation, as mentioned previously. Tubulin's critical role in this key cellular event makes it a prime target of many cancers, which characteristically elicit aberrant cell division (Goyal et al., 2010). Therefore, chemotherapeutic drugs with the ability to disrupt microtubule polymerization, stability and function have become attractive clinical treatment options for a variety of cancers including breast, ovarian and prostate cancer (Mukhtar et al., 2014). Recognized as a key factor in modulating signalling events and spatial organization of organelles, certain cellular stressors with the ability to cause microtubule disruption including hypoxia and nitric oxide can have profound impacts on the health and functionality of the cell (Eiserich et al., 1999; Parker et al., 2014).

1.7. Isothiocyanates

Organosulfur compounds known as isothiocyanates (ITCs) occur naturally as glucosinolates within cruciferous vegetables (Molina-Vargas, 2013). Treatment of plant cells with physical stress such as biting or chewing, activates the enzyme myrosinase which

hydrolyses glucosinolates into ITCs (Zhang et al., 2006). Being electrophilic, ITCs readily form conjugates with thiols, having the ability to directly bind glutathione and cellular protein including tubulin (Li et al., 2012). Numerous studies have reported the human health promoting properties of ITCs such as chemopreventive efficacy as well as prevention of neurodegenerative diseases (Zhang et al., 2006; Mi et al., 2007; 2008; 2009; Gan et al., 2010; Mi et al., 2010; Li et al., 2012; Mi et al., 2011; Sarkars et al., 2013; Giacoppo et al., 2015). Three of the most extensively studied dietary ITCs include benzyl isothiocyanate (BITC), phenethyl isothiocyanate (PEITC) and sulforaphane (SFN).

1.7.1. Benzyl and phenethyl isothiocyanate

At the cellular level, the two most efficient ITCs in inhibiting tumourigenesis and reducing cancer risk in humans are BITC and PEITC (Mi et al., 2010). Both BITC and PEITC have a high binding affinity for tubulin. Given the importance and abundance of tubulin within the cell, any chemical modification of the protein by ITCs could result in a significant conformational change. In fact, this is thought to be the main mechanism through which ITC-induced cell cycle arrest and apoptosis occurs, resulting in the suppression of oncogenic cells (Zhang et al., 2006; Sarkars et al., 2013). A recent study has shown that the thiol side chains of 12 cysteine residues which exist within α- and β-tubulin are prone to modification by ITCs (Mi et al., 2008). In human lung cancer cells treated with the 3 ITCs it was determined that the average number of thiols within a tubulin heterodimer that were modified by 160 μM BITC, PEITC or SFN were 11.7, 9.1 and 3.8, respectively. It was suggested that the lower number of thiols modified by SFN relative to the other two ITCs was due to the fact that its side chain group was much larger than those found with BITC or PEITC. Since the majority of cysteine residues in tubulin are buried within hydrophobic pockets, they may not be readily accessible to

hydrophilic SFN while BITC and PEITC were able to interact and covalently bind with cysteines. The subsequent alteration in tubulin conformation resulted in the formation of tubulin aggregates.

Recently, it was shown that ITCs induced proteasomal inhibition. For example, Mi et al. (2010) determined in human tissue culture cells that the electrophilic cap of BITC and PEITC had the ability to directly bind accessible cysteine residues within the catalytic active site of proteasome subunits, significantly inhibiting all three proteasome protease activities in a concentration-dependent manner. SFN, however, was unable to inhibit proteasome activity at concentrations up to 30 μM, likely due to the fact that similar to tubulin, cysteine residues were inaccessible to this ITC (Mi et al., 2010). As a result of the BITC- and PEITC-induced proteasomal inhibition, an accumulation of UPS substrates like IκB occurred. Normally, the NFκB inhibitor, IκB, is readily degraded by the proteasome allowing NFκB to freely translocate into the nucleus where it can then induce the expression of certain cell survival genes (Mi et al., 2010). In the presence of BITC or PEITC, IκB was not degraded and therefore inhibited NFκB, possibly contributing to arrest of the cell cycle and apoptosis. This suggested another mechanism (albeit indirectly) by which ITC-induced cell cycle arrest and apoptosis could occur.

ITCs have a promising future for their use as therapeutic and preventive agents for various diseases including multiple myeloma (MM), a neoplastic proliferation of plasma cells responsible for being one of the top 10 leading causes of cancer death among African-Americans (Mi et al., 2010). In a study by Mi et al. (2010), it was found that BITC treatment of U266 cells from a human MM cell line was effective in inhibiting cell proliferation. PEITC had less of an effect on MM cell line proliferation than BITC but greater than SFN, a pattern which was similar to their ability to inhibit the proteasome. Another potential application of BITC is its use in the

control of *Campylobacter jejuni* contamination in the food industry. *C. jejuni,* a widespread pathogen, is responsible for many severe side effects in humans as well as Guillain-Barre syndrome, a long-term neurological disorder (Nachamkin et al., 1998). Treatment of *C. jejuni* with BITC was found to enhance protein aggregation, disrupt various metabolic processes and ultimately result in apoptosis (Dufour et al., 2012; 2013). Recently, in clinical trials, PEITC was found to modestly reduce the activation of the tobacco carcinogen 4-(methylnitrosamino)-1-(3-pyridyl)-1-butanone, which was determined to be responsible for tumourigenesis initiation in the human lung (Yuan et al., 2016).

1.7.2. Sulforaphane

SFN, unlike BITC and PEITC, is relatively inert in tubulin-related biological activities as mentioned above. However, studies have investigated the role of SFN in upregulating ARE-dependent antioxidant enzymes like HO-1 through direct binding of Keap1 (Mi et al., 2011). As mentioned previously, Keap1 is a repressor protein which sequesters Nrf2 in the cytoplasm and incidentally contains various cysteine residues that function as sensors of the intracellular redox state (Tarozzi et al., 2013). It was shown that through covalent modification of vulnerable thiol groups on Keap1 by SFN, Nrf2 was able to disassociate, translocate to the nucleus and bind to the ARE of the *ho-1* gene promoter to induce expression. This finding, which demonstrated the ability of SFN to induce a direct antioxidant response, may be of potential use as an agent to combat acute and chronic neurodegenerative diseases (Giacoppo et al., 2015).

1.8. *Xenopus laevis* as a model organism

X. laevis, the South African clawed frog, has been one of the most extensively used amphibian model research organism within many branches of life science including cell biology, development, physiology and toxicology (Schmitt et al., 2014). A great deal of basic information

has been acquired at both the cellular and molecular level. For example, work with *Xenopus* oocytes, eggs and early embryos was used to elucidate the mechanisms associated with early embryogenesis and differentiation (Philpott and Yew, 2008). Since the data obtained from *Xenopus* is often applicable to human cells, the aforementioned contributions as well as many others have aided in our understanding of tumour biology and chemopreventive therapeutics.

The present study has employed the *Xenopus laevis* A6 kidney epithelial cell line as an experimental system. The growing collection of data derived from this cell line is in part due to its quick doubling time of 22 h (Rafferty, 1975). The fast growing nature of A6 cells combined with their easy maintenance as well as continuous division after reaching confluency makes this model system ideal for cellular and molecular research purposes. Originally isolated by Rafferty (1968) from the proximal renal tubules of adult male *Xenopus*, this cell line has been a model system in various areas of research from genetic profiling under zero gravity to the role of renal epithelial sodium channels in hypertension and function of Cystic Fibrosis transmembrane conductance regulator channels (Guerra et al., 2004; Ikuzawa et al., 2007; Ma, 2011; Niisato et al., 2012). Recently, A6 kidney epithelial cells have been used to assess the toxicological impact of various environmental stressors. For instance, perfluoroalkylated substances (PFAs), used for a range of chemical and industrial applications, are considered organic pollutants with adverse effects on human health when present in food or water (EFSA, 2012). Therefore, researchers have monitored changes in the physiological state of A6 cells (cells forming monolayers or differentiating into domes) in the presence of PFAs to further elucidate the effects of this toxicant (Gorrochategui et al., 2016).

A6 cells have also been employed to observe the toxicological impact of engineered copper oxide nanoparticles (CuO NP; Thit et al., 2015). Copper, a metal co-factor for enzymes

including cytochrome c oxidase used in respiration, can become very toxic at high concentrations (Zhou and Gitschier, 1997). The resulting deleterious effects include DNA damage and the formation of ROS. Cu_{2+} is able to undergo redox reactions resulting in the formation of CuO, which is classified as a polydispersed nanoparticle if less than 100 nm in size (Thit et al., 2013). Thit et al. (2015) demonstrated that when A6 cells were treated with CuO NPs, a significant increase in ROS formation was observed along with reduced glutathione levels and decreased cell viability.

Another application of the A6 kidney epithelial cell line includes the analysis of HSP accumulation after treatment with various environmental stressors including heat shock, sodium arsenite and cadmium chloride (Ohan et al., 1998; Phang et al., 1999; Gellalchew and Heikkila, 2005; Woolfson and Heikkila, 2009; Heikkila, 2010; Brunt et al., 2011; Khamis and Heikkila, 2013). Also, the A6 cell line was employed to examine HO-1 accumulation in the presence of metals and proteasomal inhibitors (Music et al., 2014; Shirriff and Heikkila, 2017). Finally, other studies have identified the ability of A6 cells to confer thermotolerance to lethal thermal challenges when pretreated with a mild heat shock, sodium arsenite or proteasomal inhibitors (Manwell and Heikkila, 2007; Young et al., 2009; Khan and Heikkila, 2011; Khan et al., 2012).

1.8.1. *Xenopus laevis* HSP70

In 1984, Bienz isolated 4 stress-inducible *X. laevis hsp70* genes (A-D). Developmentally, both *hsp70* mRNA and protein were present constitutively during *Xenopus* oogenesis and *hsp70* mRNA was first heat inducible after the midblastula transition, signalling the onset of zygotic genome activation (Bienz, 1984; Krone and Heikkila, 1988; Ovsenek and Heikkila, 1990; Heikkila et al., 1991; Lang et al., 2000). In another study, *Xenopus laevis* embryos were measured for toxicity in the presence of perfluooctane sulfonate by assessing *hsp70* mRNA as

well as pro-apoptotic proteins such as Bax, both of which were significantly upregulated in the presence of the chemical (Segundo et al., 2016). HSP70 accumulation in A6 cells was induced by a variety of stressors including heat shock, sodium arsenite, cadmium chloride, herbimycin A, hydrogen peroxide as well as proteasomal inhibitors such as MG132, lactacystin, celastrol and curcumin (Darasch et al., 1988; Briant et al., 1997; Heikkila, 2004, Muller et al., 2004; Woolfson and Heikkila, 2009; Young et al., 2009; Young and Heikkila, 2010; Walcott and Heikkila, 2010; Khan and Heikkila, 2011; Khamis and Heikkila, 2013).

1.8.2. *Xenopus laevis* HSP30

HSP30, a member of the sHSP family, is a well-characterized molecular chaperone. Multiple intronless genes have been isolated to date including *hsp30A, B, C, D* and part of *E*. *Hsp30A* and *hsp30B* genes were deemed non-functional. *Hsp30A* contained an insertional mutation with a stop codon in the coding region giving rise to only a 10 kDa protein, while *hsp30B* was a pseudogene (Bienz, 1984). Isolation and sequencing of *hsp30C* and *hsp30D* by Krone et al. (1992) determined that these two genes encoded functional 24 kDa proteins with an α-crystallin domain, a characteristic which has been conserved through evolution within the entire sHSP family (Krone et al., 1992, MacRae, 2000; Heikkila, 2017).

In *X. laevis* A6 cells, research has investigated stress-induced HSP30 accumulation and its localization. For example, treatment of cells with heat shock, sodium arsenite, cadmium chloride, herbimycin A, hydrogen peroxide or proteasomal inhibitors like MG132 induced the accumulation of HSP30 (Briant et al., 1997; Ohan et al., 1998; Phang et al., 1999; Muller et al., 2004; Woolfson and Heikkila, 2009; Young et al., 2009; Walcott and Heikkila, 2010; Khan and Heikkila, 2011; Khamis and Heikkila, 2013; Khan et al., 2015). Immunocytochemical analysis revealed that heat shock-induced HSP30 accumulation was present primarily in the perinuclear

region in a granular or punctate pattern and that proteasomal inhibitors had the ability to induce the formation of large HSP30 staining structures (Gellalchew and Heikkila, 2005; Young and Heikkila, 2010; Khan and Heikkila, 2011). A recent study with A6 cultured cells employing immunocytochemistry indicated the association of HSP30 with aggresome-like inclusion bodies after treatment with sodium arsenite, cadmium chloride or MG132 (Khan et al., 2015). As molecular chaperones, HSP30 may be involved in the sequestration of unfolded protein which is transported to the perinuclear region (Khan and Heikkila, 2014; Heikkila, 2017).

1.8.3. *Xenopus laevis* HO-1

In a report by Shi et al. (2008), cDNA data obtained from GenBank determined that the percent identity of *Xenopus* HO-1 with human and mouse amino acid sequences was 61% and 58%, respectively. *Ho-1* mRNA was detected in oocytes and during early embryogenesis from the 1-cell stage to tadpole and was found to accumulate in the dorsal region once embryos reached the neurula stage. Experiments examining stress-induced HO-1 accumulation were conducted for the first time in an amphibian cell line by our laboratory (Music et al., 2014; Shirriff and Heikkila, 2017). It was determined that HO-1 accumulation in *X. laevis* was not induced by heat shock but was induced by sodium arsenite, cadmium chloride and proteasomal inhibitors in a concentration- and time-dependent manner. Immunocytochemical analysis revealed the presence of HO-1 within the perinuclear region of cells, which was consistent with HO-1 being an anchored ER protein. Interestingly, A6 cells treated with a concurrent mild heat stress and sodium arsenite or cadmium chloride elevated HO-1 accumulation to a level greater than observed with either stressor individually.

1.9. Hypothesis

Given the ability of ITCs to bind thiol groups of cellular protein, which results in misfolding and aggregation, my hypothesis is that these electrophilic compounds will induce stress protein accumulation and enhance levels of ubiquitinated and aggregated protein. Additionally, BITC and PEITC will have an affect on tubulin levels and microtubule structure.

1.10. Objectives

As mentioned previously, BITC, PEITC and SFN were shown to be of possible therapeutic use in treating human diseases. While a number of studies have characterized the ability of ITCs to directly bind and modify thiol-containing proteins including α-tubulin, less is known regarding their ability to induce the accumulation of stress proteins such as HO-1 and HSPs and the possible formation of aggregated protein. The present study will focus on the effect of BITC, PEITC and SFN on stress protein accumulation, aggregated protein levels and the actin and microtubule filament structure in *Xenopus laevis* A6 kidney epithelial cells. Specifically, the objectives of this thesis are as follows:

1. To examine the effects of BITC, PEITC and SFN on the relative levels of HO-1, HSP70, HSP30 and HSPB6 accumulation as well as on the actin and microtubule cytoskeleton.
2. To determine the impact of ITC treatment on the level of ubiquitinated protein, aggregated protein and formation of aggresome-like structures.
3. To carry out sequence and phylogenetic analyses of a *X. laevis* small heat shock protein encoded by an *hspb6* cDNA (that was expressed in our laboratory during this research) as well as examining the accumulation of HSPB6 in A6 cells in response to ITCs, heat shock, cadmium and MG132.

Chapter 2: Materials and Methods

2.1. Maintenance and treatment of *Xenopus laevis* A6 cells

HSP accumulation patterns in response to stressful stimuli were examined in *Xenopus laevis* A6 kidney epithelial cells obtained from the American Type Culture Collection (Rockville, MD). The cell line was grown in 70% Leibovitz L-15 Media containing 10% fetal bovine serum and 1% penicillin/streptomycin (Sigma-Aldrich, Oakville, ON) at 22 ºC in T75 cm BD falcon culture flasks (BD Biosciences, Mississauga, ON). After cells reached confluency, old media was aspirated and washed with 1 mL versene [0.02% (w/v) KCl, (0.8% (w/v) NaCl, 0.02% (w/v) KH_2PO_4, 0.115% (w/v) $NaHPO_4$, 0.02% (w/v) Na_2EDTA] followed by incubation with 2 mL of fresh versene. Subsequently, 1 mL of 1X trypsin (Sigma-Aldrich) in 100% Hanks balanced salt solution (HBSS; Sigma-Aldrich) for 1 min was added to detach the cells from the bottom of the flask. Cells were resuspended in fresh media and transferred into new culture flasks.

Flasks reaching at least 90% confluency were used for treatments. Treatment of cells at 30 °C were performed in a water bath. Also, some flasks of cells were heat shocked in a 33 °C water bath for 2 h and allowed to recover at 22 °C for 2 h. BITC, PEITC and SFN (Sigma-Aldrich) were dissolved in dimethylsulphoxide (DMSO) to make a stock solution of 100 mM, from which a 1 mM working solution was created. Subsequently, A6 cells were treated with 7.5 µM BITC, 5 µM PEITC or 20 µM SFN. MG132 (Sigma-Aldrich), which was dissolved in 500 µL DMSO to prepare 21 mM stock solutions, was added to the cells at a final concentration of 30 µM. Other flasks were exposed to 100 µM cadmium chloride for 16 h at 22 °C (Khamis and Heikkila, 2013). In transcriptional inhibitor experiments, cells were pretreated for 30 min with 2 µg/mL actinomycin D (Sigma-Aldrich) before the addition of the ITC. In translational inhibitor

experiments, A6 cells were pretreated with 100 μM cycloheximide (Sigma-Aldrich) for 6 h prior to the introduction of the ITC directly into the media in the flask. In other experiments, cells were pretreated with the HSF1 inhibitor, 100 μM KNK437 (Sigma-Aldrich; dissolved in DMSO) for 6 h prior to the ITC treatments. Cell morphology was recorded using a phase contrast Nikon TMS microscope equipped with a Nikon Coolpix 995 digital camera (400X magnification; Nikon Canada, Mississauga, ON).

2.2. Protein isolation and quantification

The media was removed from the flasks followed by rinsing of the cells with 2 mL of 65% HBSS and the subsequent addition of 1 mL of 100% HBSS. A cell scraper was used to remove cells from the flask, which were then transferred to a 1.5 mL microcentrifuge tube. The cells were centrifuged at 14,000 rpm for 1 min (Eppendorf centrifuge; Model No. 5810R; Mississauga, ON). The supernatant was removed and cells were stored at -80 °C until protein isolation. Protein was isolated using 300 μL lysis buffer (200 mM sucrose, 2 mM EGTA, 1 mM EDTA, 40 mM NaCl, 30 mM HEPES, pH 7.4), which contained 1% SDS and 1% protease inhibitor cocktail (Promega; Madison, WI). For ubiquitinated protein, 10 mM N-ethylmaleimide (Sigma-Aldrich) was added to the lysis buffer to inhibit deubiquitination of proteins. Next, samples were sonicated on ice with a sonic dismembranator (Model 100, Fisher Scientific; Waltham, MA, USA) and then centrifuged at 14,000 rpm for 30 min at 4 ºC. The protein supernatant was then isolated and stored at -20 ºC until further use.

The bicinchoninic acid (BCA) method was used for protein quantification according to the manufacturer's instructions (Pierce, Rockford, IL, USA). A protein standard was made using a bovine serum albumin (BSA; Bioshop; Burlington, ON). BSA was diluted in MilliQ water to concentrations ranging from 0 to 2 mg/mL. Protein samples in 1.5 mL microcentrifuge tubes

were diluted to a concentration of 1:2 in MilliQ water. BSA standards and protein samples in 10 µL volumes were loaded in triplicate into a 96-well polystyrene plate. Eighty µL of BCA reagent A and B (Pierce) was added to each standard and protein sample and the plate was incubated at 37 °C for 30 min. Subsequently, the plate was read at 562 nm using a Versamax Tunable microplate reader (Molecular Devices, Sunnyvale, CA, USA) and Softmax Pro software. A standard curve was created using the BSA protein standards which was used to determine the concentration of the protein samples.

2.3. SDS-polyacrylamide gel electrophoresis

Proteins were subjected to sodium dodecyl sulfate-polyacrylamide gel electrophoresis employing 12% gels for HO-1, HSP70, HSP30, HSPB6, α-tubulin and actin and 10% gels for ubiquitinated protein. Separating gels [10 or 12% (w/v) acrylamide, 0.32% (v/v) n'n'-bis methylene acrylamide, 0.375 M Tris pH 8.8, 1% (w/v) SDS, 0.2% (w/v) ammonium persulfate (APS), 0.14% (v/v) tetramethylethylenediamine (TEMED)] were prepared and allowed to polymerize for 25 min after 100% ethanol was layered on top of the gel. Once the separating gel solidified, ethanol was removed and the stacking gel [4% (v/v) acrylamide, 0.11% (v/v) n'n'-bis methylene acrylamide, 0.125 M Tris pH 6.8, 1% (w/v) SDS, 0.4% (w/v) APS, 0.21% (v/v) TEMED] was added. Combs were inserted to create lanes in the stacking gel after which it was left to polymerize for another 25 min. Protein samples (30 µg) for HO-1, HSP70, HSP30 and α-tubulin, 40 µg for HSPB6, 60 µg for ubiquitinated protein or 12 µg for actin were added to loading buffer [0.0625 M Tris pH 6.8, 10% (v/v) glycerol, 2% (w/v) SDS, 5% (v/v) β-mercaptoethanol, 0.00125% (w/v) bromophenol blue]. Samples were boiled for 10 min, cooled, briefly centrifuged and loaded on to the gel. Gels were electrophoresed in 1X running buffer [25 mM Tris, 0.2 M glycine, 1 mM SDS] at 90 V until samples reached the separating gel at which

point the voltage was increased to 140 V for ubiquitinated protein or 160 V for HO-1, HSP70, HSP30, HSPB6, α-tubulin and actin.

2.4. Immunoblot analysis

Immunoblot analysis was employed to detect the relative levels of different proteins in A6 cells subjected to various stressors. Nitrocellulose membranes (BioRad, Mississauga, ON) and filter paper (BioRad) were cut to a size of 5.5 X 8.5 cm. Membranes were soaked for 30 min in 10% transfer buffer [25 mM Tris, 192 mM glycine, 10% (v/v) methanol] for ubiquitin blots, or 20% transfer buffer [25 mM Tris, 192 mM glycine, 20% (v/v) methanol] for HO-1, HSP70, HSP30, HSPB6, α-tubulin and actin. Once electrophoresis was finished, the stacking gel was removed and the remainder of the gel was soaked in transfer buffer for 15 min. Protein was transferred to the nitrocellulose membrane with a Trans-Blot Semi-dry Transfer cell (BioRad) for 25 min at 20 V. Once the transfer was complete, membranes were stained with Ponceau S stain [0.19% (w/v) Ponceau S, 5% (v/v) acetic acid] for 10 min to determine the quality of the transfer and loading of protein. Blots were rinsed with MilliQ water and scanned. Membranes were then incubated with 5% blocking [20 mM Tris pH 7.5, 0.1% Tween 20 (Sigma), 300 mM NaCl, 5% (w/v) Nestle® Carnation skim milk powder] solution for 1 h to prevent non-specific binding. Once the blocking solution was removed, the membranes were incubated with rabbit anti-HO-1 (at a dilution of 1:500, Enzo Life Sciences, Farmingdale, NY; Catalog No. BML-HC3001-0100), rabbit anti-*Xenopus* HSP70 (commercially made against a 16 amino acid C-terminal peptide fragment of HSP70B; 1:350; Gauley et al., 2008), rabbit anti-*Xenopus* HSP30 (1:500; Fernando and Heikkila, 2003) or rabbit anti-actin (1:200; Sigma; Catalog No. A2066) polyclonal antibodies or a mouse anti-α-tubulin (1:500; Sigma; Catalog No. T9026) monoclonal antibody, diluted in 5% blocking solution and left overnight. Other membranes were incubated overnight

with a polyclonal rabbit anti-human HSPB6 (1:200; Cedarlane; Catalog No. ARP48436_T100) antibody or a monoclonal mouse anti-ubiquitin (1:150; Invitrogen, Carlsbad, CA, USA; Catalog No. 13-1600) antibody diluted in 5% BSA (Sigma). After incubation with primary antibody, membranes were washed once for 15 min and twice for 10 min, with 1X TBS-T [20mM Tris, 300 mM NaCl, (pH 7.5), 0.1% (v/v) Tween 20]. Membranes were then incubated with secondary antibody in blocking solution for 1 h. Alkaline phosphatase-conjugated goat-anti-rabbit (BioRad) at a dilution of 1:30,000 dilution was employed to detect HO-1, HSP70, HSP30, HSPB6 and actin while alkaline phosphatase-conjugated goat-anti-mouse (BioRad) at a 1:1000 dilution was used to monitor α-tubulin and ubiquitin. Following incubation with secondary antibody, the membranes were washed once for 15 min with TBS-T and twice for 5 min. Membranes were then washed in alkaline phosphatase detection buffer [50 mM Tris, 50 mM NaCl, 25 mM $MgCl_2$ pH 9.5, 0.3% 4-nitro blue tetrazolium (NBT; Roche, Ayr, ON) and 0.17% 5-bromo-4-chloro-3-indolyl phosphate, toluidine salt (BCIP; Roche)] until bands or ubiquitinated protein lanes were visible and then detection buffer was removed and the blots were rinsed with MilliQ water.

2.5. Immunocytochemistry and laser scanning confocal microscopy

In order to determine the localization of HO-1, HSP30 or aggregated protein or the morphology of actin and microtubule filaments in response to various treatments, immunocytochemistry in conjunction with laser scanning confocal microscopy was employed. A6 cells were grown on flame sterilized 22 x 22 mm base-washed glass coverslips (VWR; Catalog No. 48366-067) in sterile petri dishes (VWR, Catalog No. 351029). Coverslips were washed with a base solution [49.5% (v/v) ethanol, 0.22 M NaOH] in small staining jars (Thomas Scientific Apparatus, Philadelphia, PA, USA) for 30 min and then rinsed with distilled water for 3 h.

ITC treatments involved the adjustment of 10 mL of fresh media to a final concentration of 7.5 μM BITC, 5 μM PEITC or 20 μM SFN (as indicated in section 2.1) which was then poured into the petri dishes. The petri dishes were then kept at 22 °C or wrapped with parafilm, sealed in a plastic bag and incubated at 30 °C. Following treatment, L-15 media was removed and cells were rinsed twice with phosphate buffered saline (PBS; 1.37 M NaCl, 67 mM Na_2HPO4, 26 mM KCl, 14.7 mM H_2PO_4, 1 mM $CaCl_2$, 0.5 mM $MgCl_2$ pH 7.4). Once washed, coverslips were transferred to small petri dishes and fixed with 3.7% paraformaldehyde (BDH, Toronto, ON) for 15 min. Coverslips were then rinsed with three 5 min each washes with PBS and then permeabilized using 0.3% Triton X-100 (Sigma) for 10 min. After an additional three washes with PBS, A6 cells were incubated with 3.7% (w/v) BSA (Sigma) for 1 h or overnight at 4 °C. The following day, cells were incubated with rabbit anti-HO-1 (1:200), affinity-purified rabbit anti-*Xenopus* HSP30 (1:500), rabbit anti-human HSPB6 (1:100) or monoclonal mouse anti-α-tubulin (1:250) antibodies in 3.7% BSA for 1 h. After three washes for 3 min each with PBS, indirect labeling of cells was carried out with fluorescent-conjugated secondary antibodies including goat anti-rabbit Alexa Fluor 488 (Molecular Probes) at a 1:2000 dilution (1:1000 for HSPB6) or goat anti-mouse Alexa Fluor 488 (Invitrogen Molecular Probes) at 1:1000 in 3.7% BSA for 30 min in the dark. Coverslips were then incubated with rhodamine-tetramethylrhodamine-5-isothiocyanate phalloidin (TRITC; Invitrogen Molecular Probes) for 15 min at a 1:60 in 3.7% BSA in the dark in order to visualize the actin cytoskeleton. A ProteoStat aggresome detection kit (Enzo Life Sciences, Plymouth Meeting, PA) was used to monitor the presence of aggregated protein and/or aggresome-like structures as per manufacturer's instructions. Coverslips were dried and mounted on a glass microscope slide with Vectashield (Vector Laboratories Inc., Burlingame, CA) containing 4,6-diamidino-2-phenylindole (DAPI;

Vector Laboratories Inc.) to stain nuclei followed by three washes of 5 min each. Clear nail polish was used to permanently attach coverslips to glass slides and the slides were stored at 4 °C. Slides were examined using a Zeiss Axiovert 200 confocal microscope with LSM 510 META software (Carl Zeiss Canada Ltd., Mississauga, ON).

2.6. DNA sequence alignment and phylogenetic analysis

The *X. laevis* HSPB6 amino acid sequence was aligned with human, rat and mouse HSPB6 proteins using the multiple sequence alignment program of Clustal Omega (Version O.2.1; Sievers et al., 2011). For phylogenetic analysis, representative HSPB6 and HSPB5 amino acid sequences obtained from amphibians, reptiles, mammals and fish were aligned using Clustal. A maximum-likelihood tree was constructed using a Jones-Taylor-Thornton model and Nearest Neighbor-Interchange as the heuristic method using MEGA 7.0.14 (Jones et al., 1992; Kumar et al., 2016). The tree was rooted with *S. cerevisiae* HSP26. The reliability of the tree was estimated by bootstrapping with 1000 replicates.

2.7. Densitometry and statistical analysis

Densitometric analysis of all blots were performed with at least 3 separate replicates, using Image J software (Version 1.44; National Institute of Health http://rsb.info.nih.gov/ij/). In cases where 2 HSP70 bands or multiple HSP30 bands were observed, the entire HSP signal detected by each respective antibody was used for analysis. The average densitometric values of HO-1, HSP70 or HSP30 were expressed as a percentage of the maximum signal obtained for each stress protein. The densitometric values obtained for HSPB6, α-tubulin or ubiquitin were compared to control. The standard error is represented by vertical error bars. To determine if any statistically significant differences existed between samples, a one-way ANOVA with a Tukey's post-test was performed on the data.

Chapter 3: Results

3.1. Examination of ITC treatment on HO-1 and HSP accumulation.

3.1.1. Morphology of A6 cells treated with BITC, PEITC or SFN.

Preliminary studies employed phase contrast microscopy to observe the effects of ITCs on the morphology of *Xenopus laevis* A6 kidney epithelial cells (Fig. 6). The concentrations used were similar to studies examining the effects of BITC, PEITC and SFN in mammalian systems (Gibbs et al., 2009; Sarkars et al., 2013; Sehrawat et al., 2016; Yeh et al., 2016). Compared to control, cells treated with 7.5 μM BITC for 12 h at 22 °C displayed an elongated structure with numerous cell processes and a lower overall density. In contrast, cells treated with 5 μM PEITC had a control-like appearance whereas SFN-treated cells displayed a slightly elongated polygonal morphology. After completion of the ITC treatments, the cells were allowed to recover in fresh media for 72 h. Regardless of the ITC treatment, the number of cells increased during recovery and were morphologically similar to control cells. Given these latter results, subsequent studies employed primarily the aforementioned concentrations of the three ITCs to examine their effect on HO-1 and HSP accumulation in A6 cells.

3.1.2. Immunoblot analysis of HO-1, HSP70 and HSP30 accumulation in BITC-, PEITC- and SFN-treated cells.

In this study, the effect of different BITC concentrations on the relative levels of HO-1, HSP70 and HSP30 at 22 °C were examined. Given that HSP70 and HSP30 are heat-inducible, the effect of A6 cells treated with BITC at 30 °C was also evaluated. MG132, a proteasomal inhibitor which was found previously to induce both HO-1 and HSPs in *Xenopus* A6 cells, was used a positive control (Gauley et al., 2008; Young and Heikkila, 2010; Khamis and Heikkila,

Figure 6. Effect of BITC, PEITC and SFN treatment and recovery on the morphology of A6 cells. Cells were maintained at 22 °C (Control) or treated with either 7.5, 5 or 20 μM of BITC, PEITC or SFN, respectively, for 12 h followed by recovery (Rec) in fresh media for 72 h at 22 °C. Phase contrast microscopy was employed to observe the morphology of ITC-treated cells. A6 cells were photographed using a Nikon Coolpix 995 digital camera (400X magnification).

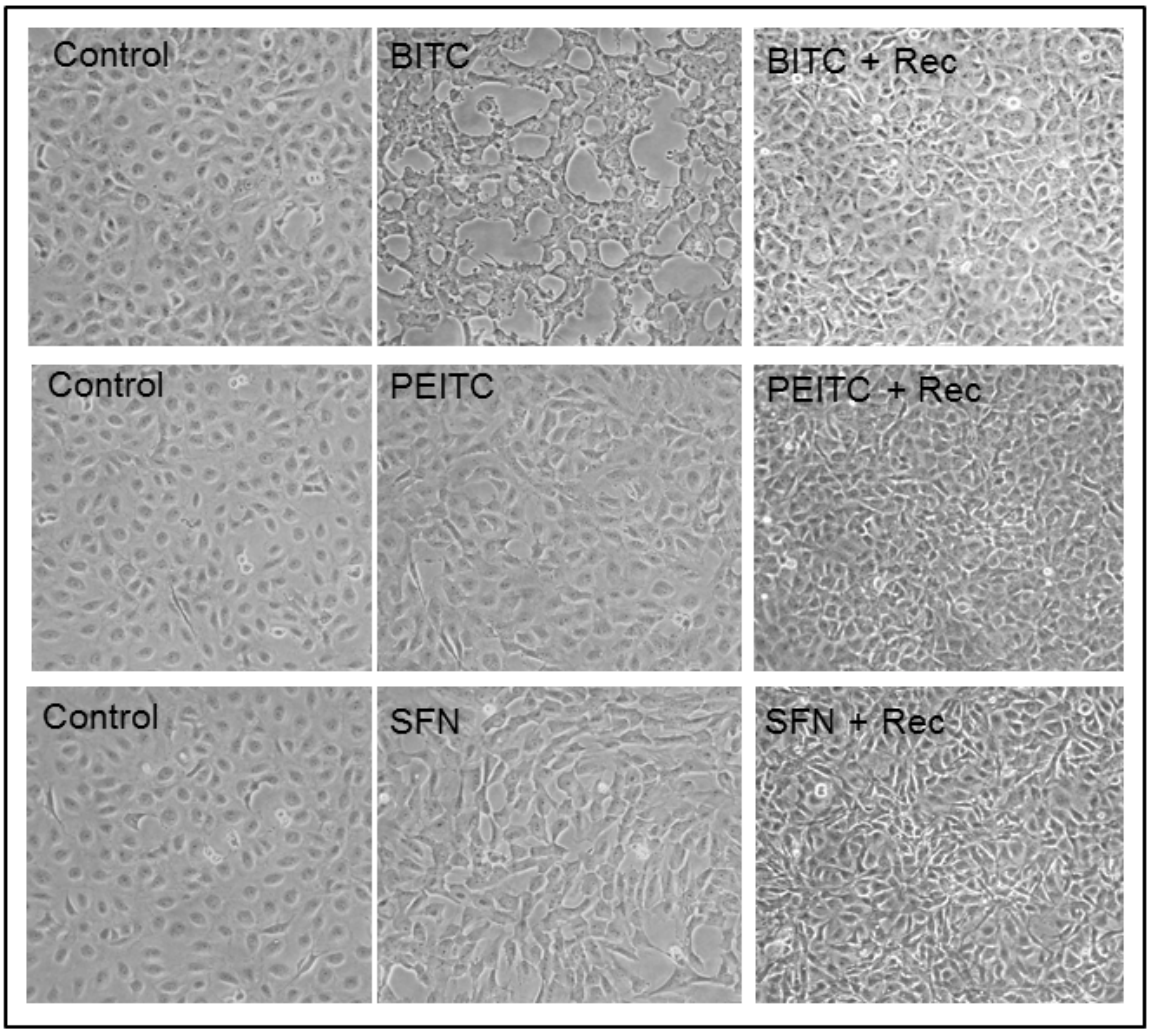
Control
BITC
BITC + Rec
Control
PEITC
PEITC + Rec
Control
SFN
SFN + Rec

2013; Music et al., 2014). The analysis of HO-1 accumulation utilizing immunoblotting and immunocytochemistry employed an antibody that was made against a synthetic peptide (DLSEALKEATKEVH), which shared 100% identity with *X. laevis* HO-1 (Music et al., 2014). Previous studies employed this anti-HO-1 antibody to analyze stress-induced HO-1 accumulation in human cells (Hock et al., 2004; Hanneken et al., 2006). As shown in Figure 7, treatment of cells with 5 and 7.5 μM BITC for 12 h resulted in a greater accumulation of HO-1 than found with 10 μM. Densitometric analysis revealed that A6 cells treated with these two different BITC concentrations at 30 °C had HO-1 levels that were 56 and 28% less, respectively, than found with treatments at 22 °C. While HSP70 was induced to low levels in cells treated with 5 μM BITC compared to control, larger accumulations were observed when cells were exposed to either 7.5 or 10 μM (at 22 or 30 °C). Very low levels of HSP30 were observed in cells treated with all three concentrations of BITC at 22 °C. However, treatment of cells with 7.5 or 10 μM BITC at 30 °C produced an increase in HSP30 accumulation compared to the responses observed at 22 °C or with 30 °C alone. Densitometric analysis revealed that treatment of cells with 7.5 μM BITC at 30 °C resulted in a 40-fold increase in HSP30 compared to the sum of responses obtained with the same concentration at 22 °C or at 30 °C alone. Exposure of cells to DMSO alone did not induce stress protein accumulation (data not shown). Throughout these experiments, the levels of actin remained relatively constant.

The next set of experiments examined the effect of different concentrations of PEITC or SFN on HO-1, HSP70 and HSP30 accumulation at 22 and 30 °C for 12 h. As shown in Figure 8, higher levels of HO-1 and HSP70 accumulation were observed in cells treated with 5 μM PEITC at 22 °C compared to cells treated with 7.5 μM. Exposure of cells to 5 μM PEITC at 30 °C resulted in a 59 and 58% decrease in HO-1 and HSP70 accumulation, respectively, compared to

Figure 7. Relative levels of HO-1, HSP70 and HSP30 in cells subjected to BITC treatment at 22 or 30 °C. A6 cells were maintained at 22 °C (C) or exposed to either 5, 7.5 or 10 μM BITC at 22 or 30 °C for 12 h. Additionally cells were exposed to a temperature of 30 °C for 12 h or treated with 30 μM MG132 (MG) for 12 h at 22 °C as a positive control since MG132 was shown to induce the accumulation of all 3 stress-inducible proteins. A) Total protein was isolated and 30 μg (or 15 μg of protein from MG132-treated cells, 12 μg for actin) was subjected to immunoblot analysis using an anti-HO-1, anti-HSP70, anti-HSP30 or anti-actin antibody as described in Materials and methods, with the representative immunoblot shown. B) ImageJ software was used to perform densitometric analysis of signals obtained for HO-1, HSP70 and HSP30 as described in Materials and methods. The data were expressed as a percentage of the maximum band obtained for each protein, while standard errors were indicated with vertical bars. A one-way ANOVA with a Tukey's Multiple Comparisons post-test was used to determine significance. Significant differences between the control cells and treated cells are indicated with an asterisk ($p < 0.05$). These data are representative of 4 separate experiments.

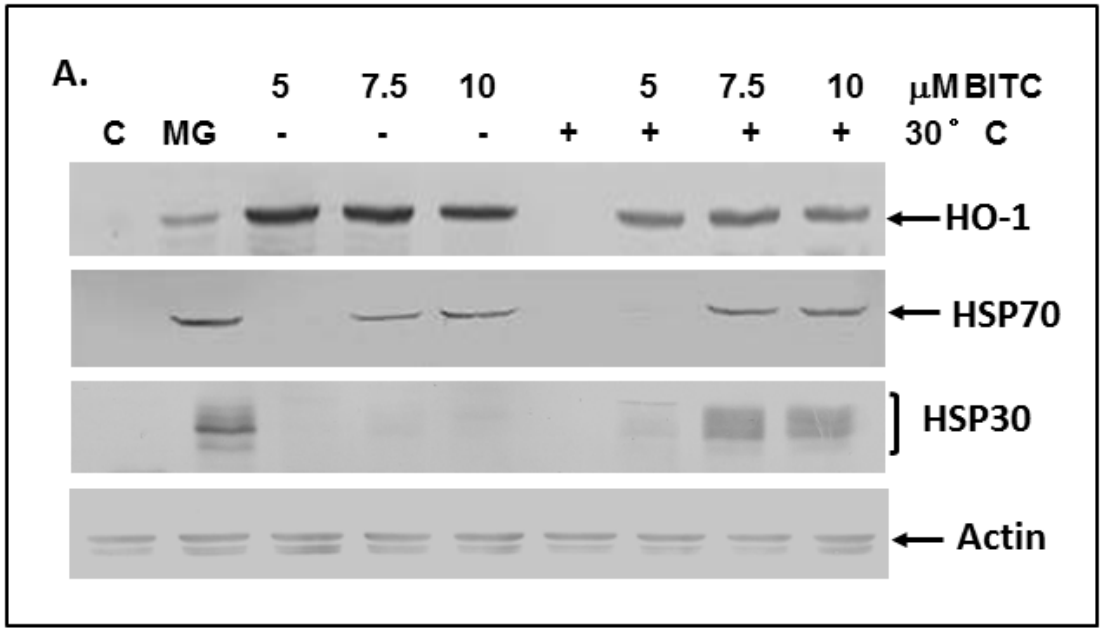
A.
5
7.5
10
5
7.5
10
μM BITC
C
MG
-
-
-
+
+
+
+
30 ° C
HO-1
HSP70
HSP30
Actin

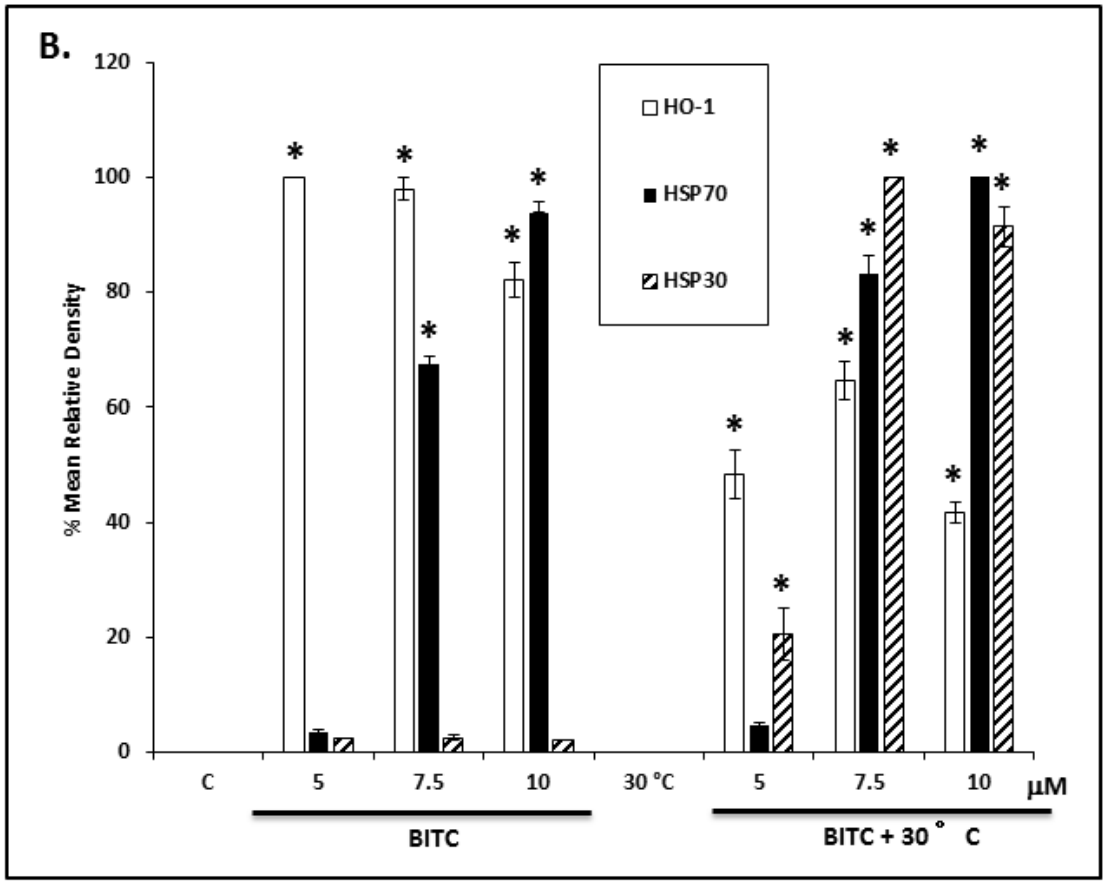
B.
120
100
80
60
40
20
0
% Mean Relative Density
HO-1
HSP70
HSP30
C
5
7.5
10
30 °C
5
7.5
10
μM
BITC
BITC + 30 ° C

Figure 8. Representative immunoblot showing the effect of PEITC on HO-1, HSP70 and HSP30 accumulation at 22 or 30 °C. Cells were maintained at 22 °C (C), exposed to a temperature of 30 °C for 12 h, or treated with 30 μM MG132 (MG) for 12 h at 22 °C. Some flasks were incubated with 5 or 7.5 μM PEITC at 22 or 30 °C for 12 h. A) Following treatments, total protein was isolated and subjected to immunoblot analysis using an anti-HO-1, anti-HSP70, anti-HSP30 or anti-actin antibody. B) Densitometric analysis of the band densities obtained for HO-1 and HSP70 utilized ImageJ software. The data were expressed as a percentage of the maximum band obtained for either HO-1 or HSP70 (5 μM PEITC at 22 °C for both), while the standard errors were represented by vertical bars. Densitometry was not carried out with HSP30 immunoblots since the relative levels induced by PEITC were very low or undetectable. Statistical analysis was performed and the significant differences were indicated with an asterisk ($p < 0.05$). These data are representative of 3 separate experiments.

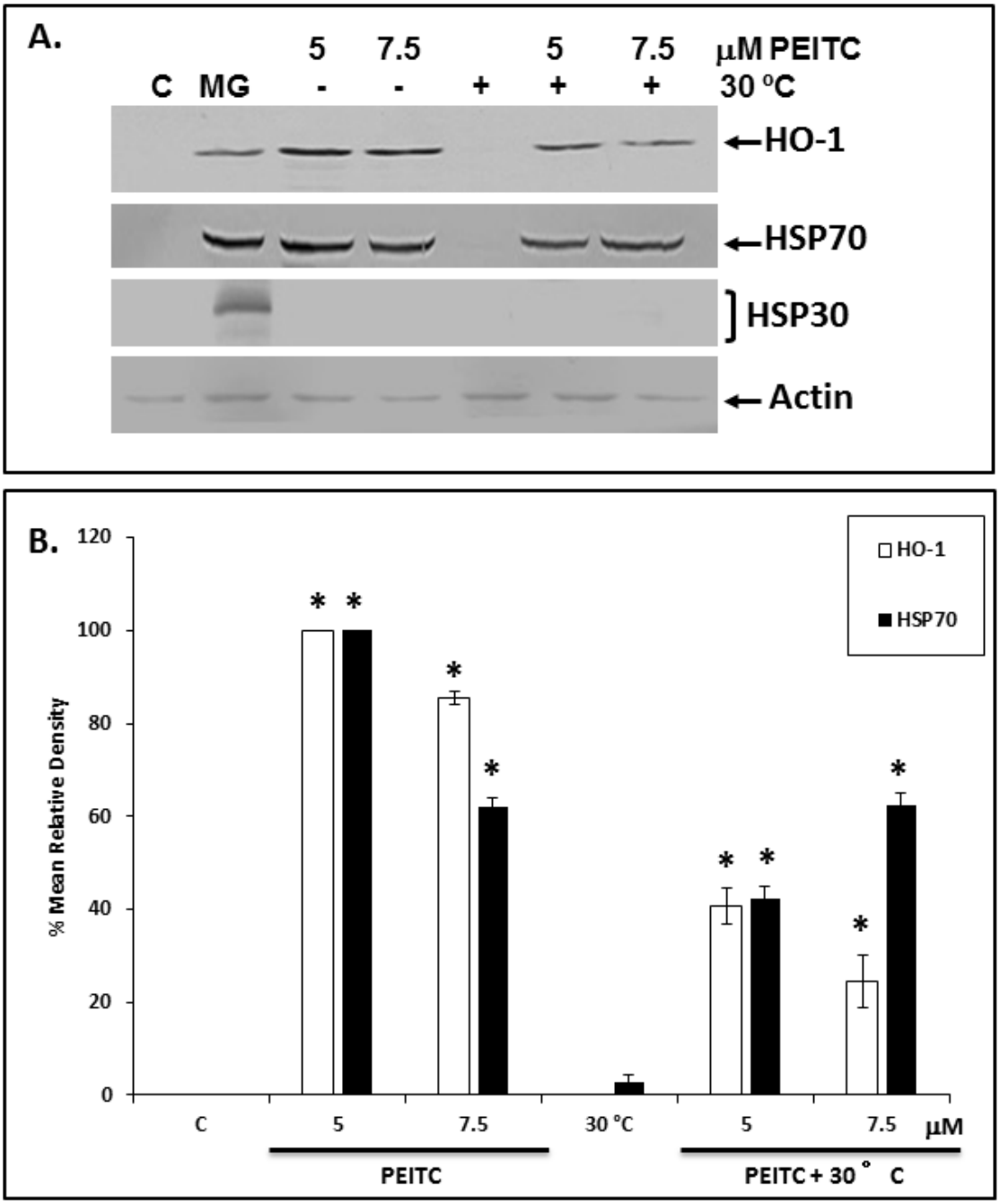
A.
C
MG
5
-
7.5
-
+
5
+
7.5
+
μM PEITC
30 °C
HO-1
HSP70
HSP30
Actin
B.
HO-1
HSP70
% Mean Relative Density
120
100
80
60
40
20
0
C
5
7.5
30 °C
5
7.5
μM
PEITC
PEITC + 30 ° C

values obtained at 22 °C. A decrease in HO-1 levels but not HSP70 was evident when cells were treated with 7.5 μM PEITC at 30 °C compared to 22 °C. HSP30 accumulation was not detected after PEITC treatment at either temperature. Additionally, high levels of HO-1 were observed when cells were treated with 10 or 20 μM SFN at 22 °C for 12 h compared to control with lower levels when SFN treatment was carried out at 30 °C (Fig. 9). HSP70 levels were detected in cells treated with 10 μM SFN at 22 °C with higher amounts at 20 μM. SFN exposure at 30 °C resulted in higher levels of HSP70. For example, at 30 °C, 20 μM SFN treatment was enhanced by 47% compared cells treated with the same concentration at 22 °C. HSP30 was not detected in cells treated with SFN at either 22 or 30 °C. The levels of actin remained relatively constant throughout these experiments.

3.1.3. Time course studies investigating levels of HO-1, HSP70 and HSP30 accumulation in BITC-treated cells.

In time course studies, the exposure of cells to 7.5 μM BITC at 22 °C resulted in relatively low levels of HO-1 and HSP70 accumulation at 4 and 6 h with higher levels observed at 12, 16 and 24 h (Fig. 10A). Densitometric analysis revealed a 68% increase in HO-1 at 12 h compared to 4 h (Fig. 10B). HSP70 levels increased by 63% and 80% at the 12 and 16 h time points, respectively compared to 4 h. HSP30 was not included in this analysis since the relative levels of protein were too low for accurate densitometric measurements. The next series of time course experiments explored the effect of BITC on stress protein accumulation in cells incubated at 30 °C from 4 to 24 h. As shown in Figure 11, HO-1 accumulation was detected at 4 h, with a 29% increase at 6 h and a 36% increase at 12 h. A subsequent decline in HO-1 protein levels was observed at the 16 and 24 h time points. HSP70 and HSP30 were both detectable at 4 h, with the largest increase observed at 16 h followed by a decline at 24 h. The levels of actin remained

Figure 9. Effect of SFN on HO-1, HSP70 and HSP30 accumulation at 22 or 30 °C. Cells were maintained at 22 °C (C) or incubated with 10 or 20 μM SFN at 22 or 30 °C for 12 h. Also, some cells were exposed to a temperature of 30 °C for 12 h or treated with 30 μM MG132 (MG) at 22 °C. In panel A, a representative immunoblot is shown. Following treatments, total protein was isolated and subjected to immunoblot analysis using an anti-HO-1, anti-HSP70, anti-HSP30 or anti-actin antibody. B) Densitometric analysis of the bands obtained for HO-1 and HSP70 utilized ImageJ software. The data was expressed as a percentage of the maximum band obtained for either HO-1 (10 μM SFN at 22 °C) or HSP70 (20 μM SFN at 30 °C), with vertical bars denoting the standard errors. Densitometry was not carried out with HSP30 immunoblots since the relative levels induced by SFN were very low or undetectable. Statistical analysis was performed and the significant differences were indicated with an asterisk ($p < 0.05$). These data are representative of 3 separate experiments.

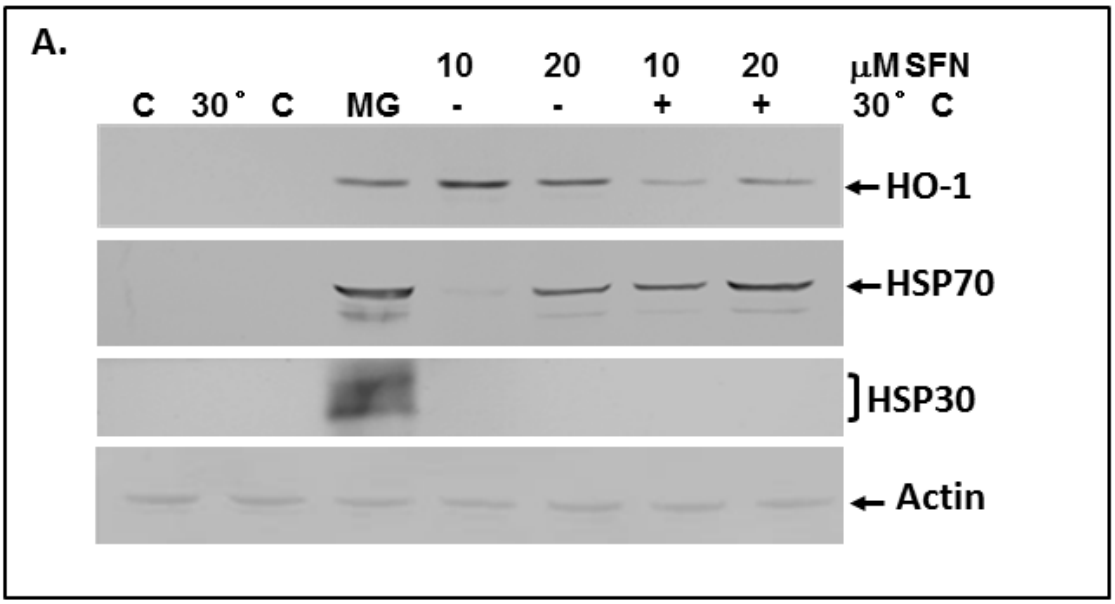
A.
C
30˚ C
C
MG
10
-
20
-
10
+
20
+
μM SFN
30˚ C
HO-1
HSP70
HSP30
Actin

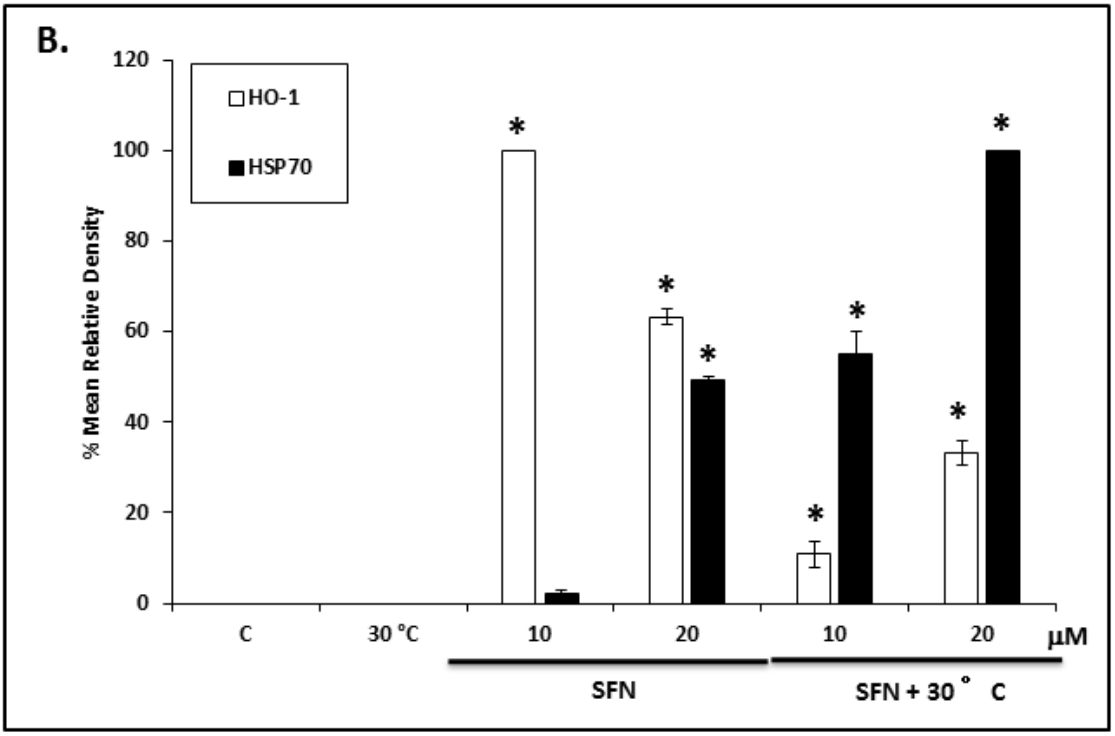
B.
HO-1
HSP70
% Mean Relative Density
120
100
80
60
40
20
0
C
30 °C
10
20
10
20
μM
SFN
SFN + 30 ˚ C

Figure 10. Time course of HO-1, HSP70 and HSP30 accumulation in A6 cells treated with BITC at 22 °C. A6 cells were maintained at 22 °C (C), treated with 30 μM MG132 (MG) for 12 h or incubated with 7.5 μM BITC from 4 to 24 h at 22 °C. A) Total protein was isolated and subjected to immunoblot analysis using an anti-HO-1, anti-HSP70, anti-HSP30 or anti-actin antibody, with the representative immunoblot shown. B) ImageJ software was used to perform densitometric analysis of signal intensity for HO-1 and HSP70 protein bands. The data were expressed as a percentage of the maximum band obtained for either stress-inducible protein (24 h for HO-1 and 16 h for HSP70), while the standard errors were represented by vertical bars. Statistical analysis was performed and the significant differences are indicated with an asterisk ($p < 0.05$) or a triangle ($p < 0.1$). These data are representative of 4 separate experiments.

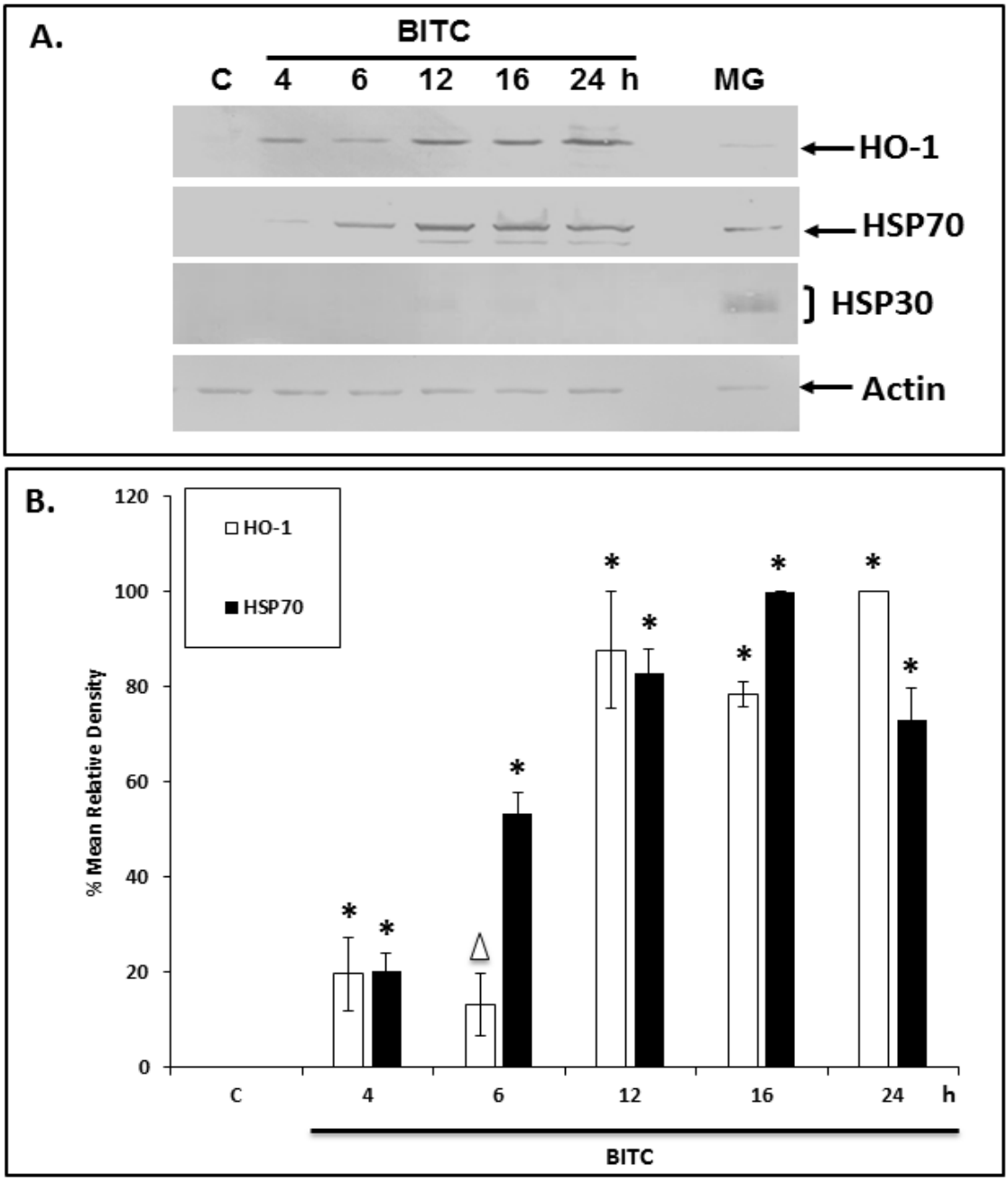
A.
BITC
C
4
6
12
16
24 h
MG
HO-1
HSP70
HSP30
Actin
B.
HO-1
HSP70
% Mean Relative Density
120
100
80
60
40
20
0
C
4
6
12
16
24
h
BITC

Figure 11. Time course of BITC-induced HO-1, HSP70 and HSP30 accumulation at 30 °C. Cells were maintained at 22 °C (C), incubated at 30 °C for 12 h, or treated with 7.5 μM BITC at 30 °C for 4 to 24 h. In panel A, a representative immunoblot is shown. After treatment, total protein was isolated and subjected to immunoblot analysis using an anti-HO-1, anti-HSP70, anti-HSP30 or anti-actin antibody. B) Densitometric analysis of the band intensity for HO-1, HSP70 and HSP30 utilized ImageJ software. The results were expressed as a percentage of the maximum band intensity acquired for each protein in each trial. Vertical error bars denote standard error. Statistical analysis was performed and the significant differences are indicated with an asterisk ($p < 0.05$). These data are representative of 4 separate experiments.

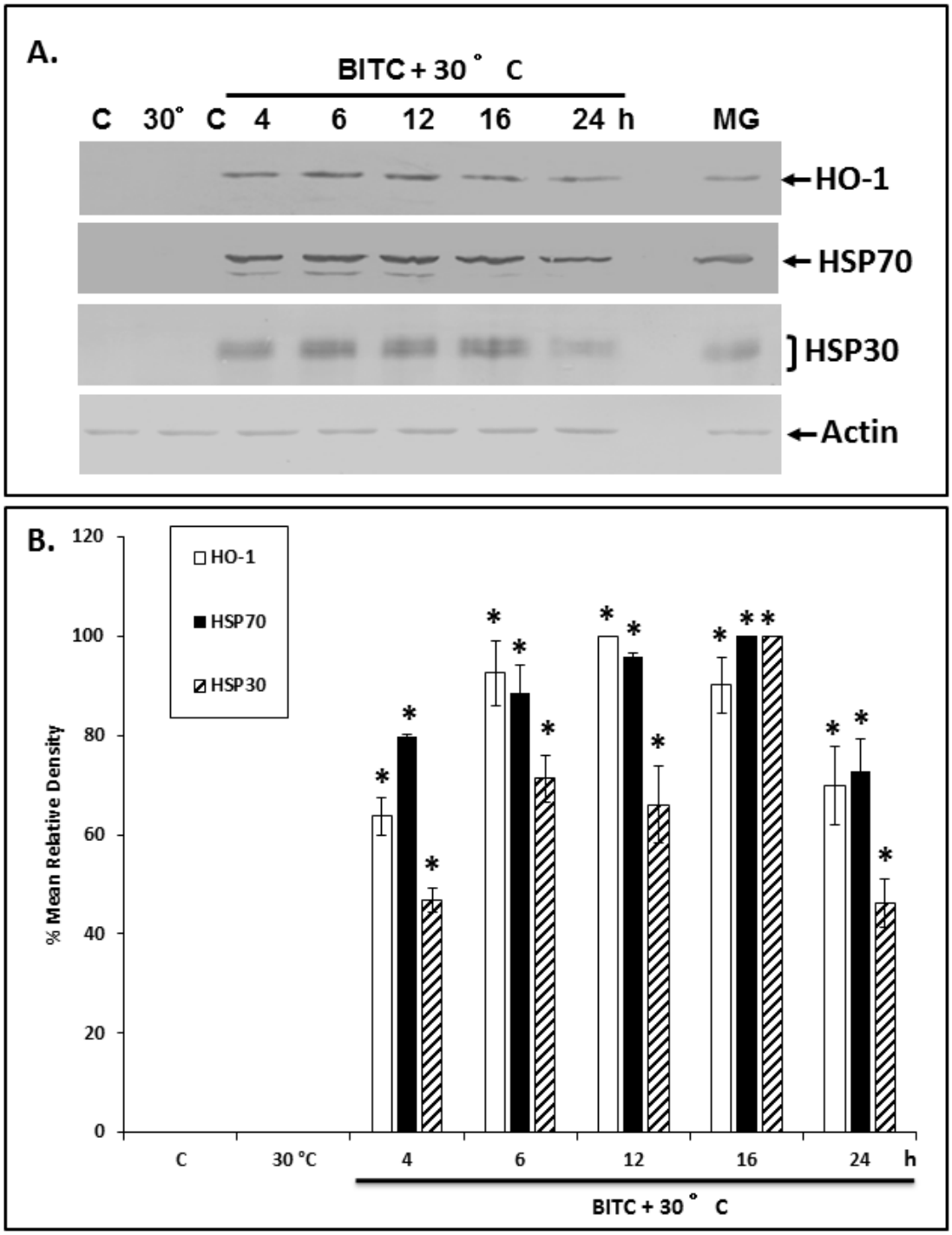
A.
BITC + 30 ° C
C 30° C 4 6 12 16 24 h MG
HO-1
HSP70
HSP30
Actin
B.
HO-1
HSP70
HSP30
% Mean Relative Density
120
100
80
60
40
20
0
C
30 °C
4
6
12
16
24
h
BITC + 30 ° C

relatively constant throughout these experiments.

3.1.4. Immunoblot analysis of HSPB6 accumulation in ITC-treated cells.

The effect of ITCs on HSPB6 levels in A6 cells employed a rabbit polyclonal antibody made against a proprietary human HSPB6 14 amino acid peptide sequence located within A101 to S150 (additional information is shown in Fig. 30). According to the manufacturer, 11 out of 14 amino acids of the human HSPB6 peptide immunogen were identical with the comparable region in *X. laevis* HSPB6. In preliminary experiments, I confirmed the ability of the anti-human HSPB6 antibody in detecting two dilutions of *X. laevis* recombinant HSPB6, produced by a former undergraduate student in our laboratory (D. Chan; data not shown). The antibody was then used to examine the accumulation of HSPB6 in cells treated with BITC, PEITC and SFN at 22 and 30 °C. As shown in Figure 12, none of the treatments resulted in significant changes in HSPB6 accumulation relative to control. The levels of actin remained relatively constant in this experiment.

3.1.5. Effect of actinomycin D, cycloheximide and KNK437 on HO-1 and HSP accumulation in ITC-treated cells.

In the present study, pretreatment of A6 cells with actinomycin D (ActD), a transcriptional inhibitor, inhibited BITC, PEITC and SFN-induced HO-1 and HSP70 accumulation at both 22 and 30 °C (Fig. 13). Furthermore, ActD treatment prior to the introduction of 7.5 μM BITC at 30 °C resulted in an inhibition of HSP30 accumulation. As already determined, PEITC and SFN did not induce the accumulation of HSP30 at 22 or 30 °C. In the next series of experiments, pretreatment of cells with cycloheximide (CHX), an inhibitor of protein synthesis, also prevented BITC-, PEITC- and SFN-induced HO-1 and HSP70 accumulation, as well as HSP30 accumulation in cells treated with BITC at 30 °C (Fig. 14).

Figure 12. Representative immunoblot showing the effect of BITC, PEITC and SFN on HSPB6 accumulation. Cells were maintained at 22 °C (C), incubated at 30 °C, or treated individually with either 7.5 μM BITC, 5 μM PEITC or 20 μM SFN at 22 or 30 °C for 12 h. A) Following treatments, total protein was isolated and 40 μg was subjected to immunoblot analysis using an anti-HSPB6 or anti-actin antibody as described in Materials and methods. ImageJ software was used to perform densitometric analysis of signal intensity for HSPB6 (panel B) as described in Materials and methods. The data for HSPB6 are expressed as a ratio to control levels and vertical error bars denote standard error. Statistical analysis was performed as described in Materials and methods. These data are representative of 3 separate experiments.

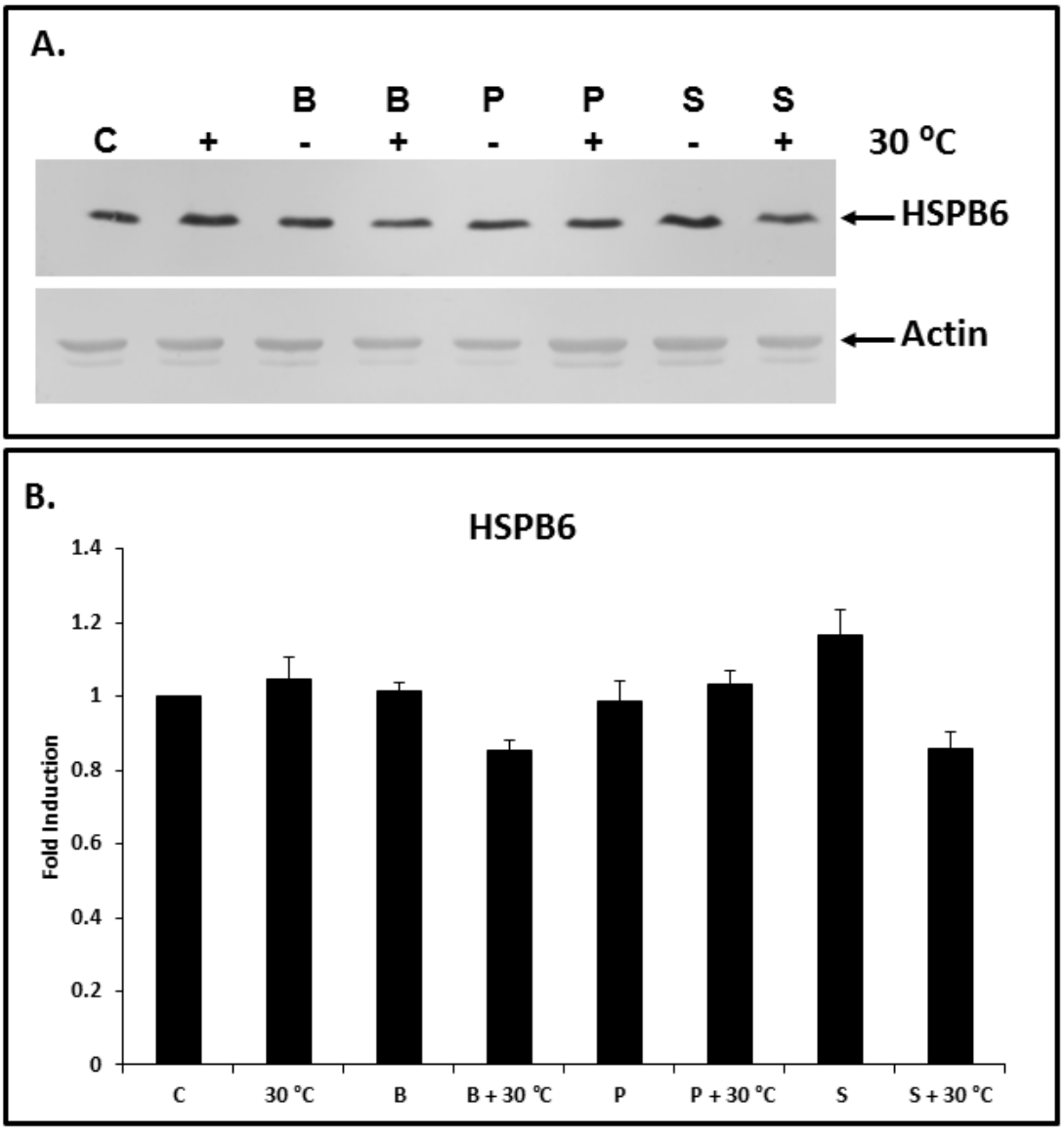
A.
C
+
B
-
B
+
P
-
P
+
S
-
S
+
30 °C
HSPB6
Actin
B.
HSPB6
Fold Induction
1.4
1.2
1
0.8
0.6
0.4
0.2
0
C
30 °C
B
B + 30 °C
P
P + 30 °C
S
S + 30 °C

Figure 13. Effect of actinomycin D on ITC-treated cells. A) Cells were maintained at 22 °C (C) or treated with 7.5, 5, or 20 μM of BITC, PEITC or SFN, respectively, for 12 h at 22 °C, with or without a 30 min pretreatment of 2 μg/mL actinomycin D (ActD) at 22 °C. B) Cells were maintained at 22 °C (C) or incubated at 30 °C for 12 h. Some flasks were treated with 7.5, 5, or 20 μM BITC, PEITC or SFN, respectively, for 12 h at 30 °C, with and without a 30 min pretreatment of 2 μg/mL ActD at 22 °C. Following treatments, total protein was isolated and subjected to immunoblot analysis using an anti-HO-1, anti-HSP70, anti-HSP30 or anti-actin antibody. These results are representative of 2 separate experiments.

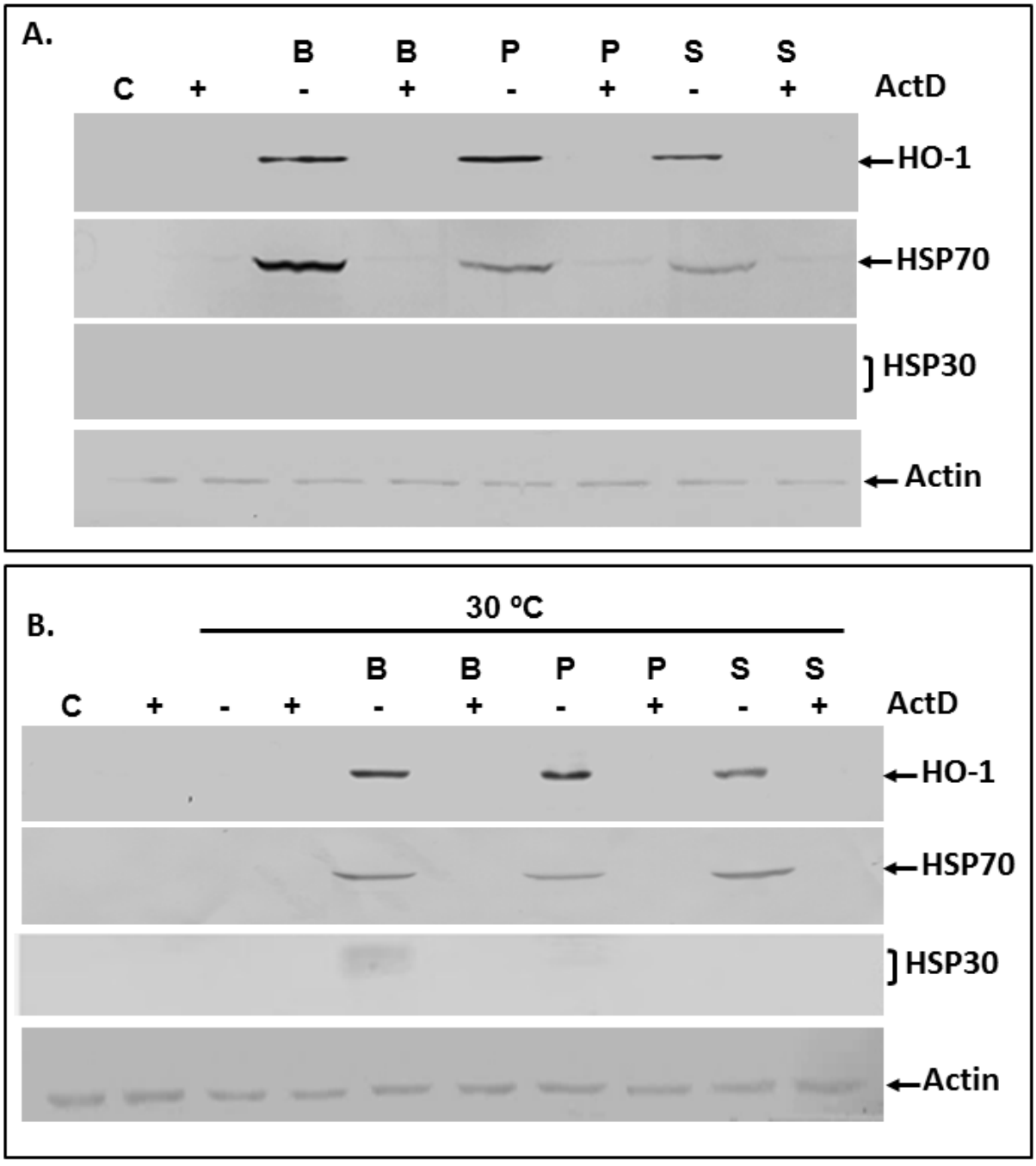
A.
C
+
B
-
B
+
P
-
P
+
S
-
S
+
ActD
HO-1
HSP70
HSP30
Actin
B.
30 ºC
C
+
-
+
B
-
B
+
P
-
P
+
S
-
S
+
ActD
HO-1
HSP70
HSP30
Actin

Figure 14. Effect of cycloheximide on ITC-treated cells. A) Cells were maintained at 22 °C (C) or treated with 7.5, 5 or 20 μM of BITC, PEITC or SFN, respectively, for 12 h at 22 °C with or without a 6 h pretreatment with 100 μM cycloheximide (CHX) at 22 °C. B) Cells were maintained at 22 °C (C) or incubated at 30 °C for 12 h. Other cells were treated with 7.5, 5 or 20 μM of BITC, PEITC or SFN for 12 h at 30 °C, with or without a 6 h pretreatment with 100 μM CHX at 22 °C. Following treatments, total protein was isolated and subjected to immunoblot analysis using an anti-HO-1, anti-HSP70, anti-HSP30 or anti-actin antibody. These results are representative of 2 separate experiments.

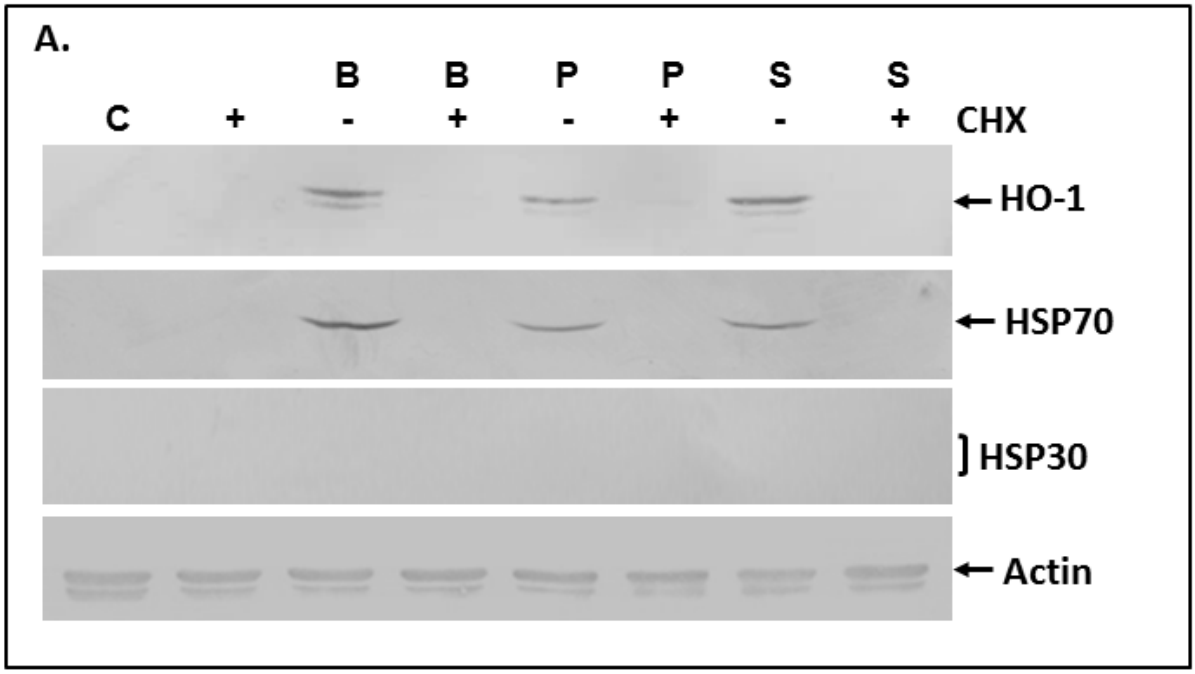
A.
B B P P S S
C + - + - + - + CHX
HO-1
HSP70
HSP30
Actin

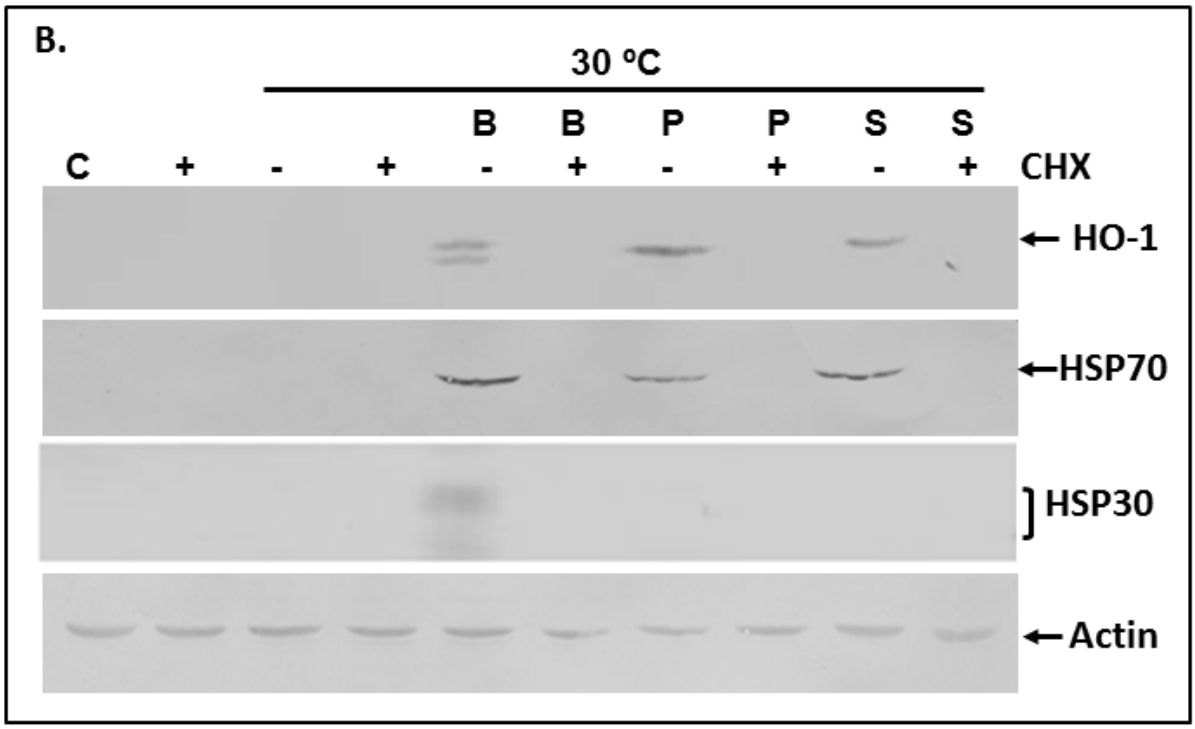
B.
30 °C
B B P P S S
C + - + - + - + - + CHX
HO-1
HSP70
HSP30
Actin

Finally, the effect of the HSP transcriptional inhibitor, KNK437, on ITC-induced HO-1, HSP70 and HSP30 accumulation was examined (Fig. 15). Treatment of cells with 100 μM KNK437, an HSF1 inhibitor, prior to their exposure to BITC, PEITC or SFN at either 22 or 30 °C inhibited both HO-1 and HSP70 accumulation. The induction of HSP30 accumulation with BITC at 30 °C was also inhibited by KNK437. The levels of actin remained relatively constant throughout these experiments.

3.1.6. Cytoskeletal structure and localization of HO-1 and HSP30 in MG132- and ITC-treated cells.

Immunocytochemistry and laser scanning microscopy (LSCM) was used to compare the effect of MG132 (MG) and ITCs on HO-1 and HSP30 localization in A6 cells. HSP70 localization was not examined since the affinity-purified polyclonal anti-HSP70 antibody, used successfully in immunoblot detection, was unable to detect HSP70 by immunocytochemistry (Gauley et al., 2008; Khamis and Heikkila, 2013). As shown in Figure 16, control and MG132-treated A6 cells at 22 °C displayed actin stress fibers transversing the entire length of cells in mostly axial bundles, with the appearance of a few radial bundles located at the periphery. Some cells treated with MG132 showed signs of membrane ruffling and disorganization of F-actin (yellow arrows). HO-1 and HSP30 were undetectable in control cells maintained at 22 °C. However, treatment of A6 cells with MG132 induced HO-1 and HSP30 accumulation in 90 and 60% of the cells, respectively, in a punctate pattern primarily located in the perinuclear region.

Treatment of A6 cells with BITC revealed the presence of ruffled edges in some cells and when this ITC treatment occurred at 30 °C, cellular cytoskeletal disorganization (yellow arrows) was observed with numerous cells undergoing F-actin bundle collapse around the nucleus (Fig. 17). Additionally, larger F-actin structures were also present in the periphery of cells. Following

Figure 15. Effect of KNK437 on ITC-treated cells. A) Cells were maintained at 22 °C (C) or treated with 7.5, 5, or 20 μM of BITC, PEITC or SFN, respectively, for 12 h at 22 °C, with or without a 6 h pretreatment with 100 μM KNK437 at 22 °C. B) Cells were maintained at 22 °C (C) or incubated at 30 °C for 12 h. Other flasks were treated with 7.5, 5, or 20 μM of BITC, PEITC or SFN, respectively, for 12 h at 30 °C with or without a 6 h pretreatment with 100 μM KNK437 at 22 °C. Following treatments, total protein was isolated and subjected to immunoblot analysis using an anti-HO-1, anti-HSP70, anti-HSP30 or anti-actin antibody. These results are representative of 2 separate experiments.

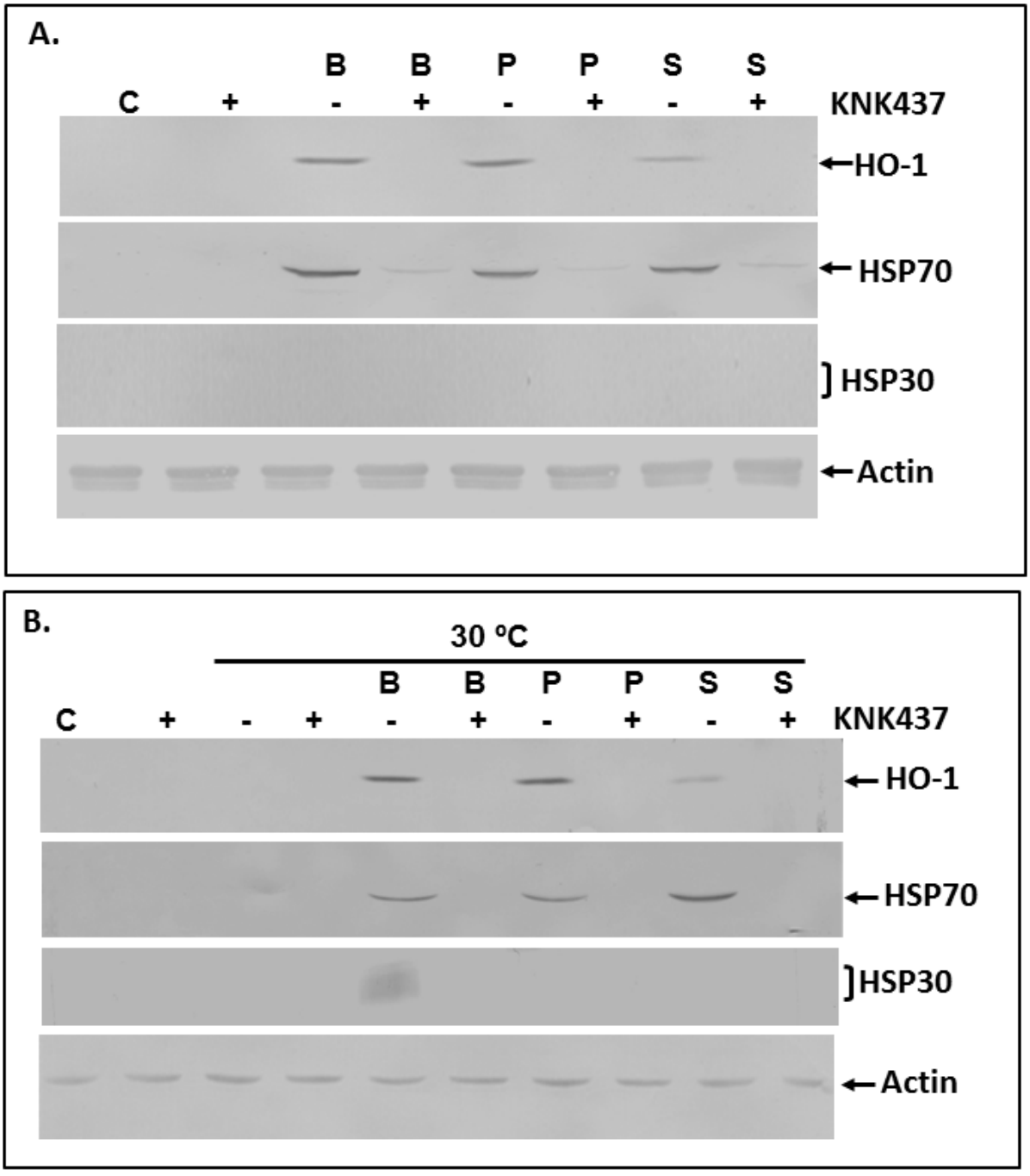
A.
B B P P S S
C + - + - + - + KNK437
HO-1
HSP70
HSP30
Actin
B.
30 °C
B B P P S S
C + - + - + - + - + KNK437
HO-1
HSP70
HSP30
Actin

Figure 16. Localization of HO-1 and HSP30 in MG132-treated A6 cells at 22 °C. A6 cells were cultured on base-washed glass coverslips and then maintained at 22 °C (C) or incubated with 30 μM MG132 (MG) for 12 h at 22 °C. HO-1 and HSP30 were detected with a rabbit anti-HO-1 or anti-HSP30 antibody, respectively, and a secondary antibody conjugated to Alexa-488 (green). Actin and nuclei staining utilized phalloidin conjugated to TRITC (red) or DAPI (blue), respectively. The columns, from left to right, show the fluorescence detection channels for actin, HO-1 or HSP30, and merged images, which also includes DAPI staining. Yellow arrows indicate membrane ruffling or disorganization of the F-actin cytoskeleton. The laser scanning confocal microscopy (LSCM) procedure was followed as outlined in the Materials and methods. The 20 μm scale bars are indicated at the bottom right corner of each panel. These results are representative of 3 different experiments.

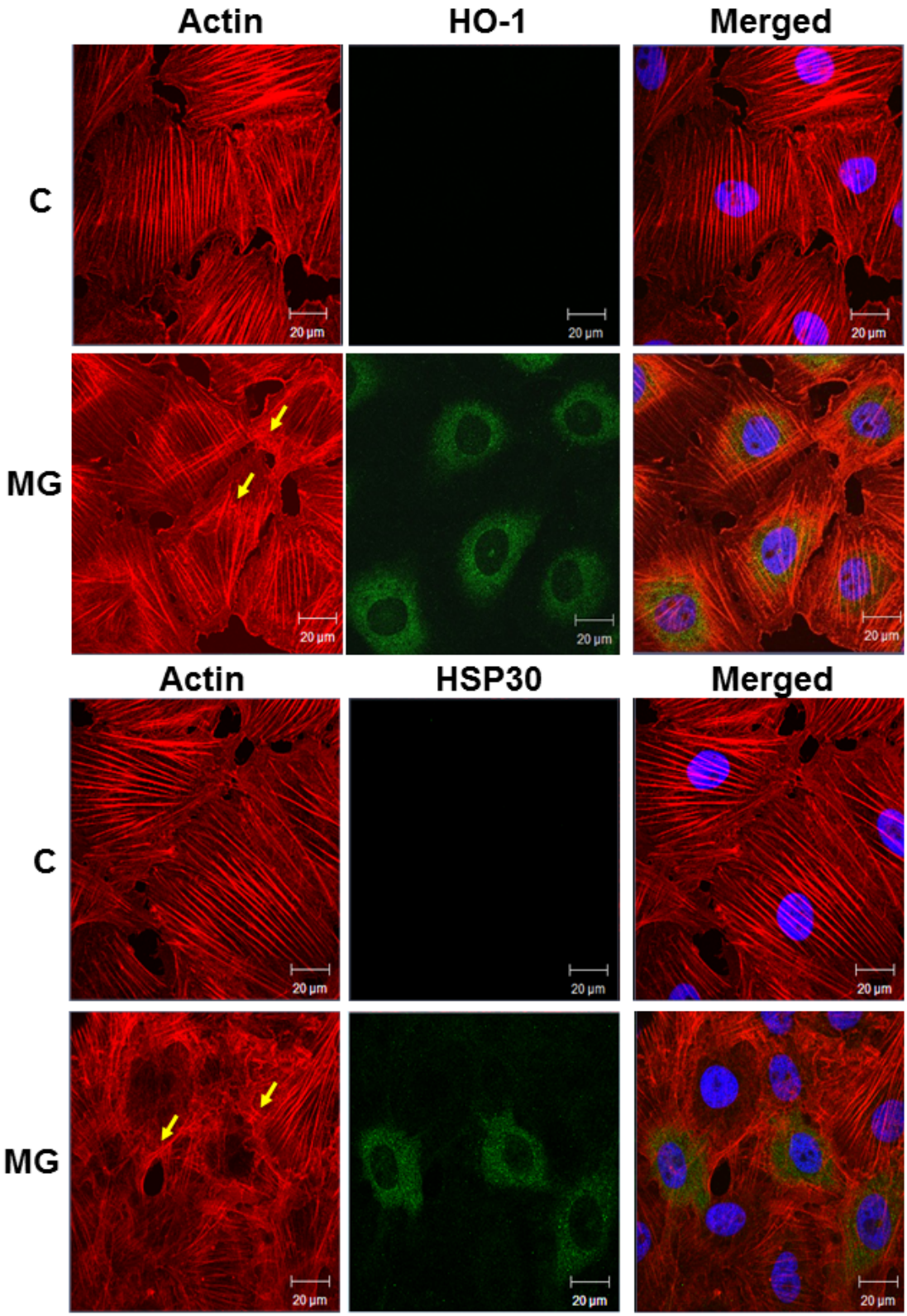
Actin
HO-1
Merged
C
MG
20 μm
Actin
HSP30
Merged
C
MG
20 μm

Figure 17. Effect of ITCs on the localization of HO-1 in A6 cells. In panels A and B, cells were cultured on glass coverslips and then maintained at 22 °C (C) or incubated with 30 μM MG132 (MG) for 12 h. Other cells were treated with 7.5, 5 or 20 μM of BITC, PEITC or SFN, respectively, for 12 h at 22 or 30 °C. HO-1 was detected with a rabbit anti-HO-1 antibody, and a secondary antibody conjugated to Alexa-488 (green). Actin and nuclei staining utilized phalloidin conjugated to TRITC (red) or DAPI (blue), respectively. The columns, from left to right, show the fluorescence detection channels for actin, HO-1, and merged images, which also includes DAPI staining. Yellow arrows indicate membrane ruffling or disorganization of the F-actin cytoskeleton. White arrows indicate larger HO-1 staining structures. The 20 μm scale bars are indicated at the bottom right corner of each panel. These results are representative of 3 different experiments.

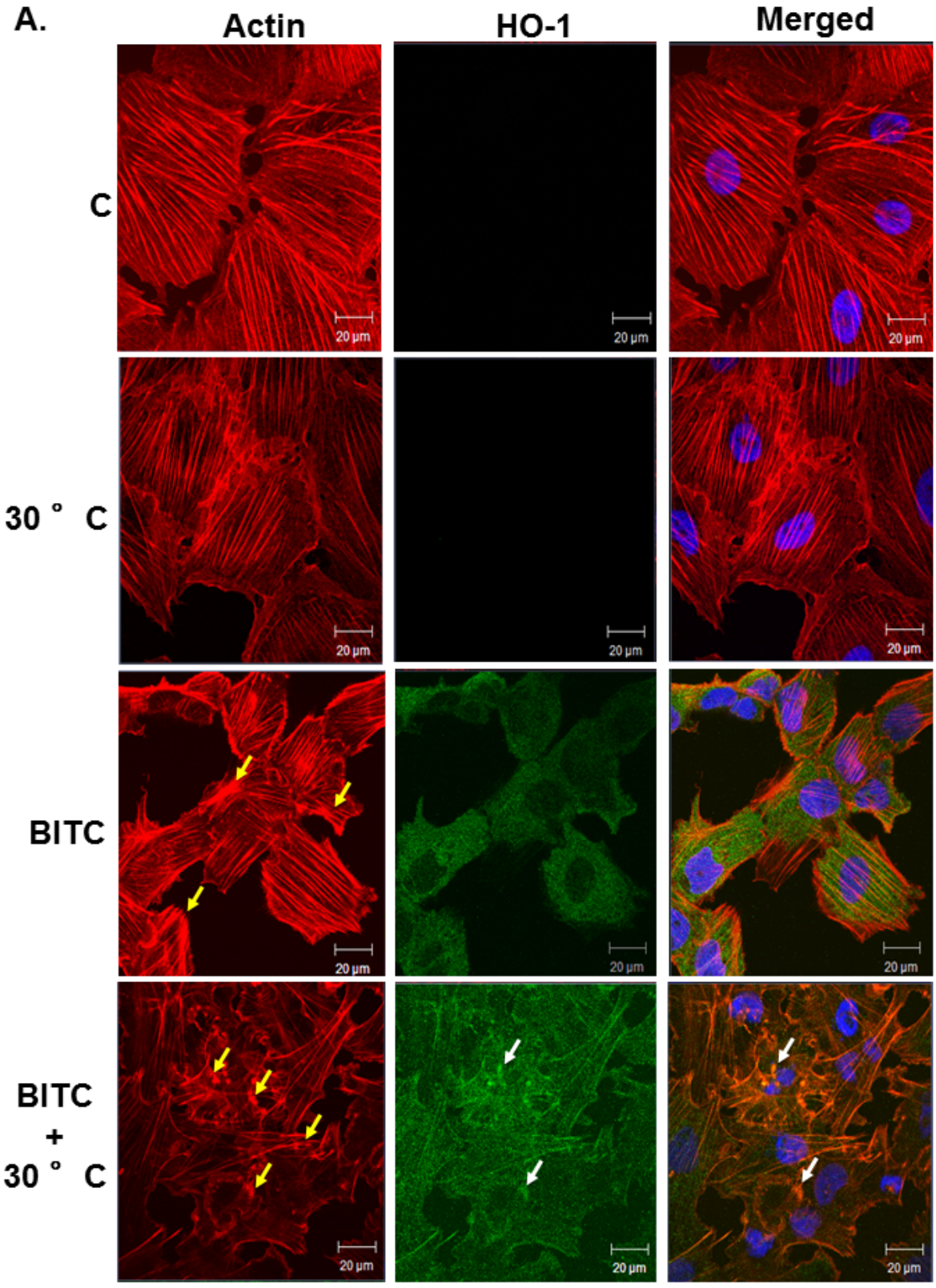
A.
Actin
HO-1
Merged
C
30 ° C
BITC
BITC
+
30 ° C
20 μm

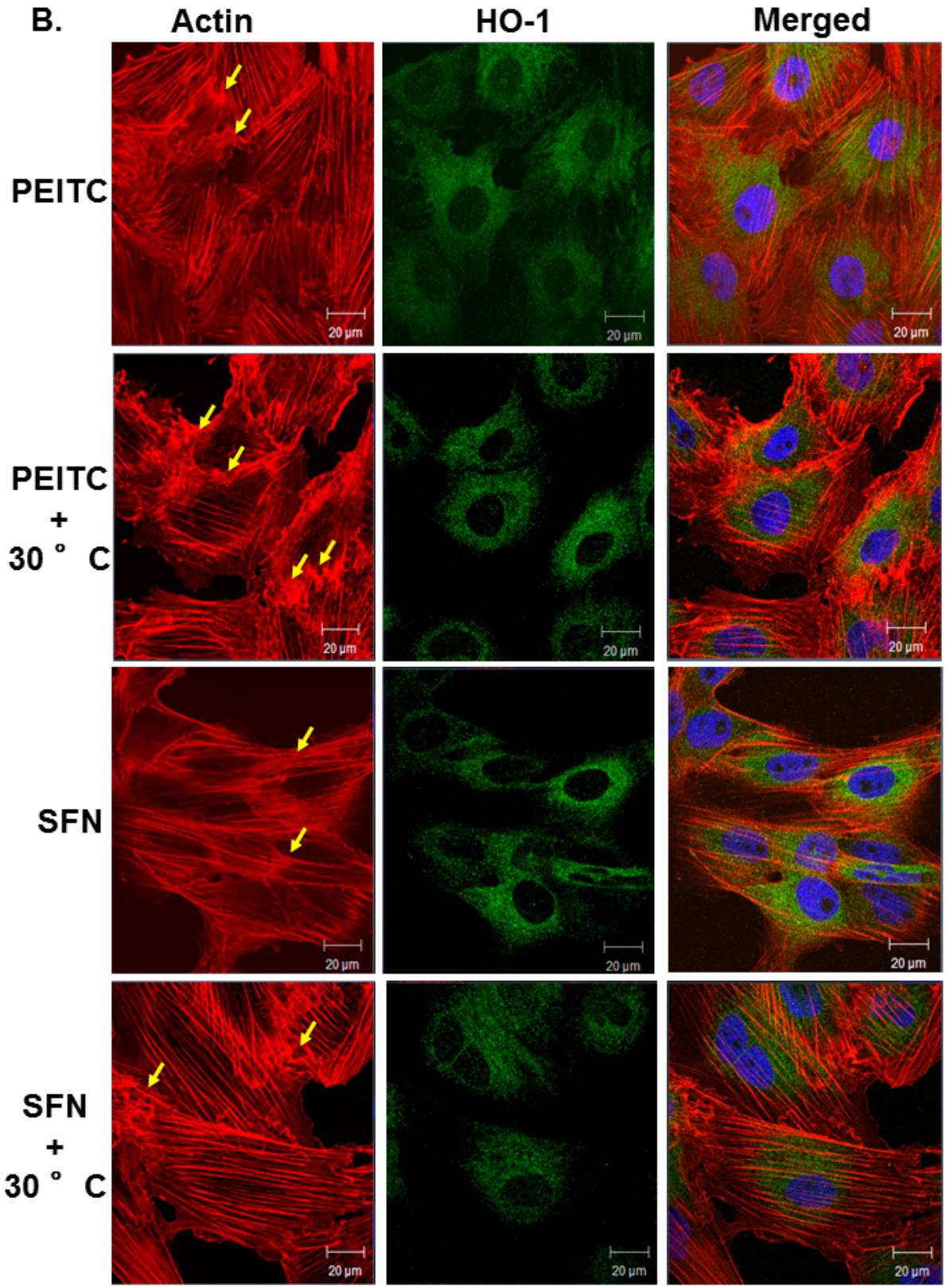
B.
Actin
HO-1
Merged
PEITC
PEITC + 30 ° C
SFN
SFN + 30 ° C
20 μm

PEITC treatment at 22 °C, slight F-actin ruffling was localized to the periphery of most cells. This effect on F-actin disorganization was enhanced when A6 cells were incubated with PEITC at 30 °C. Finally, some A6 cells treated with SFN at 22 °C displayed cytoskeletal collapse around the nucleus, while this ITC treatment at 30 °C resulted in dysregulation of actin stress fibers in cell regions associated with cell-cell contact.

Immunocytochemistry revealed that treatmentof cells with 7.5 μM BITC at 22 °C induced the accumulation of HO-1 in 85% of cells in a diffuse pattern throughout the cytosol with some in the nucleus. Treatment of cells with 7.5 μM BITC at 30 °C resulted in 70% of cells displaying a diffuse pattern of HO-1 accumulation with some larger staining structures present at the cell periphery in 30% of cells (white arrows). Interestingly, the merger of the immunostained images for this treatment revealed a possible co-localization of the larger HO-1 staining structures with actin-stained structures (see white arrows). Following a 5 μM PEITC treatment at 22 °C, 80% of cells displayed HO-1 accumulation primarily in the cytoplasm in a punctate pattern. PEITC treatment at 30 °C resulted in 75% of cells inducing HO-1, which was localized to the cytoplasm. Finally, SFN-induced HO-1 accumulation at 22 °C was observed in 70% of cells, with HO-1 being distributed throughout the cytoplasm with enrichment in the perinuclear region in some cells, while SFN treatment at 30 °C resulted in 60% of cells displaying cytoplasmic and some nuclear HO-1 accumulation in a punctate pattern.

The next set of experiments examined the effect of ITCs on HSP30 localization. As shown in Figure 18, HSP30 was not detected in control cells or cells treated at 30 °C. Following BITC treatment at 22 °C, a low amount HSP30 accumulation was detectable. In contrast, at the elevated temperature of 30 °C, BITC-induced HSP30 was present in 65% of cells in a punctate

Figure 18. Effect of ITCs on the localization of HSP30 in A6 cells. In panels A and B, cells were cultured on glass coverslips and then maintained at 22 °C (C), incubated at 30 °C for 12 h or treated with 7.5, 5 or 20 μM of BITC, PEITC or SFN, respectively, for 12 h at 22 or 30 °C. HSP30 was detected with a rabbit anti-HSP30 antibody, and a secondary antibody conjugated to Alexa-488 (green). Actin and nuclei staining utilized phalloidin conjugated to TRITC (red) or DAPI (blue), respectively. The columns, from left to right, show the fluorescence detection channels for actin, HSP30, and merged images, which also includes DAPI staining. Yellow arrows indicate membrane ruffling or disorganization of the F-actin cytoskeleton while the red arrows highlight larger HSP30 staining structures. The 20 μm scale bars are indicated at the bottom right corner of each panel. These results are representative of 3 different experiments.

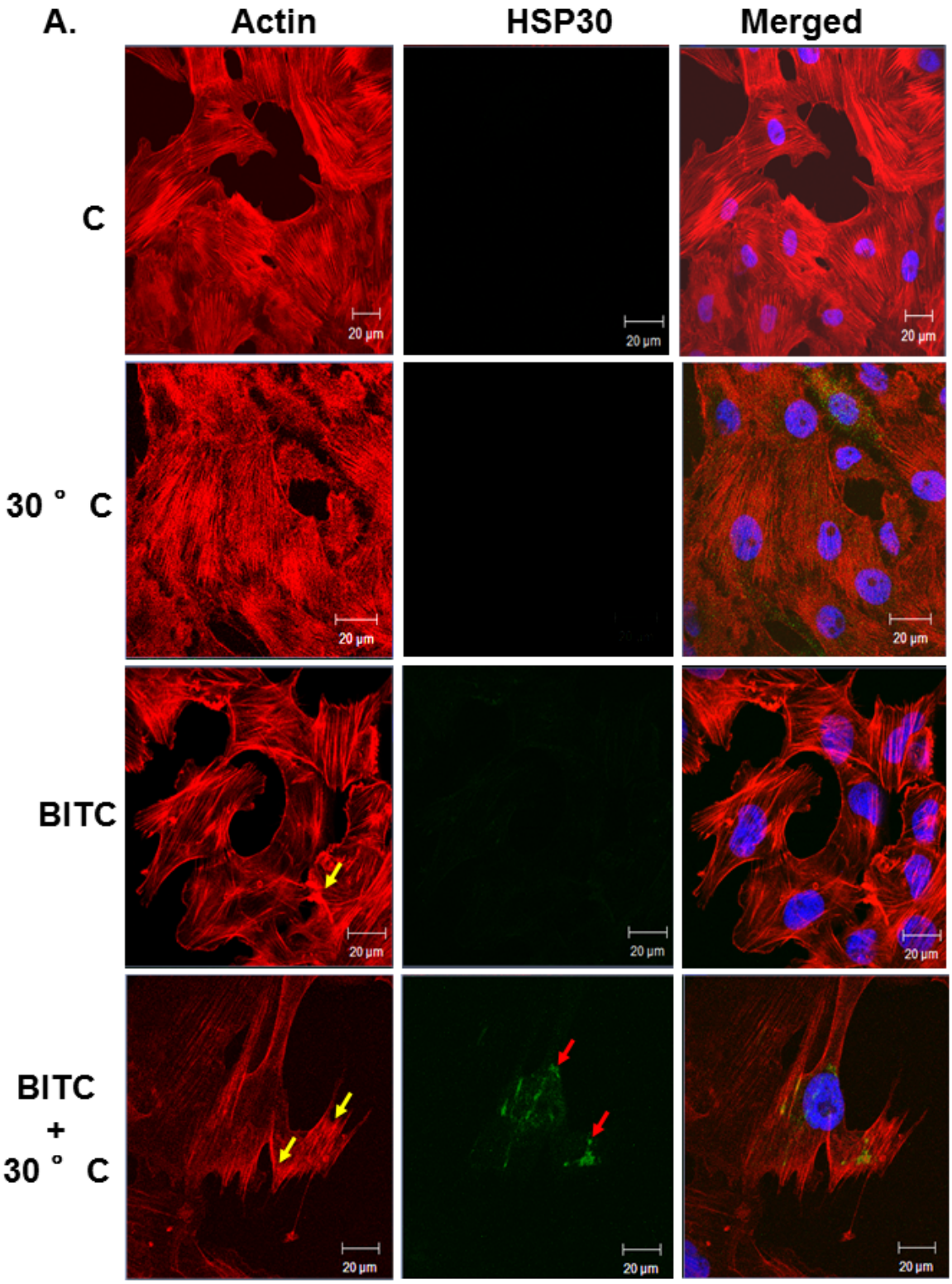
A.
Actin
HSP30
Merged
C
30 ° C
BITC
BITC
+
30 ° C
20 μm

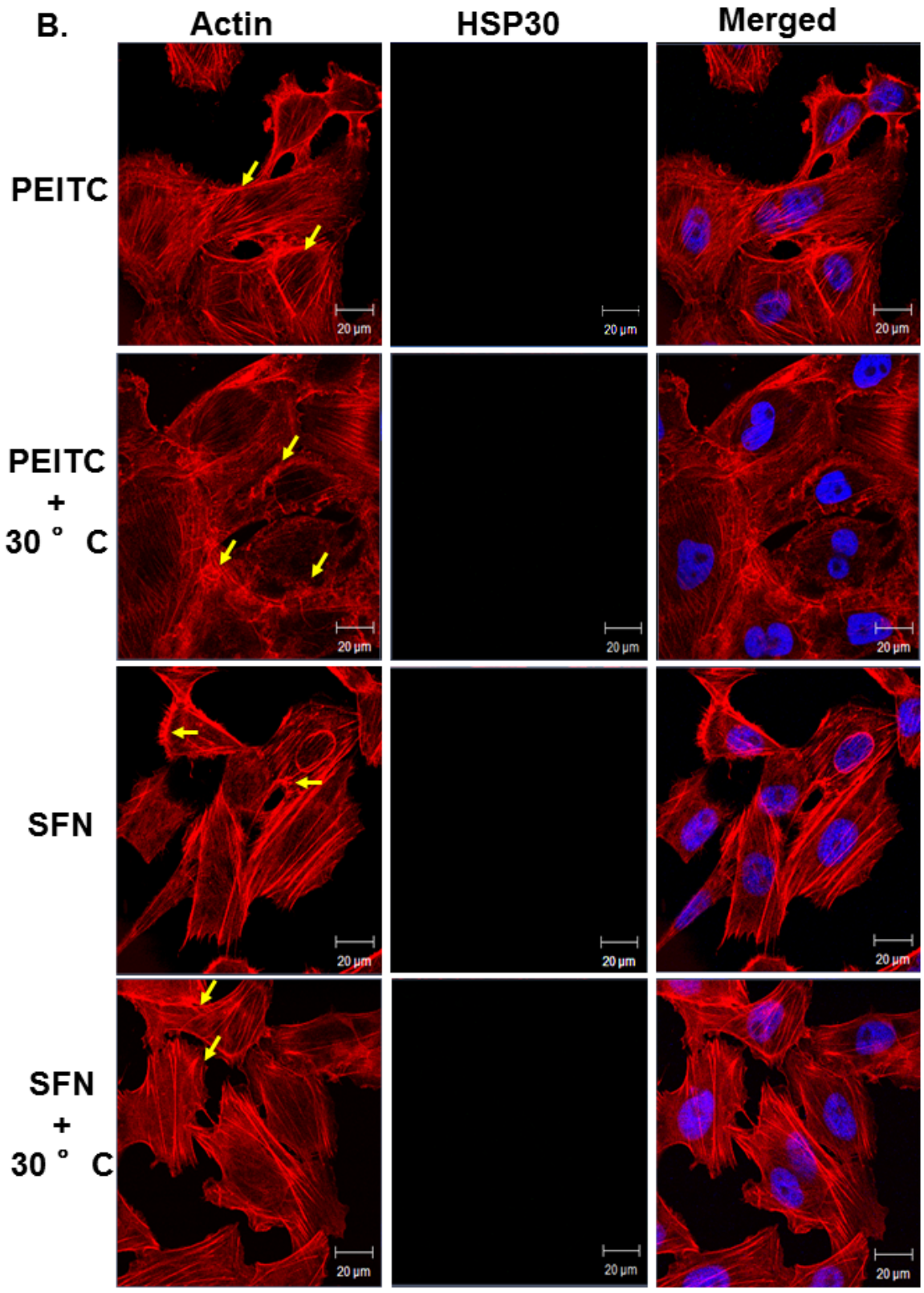
B.
Actin
HSP30
Merged
PEITC
PEITC + 30 ° C
SFN
SFN + 30 ° C
20 µm

pattern as well as additional slightly larger HSP30 structures (red arrows). HSP30 accumulation was not observed in A6 cells treated with PEITC or SFN at 22 or 30 °C.

3.2. Effect of BITC and PEITC on ubiquitinated, aggregated and α-tubulin protein accumulation and microtubule filament structure.

3.2.1. Relative levels of ubiquitinated protein accumulation in MG132-, BITC- and PEITC-treated cells.

In this section I examined the effect of BITC and PEITC on the accumulation of ubiquitinated protein in A6 cells. In previous studies, our laboratory and others found that MG132, a reversible proteasomal inhibitor, induced a strong accumulation of ubiquitinated protein (Malik et al., 2001; Lehman, 2009; Young and Heikkila, 2010; Brunt et al., 2012; Khamis and Heikkila, 2013). Thus, MG132-treated cells were employed as a positive control showing elevated levels of ubiquitinated protein as indicated in Figure 19. Exposure of cells to BITC for 12 h at 22 °C resulted in a 0.5-fold increase in ubiquitinated protein accumulation, while a 3-fold increase was observed in cells treated with PEITC at 22 °C relative to control (Fig. 20 and 21). Treatment with either ITC at 30 °C resulted in levels of ubiquitinated protein that relatively equivalent to control. Unlike BITC or PEITC, exposure of cells to SFN did not alter the levels of ubiquitinated protein compared to control (data not shown).

3.2.2. Comparison of MG132-, BITC- and PEITC-induced protein aggregation and HSP30 localization in A6 cells.

Given that BITC and PEITC bound and modified protein thiol groups in mammalian systems, it was possible that these ITCs could induce an accumulation of aggregated protein in A6 cells (Mi et al., 2008; 2009; 2010; Xiao et al., 2012). In the present study, a ProteoStat aggresome detection assay, which identifies aggregated protein and aggresome-like structures,

Figure 19. Examination of ubiquitinated protein levels in A6 cells treated with MG132. Cells were maintained at 22 °C (C) or treated with 30 μM MG132 (MG) for 12 h at 22 °C. After treatment, total protein was isolated and 60 μg was subjected to immunoblot analysis, utilizing an anti-ubiquitin antibody as described in Materials and methods. Detection of higher molecular mass ubiquitinated protein was close to reaching saturation near the top of the gel, and as a result the values obtained by densitometry in subsequent ubiquitinated protein experiments may be underestimated slightly. The positions of molecular mass standards in kDa are shown in the first lane as a marker. A section of a representative Ponceau S stained membrane is shown below. These results are representative of 2 separate experiments.

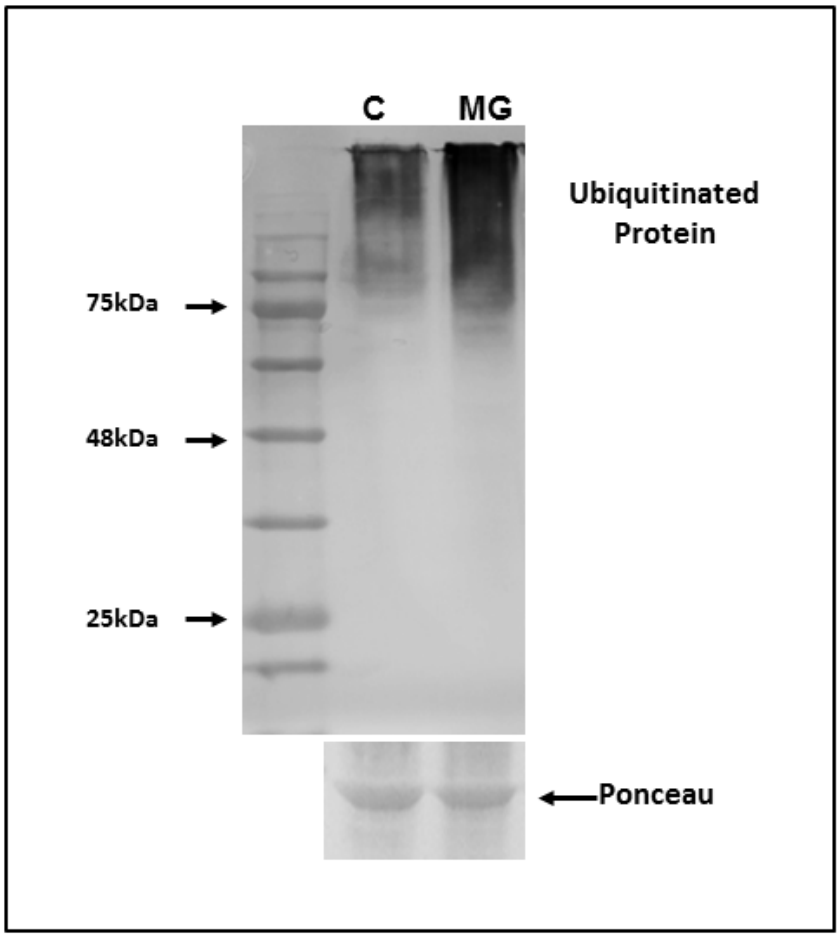
C
MG
Ubiquitinated
Protein
75kDa
48kDa
25kDa
Ponceau

Figure 20. Effect of BITC on ubiquitinated protein levels. Cells were maintained at 22 °C (C), incubated at 30 °C, or exposed to 7.5 μM BITC at 22 or 30 °C for 12 h. A) After treatments, total protein was isolated and subjected to immunoblot analysis, utilizing an anti-ubiquitin antibody, with the representative immunoblot shown. B) Densitometric analysis of the band intensity utilized ImageJ software, and the data is expressed as a ratio of ubiquitinated protein to control levels. The standard error is represented by vertical error bars. Statistical analysis was performed and the significant differences are indicated with an asterisk ($p < 0.05$) or a triangle ($p < 0.1$). These data are representative of 4 separate experiments.

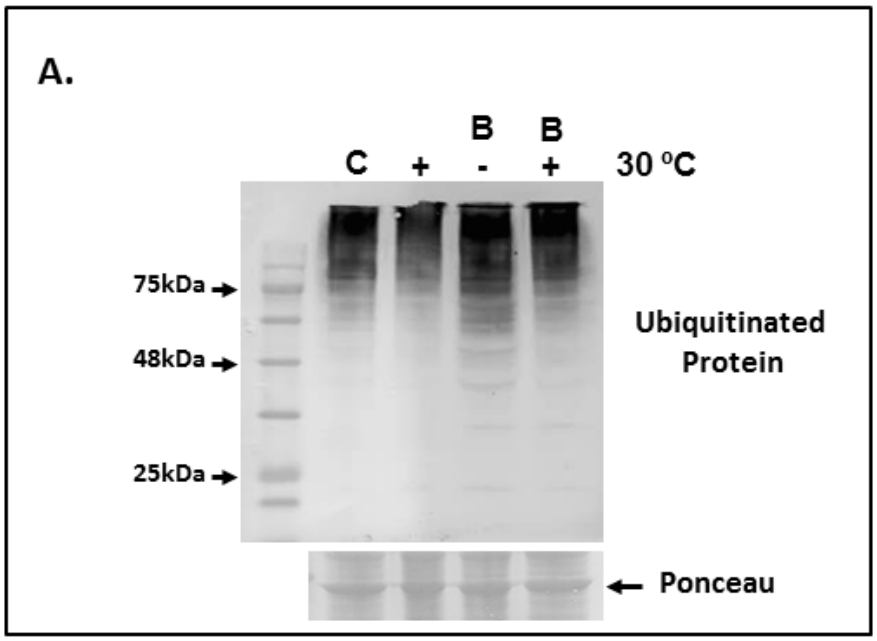
A.
C
+
B
-
B
+
30 °C
75kDa
48kDa
25kDa
Ubiquitinated Protein
Ponceau

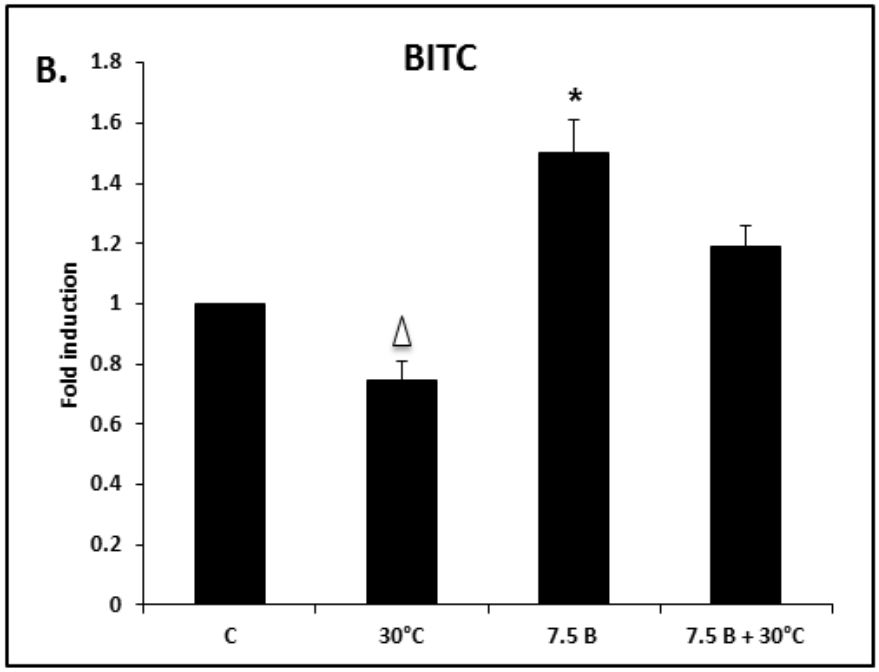
B.
BITC
Fold induction
1.8
1.6
1.4
1.2
1
0.8
0.6
0.4
0.2
0
*
C
30°C
7.5 B
7.5 B + 30°C

Figure 21. Representative immunoblot showing the relative levels of ubiquitinated protein in cells treated with PEITC. Cells were maintained at 22 °C (C), incubated at 30 °C or exposed to 5 μM PEITC at 22 or 30 °C for 12 h. A) After treatments, total protein was isolated and subjected to immunoblot analysis, utilizing an anti-ubiquitin antibody. B) Densitometric analysis of the band intensity utilized ImageJ software, and the data is expressed as a ratio of ubiquitinated protein to control levels. Vertical error bars denote standard error. Statistical analysis was performed as described in the Materials and methods and the significant differences are indicated with an asterisk ($p < 0.05$) or a triangle ($p < 0.1$). These data are representative of 4 separate experiments.

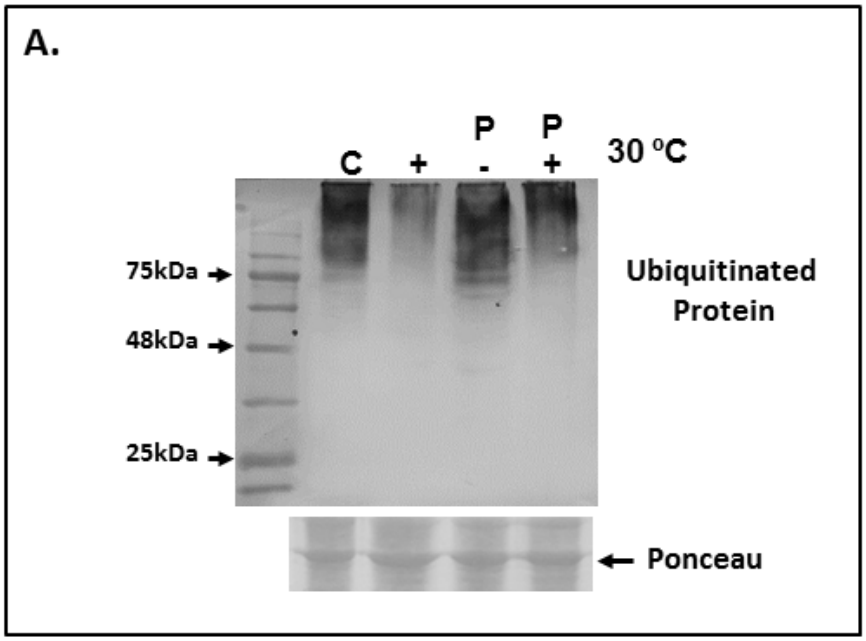
A.
C
+
P
-
P
+
30 °C
75kDa
48kDa
25kDa
Ubiquitinated
Protein
Ponceau

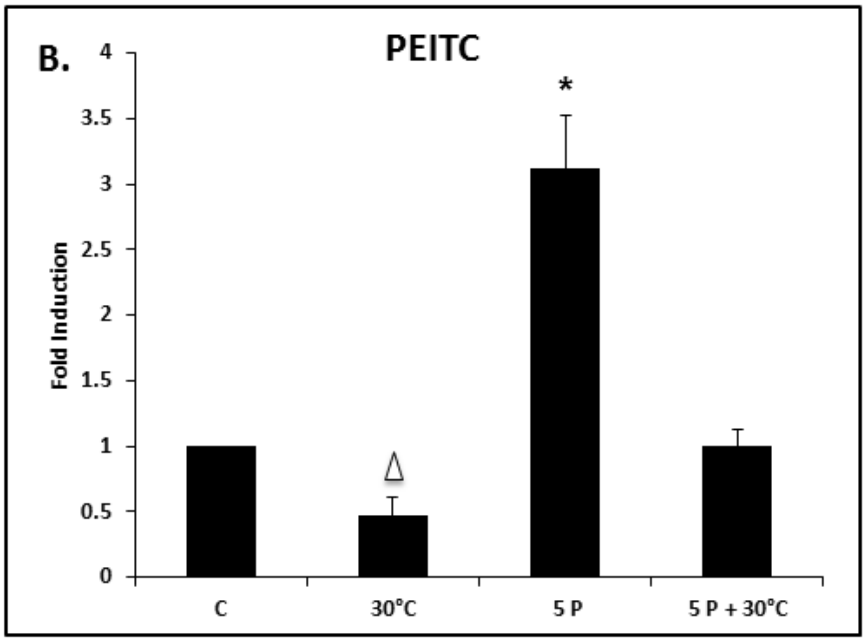
B.
PEITC
Fold Induction
4
3.5
3
2.5
2
1.5
1
0.5
0
*
C
30°C
5 P
5 P + 30°C

was employed to examine the effect of BITC and PEITC in comparison to MG132, a known inducer of protein aggregation and aggresome formation (Zaarur et al., 2008; Bolhuis and Richter-Landsberg, 2010; Xiong et al., 2013; Khan et al., 2014). Cells maintained at 22 or 30 °C displayed minimal staining of the ProteoStat dye in contrast to MG132-treated cells which induced the formation of numerous (approximately 30-50 per cell) and intensely stained aggresome-like structures in the perinuclear regions, which appeared to co-localize with HSP30 as determined by Z-stacking (white arrows; Fig. 22). BITC treatment at 22 °C resulted in a diffuse punctated pattern of aggregated protein (green arrows) throughout the cytoplasm. Treatment of cells with BITC at 30 °C also induced a granular pattern of aggregated protein as well as large aggregated protein structures (less than 1 per cell; white arrows). Some of these structures potentially co-localized with HSP30. PEITC treatment at 22 or 30 °C resulted in an increased accumulation of aggregated protein in a granular pattern compared to control, with some larger aggregated protein structures detected at the 30 °C temperature. It should be emphasized that the weakly-stained aggregated protein structures found with BITC or PEITC treatment were detected throughout the cytoplasm whereas MG132-induced numerous strongly stained aggregated protein structures per cell that were concentrated in the perinuclear region.

3.2.3. Effect of BITC and PEITC on α-tubulin and HO-1 levels in A6 cells.

Since studies with mammalian cells determined that ITCs bind and modify thiols associated with tubulin dimers, the next set of experiments investigated the effect of BITC and PEITC at 22 or 30 °C on α-tubulin and HO-1 levels. As shown in Figure 23, treatment with BITC for 4, 8 or 12 h at either 22 or 30 °C produced a decline in α-tubulin levels relative to control. Densitometric analysis revealed that cells treated with BITC for 4 h at 22 °C resulted in a 61% decrease in α-tubulin levels relative to control and a 91% decrease at 12 h. Cells incubated

Figure 22. Examination of aggregated protein and HSP30 localization in A6 cells treated with MG132, BITC or PEITC. In panels A and B, cells were grown on glass coverslips and maintained at 22 °C, incubated at 30 °C or exposed to 30 μM MG132 (MG) at 22 °C. Other coverslips were treated with 7.5 μM BITC or 5 μM PEITC at 22 or 30 °C for 12 h. The Proteostat aggresome detection kit was used to directly stain aggregated protein (red), while nuclei were stained directly with DAPI (blue). HSP30 was detected with a rabbit anti-HSP30 antibody, and a secondary antibody conjugated to Alexa-488 (green). From left to right, the columns display fluorescence detection channels for the Proteostat dye, HSP30 and merger of ProteoStat dye, HSP30 and DAPI. In MG-treated cells, white arrows indicate a large number of aggresome-like structures that co-localize with large HSP30 staining structures in the perinuclear region. Green arrows highlight BITC- or PEITC-induced accumulation of aggregated protein. In cells exposed to BITC at 30 °C, two large Proteostat stained structures are indicated with white arrows which co-localize with large HSP30 staining structures. The 20 μm scale bars are indicated at the bottom right corner of each panel. These results are representative of 3 different experiments.

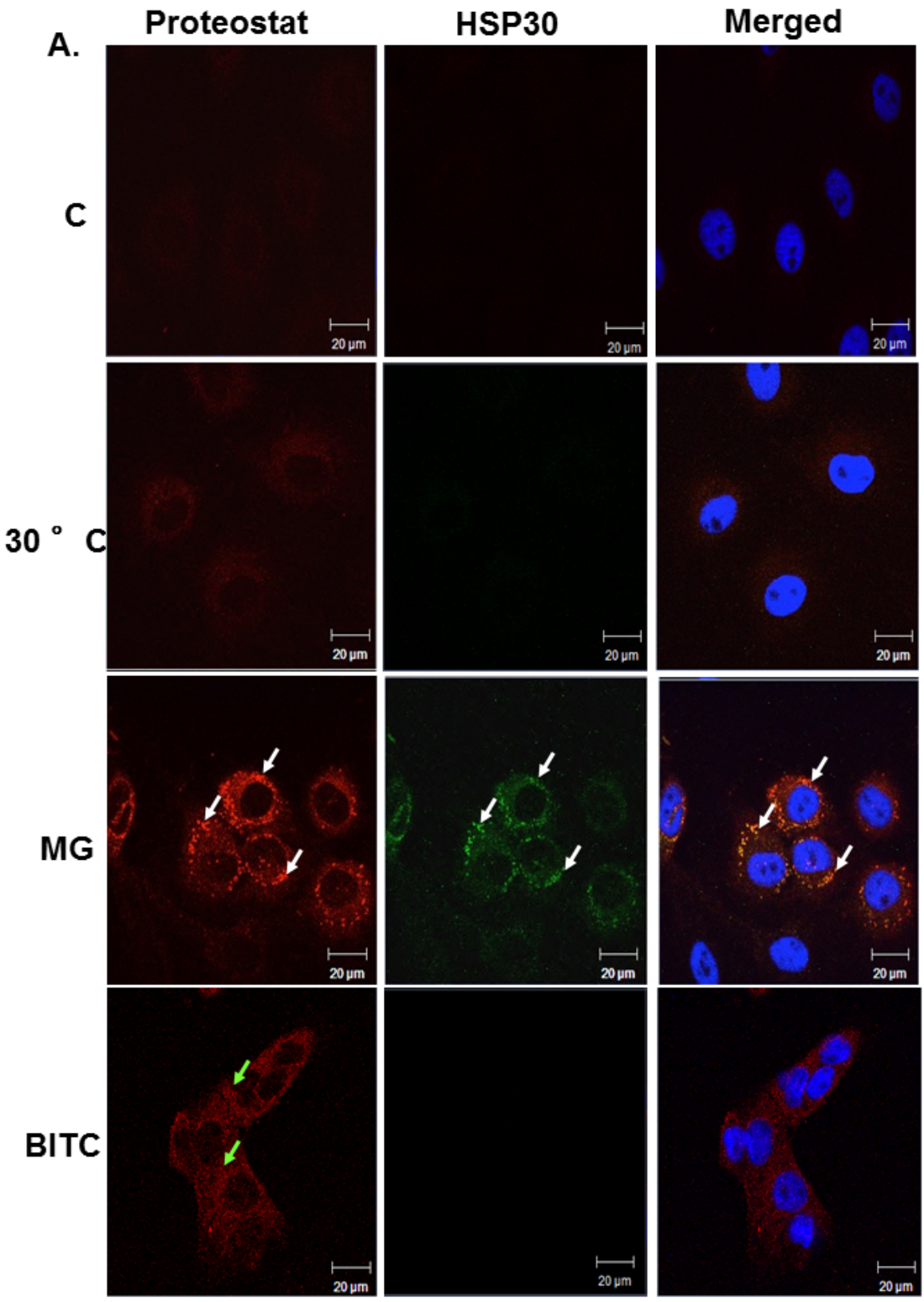
A.
Proteostat
HSP30
Merged
C
30 ° C
MG
BITC
20 µm

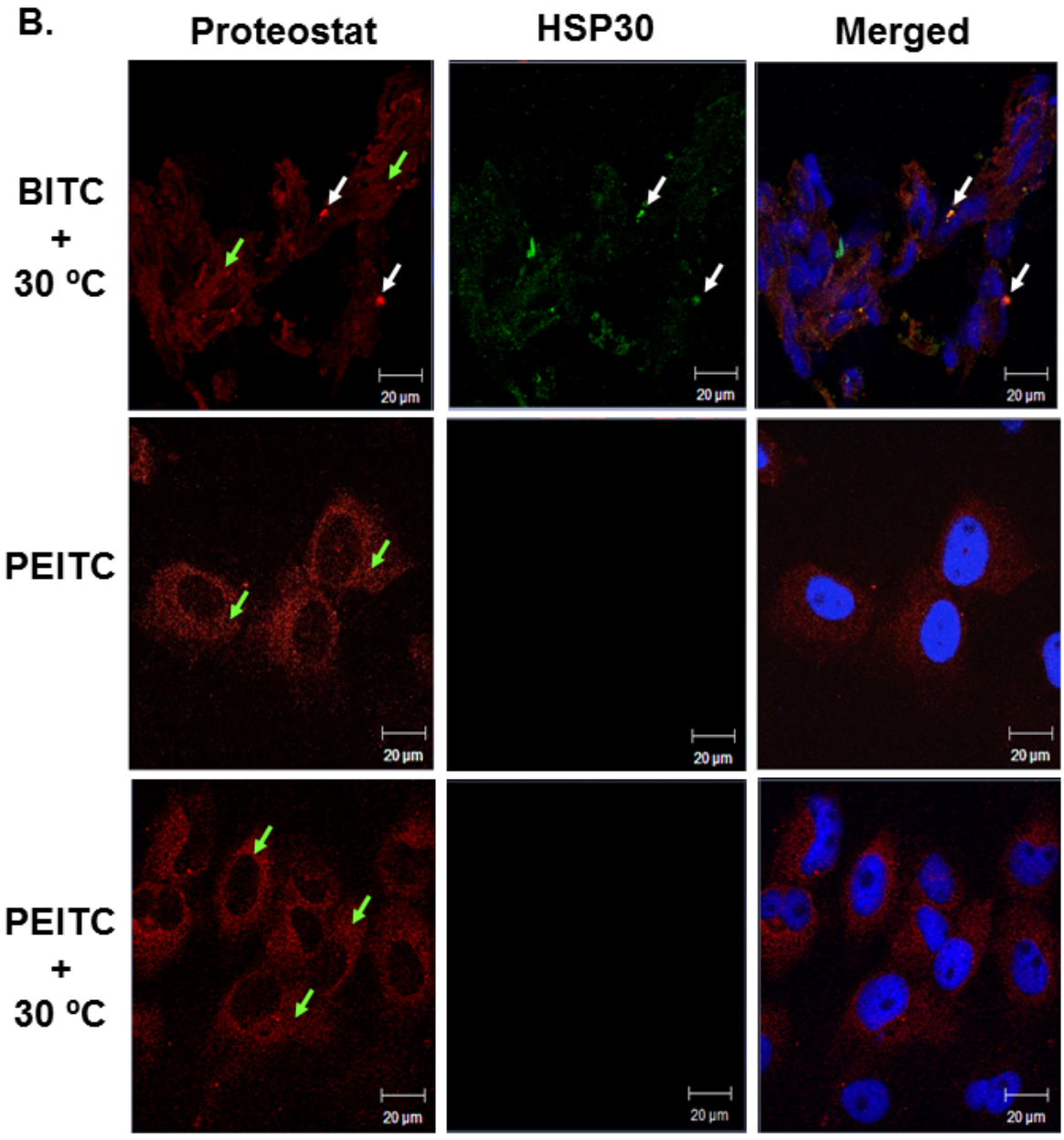
B.
Proteostat
HSP30
Merged
BITC
+
30 °C
PEITC
PEITC
+
30 °C
20 µm

Figure 23. Time course of the relative levels of α-tubulin and HO-1 in cells subjected to BITC exposure. A6 cells were maintained at 22 °C (C), incubated at 30 °C for 12 h or treated with 7.5 μM BITC for 4, 8 or 12 h at 22 or 30 °C. A) Total protein was isolated and 30 μg was subjected to immunoblot analysis using an anti-α-tubulin, anti-HO-1 or anti-actin antibody as described in Materials and methods, with the representative immunoblot shown. B) Image J software was used to perform densitometric analysis for the signal intensity for α-tubulin and HO-1. The data are expressed as percentage of control levels for α-tubulin and as a percentage of the maximum signal for HO-1 (12 h at 22 °C). The standard error is represented by vertical bars. Statistical analysis was performed as described in Materials and methods, and significant differences are indicated with an asterisk ($p < 0.05$). These results are representative of 3 different experiments.

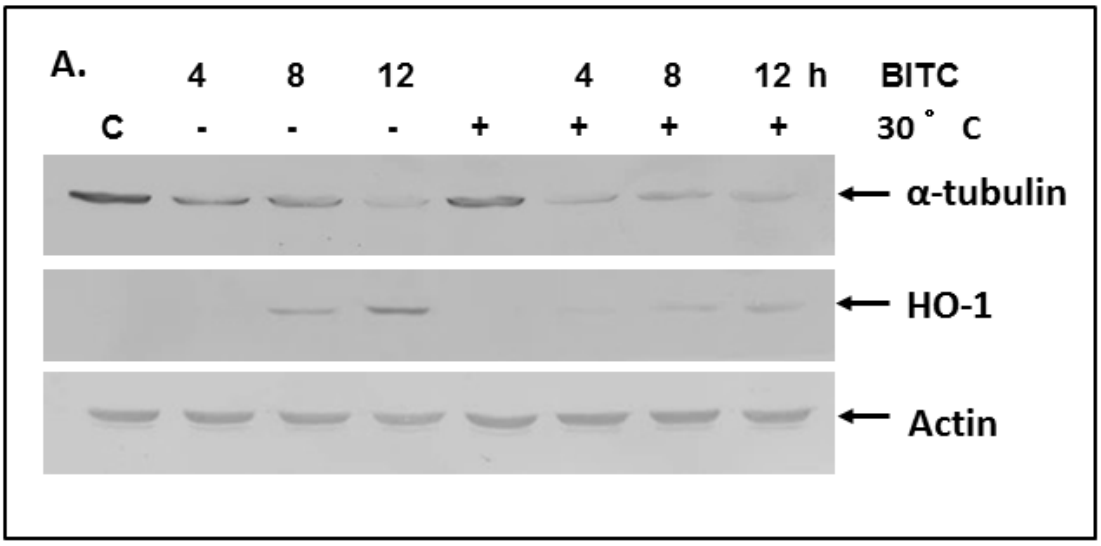
A.
4
8
12
4
8
12 h
BITC
C
-
-
-
+
+
+
+
30 ° C
α-tubulin
HO-1
Actin

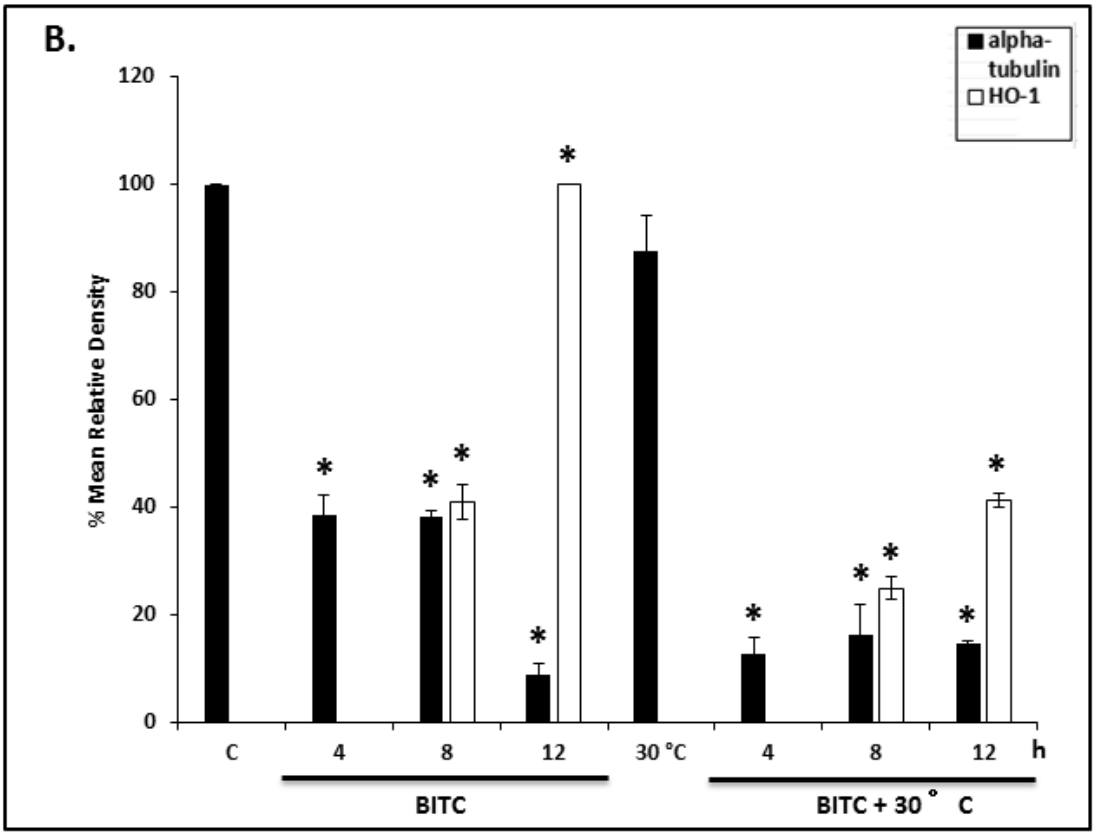
B.
alpha-tubulin
HO-1
% Mean Relative Density
120
100
80
60
40
20
0
C
4
8
12
30 °C
4
8
12
h
BITC
BITC + 30 ° C

at 30 °C without ITC treatment had approximately 12% less α-tubulin than control levels. Treatment of cells with BITC at 30 °C resulted in a rapid 87% drop in α-tubulin relative to control after 4 h with similar levels after 8 and 12 h. HO-1 levels were first detected after 8 h of BITC treatment time at 22 °C with the highest levels at 12 h. Additionally, BITC treatment at 30 °C resulted in 75 and 59% less HO-1 accumulation after the 8 and 12 h treatment, respectively, compared to 12 h at 22 °C.

While the effect of PEITC on α-tubulin was not as great as observed with BITC, a consistent decline in α-tubulin protein levels was evident with increasing exposure time of A6 cells to PEITC at either 22 or 30 °C (Fig. 24). Densitometric analysis revealed a 22% decrease in α-tubulin levels after 4 h of PEITC treatment at 22 °C and 32% after 12 h. In cells treated with PEITC at 30 °C, a 27% decrease in α-tubulin levels were observed after 4 h with a 49% decline after 12 h. At both 22 and 30 °C, HO-1 accumulation was first observed at 4 h, with increased amounts after longer treatment times. Finally, cells treated with PEITC at 22 °C for 12 h had the highest level of HO-1 accumulation compared to cells treated for 8 or 12 h of PEITC at 30 °C which had 23 and 22% less HO-1, respectively.

3.2.4. Immunocytochemical analysis of the effect of BITC on microtubule filament structure.

A6 cells incubated at 22 or 30 °C for 12 h had a similar tubulin cytoskeleton structure, consisting of long polymerized microtubule filaments emanating from microtubule-organizing centres within the perinuclear region (Fig. 25). However, disruption and microtubule filament fragmentation was evident after BITC treatment at 22 °C, which was enhanced when the experiments was performed at 30 °C (white arrows). As shown in Figure 25B, cells exposed to PEITC at 22°C revealed some microtubule disruption relative to control with microtubule filaments losing their long continuous structure. Treatment of cells with PEITC at 30 °C induced

Figure 24. Time course of the relative levels of α-tubulin and HO-1 in PEITC-treated A6 cells. Cells were maintained at 22 °C (C) or incubated at 30 °C for 12 h. Other cells were treated with 5 μM PEITC for 4, 8 or 12 h at 22 or 30 °C. In panel A, a representative immunoblot is shown. Total protein was isolated and subjected to immunoblot analysis using an anti-α-tubulin, anti-HO-1 or anti-actin antibody. B) Image J software was utilized for densitometric analysis of α-tubulin and HO-1 band intensity. The data are expressed as a percentage of control levels for α-tubulin and as a percentage of the maximum signal for HO-1 (12 h at 22 °C). The standard error is represented by vertical bars. Statistical analysis was performed and significant differences are indicated with an asterisk ($p < 0.05$). These results are representative of 5 different experiments.

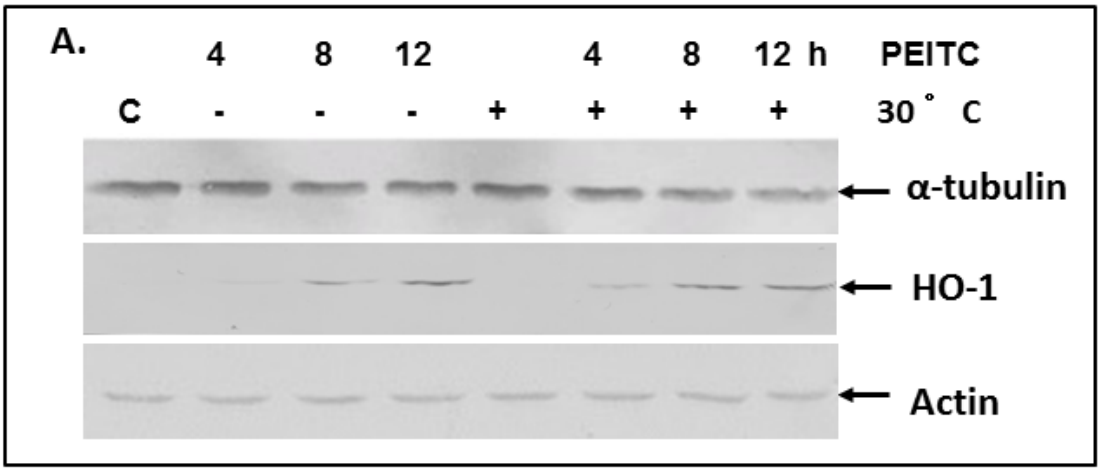
A.
4
8
12
4
8
12 h
PEITC
C
-
-
-
+
+
+
+
30 ° C
α-tubulin
HO-1
Actin

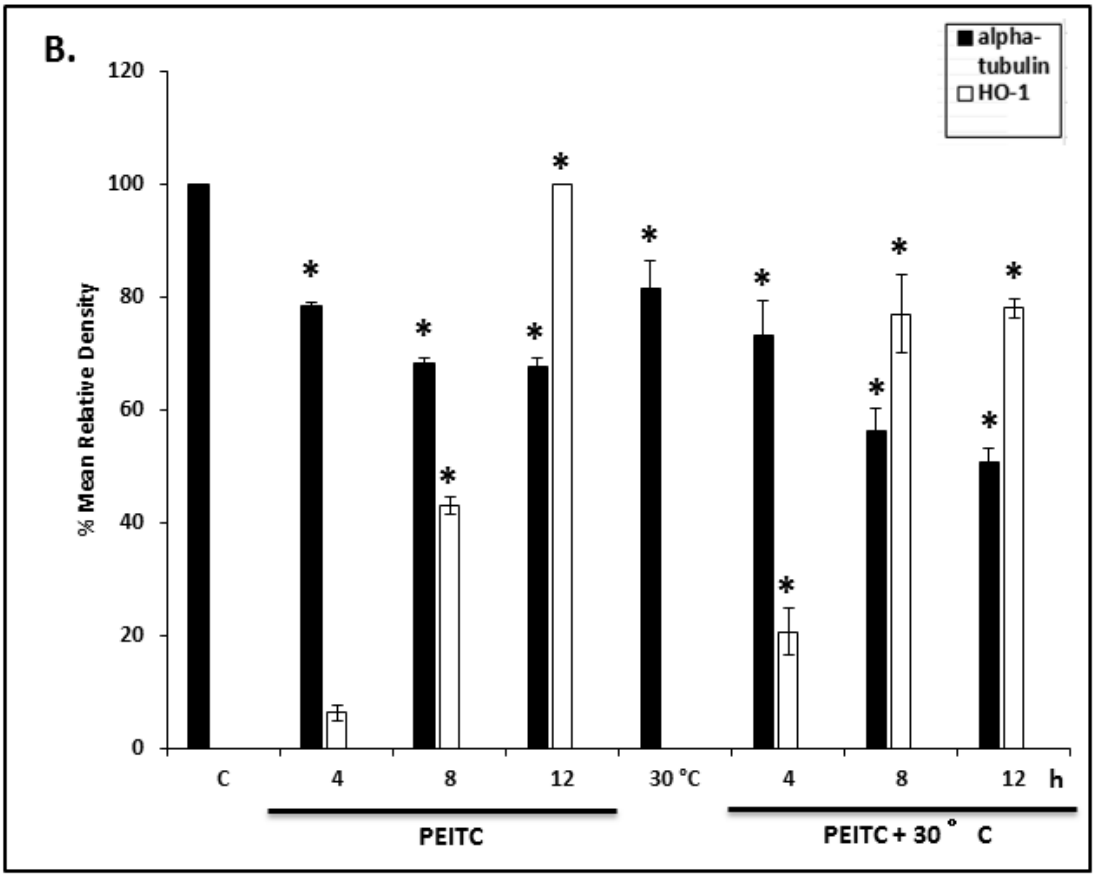
B.
alpha-tubulin
HO-1
% Mean Relative Density
120
100
80
60
40
20
0
C
4
8
12
30 °C
4
8
12
h
PEITC
PEITC + 30 ° C

Figure 25. Effect of BITC and PEITC on actin and microtubule filament structure. A) A6 cells were cultured on glass coverslips and then maintained at 22 °C (C), exposed to a temperature of 30 °C or treated with 7.5 μM BITC at 22 or 30 °C for 12 h. Microtubule filaments were detected with a mouse anti-α-tubulin antibody, and a secondary antibody conjugated to Alexa-488 (green). Actin filaments and nuclei were stained with phalloidin conjugated to TRITC (red) or DAPI (blue), respectively. The columns, from left to right, show the fluorescence detection channels for actin, α-tubulin, and merged images plus DAPI. Enlarged α-tubulin antibody-stained images are shown in panel B, comparing microtubule structure of A6 cells in response to treatments with 7.5 μM BITC or 5 μM PEITC at 22 or 30 °C for 12 h. Yellow arrows indicate membrane ruffling or disorganization of the F-actin cytoskeleton and white arrows indicate microtubule fragmentation. The 20 μm scale bars are indicated at the bottom right corner of each panel. These results are representative of 3 different experiments.

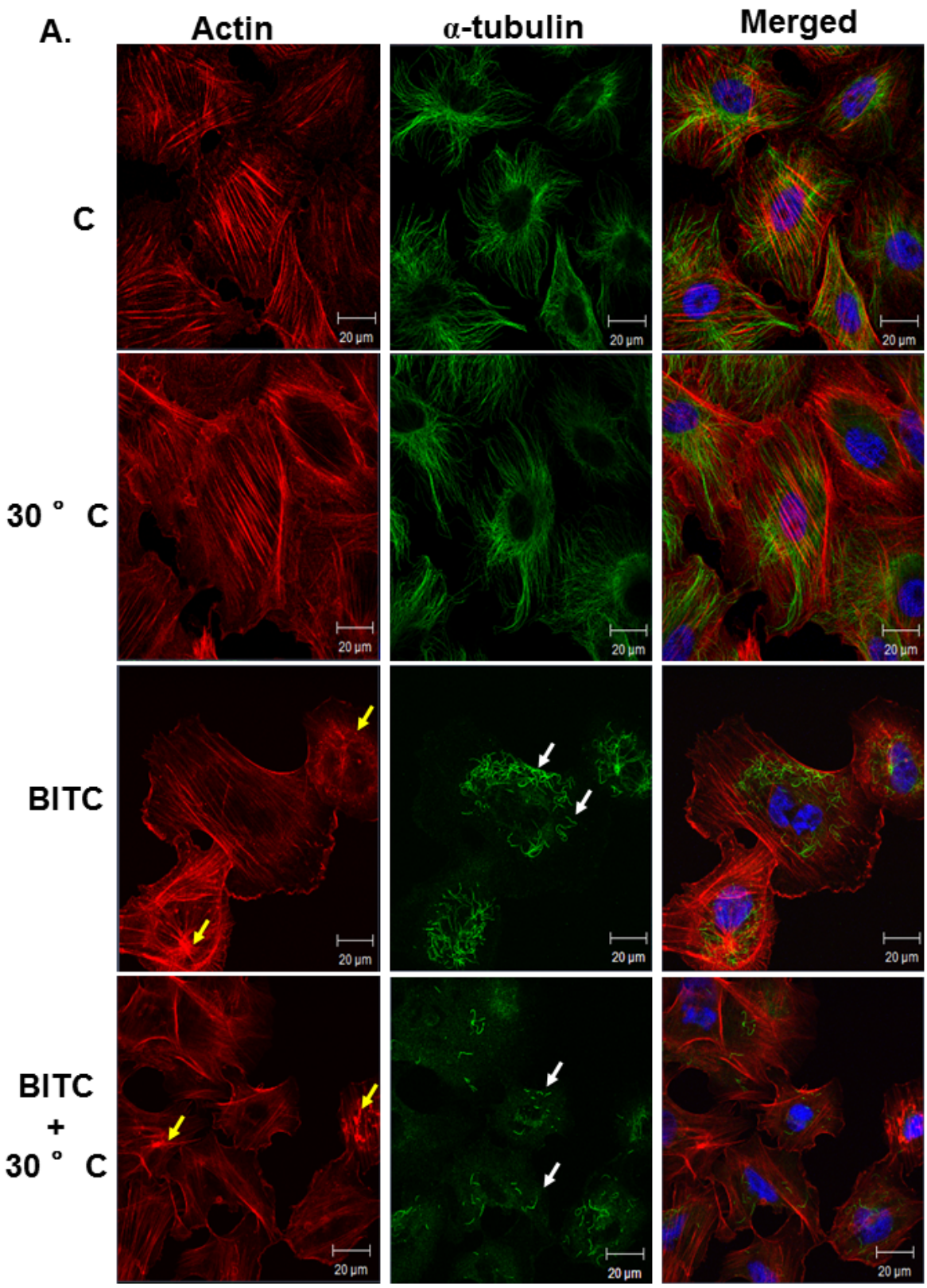
A.
Actin
α-tubulin
Merged
C
30 ° C
BITC
BITC
+
30 ° C
20 μm

B.

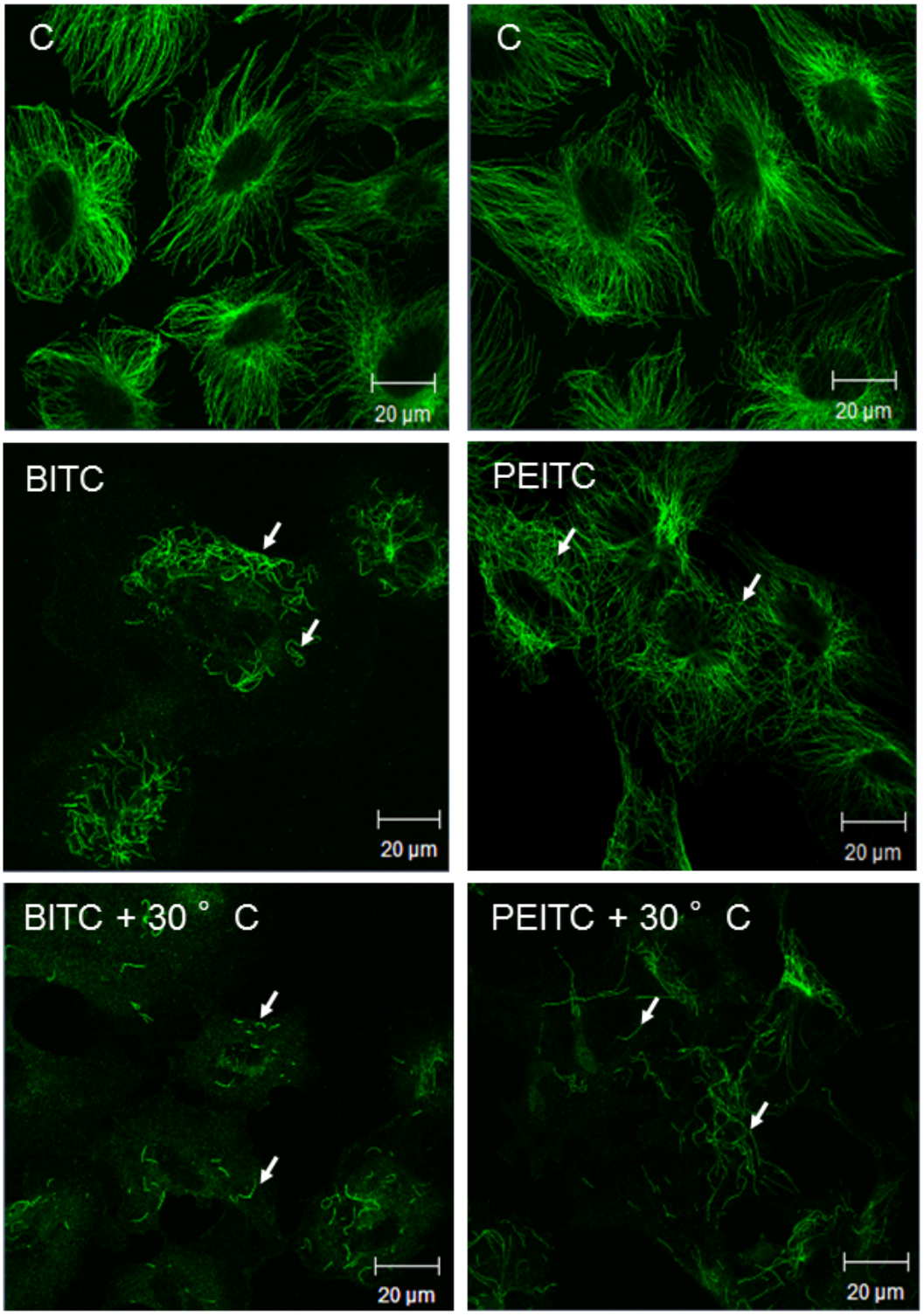
C
20 µm
C
20 µm
BITC
20 µm
PEITC
20 µm
BITC + 30 ° C
20 µm
PEITC + 30 ° C
20 µm

tubulin fragmentation but to a lesser extent than found with BITC-treated cells at 30 °C. Exposure of cells to DMSO alone did not affect α-tubulin levels or microtubule filament structure (data not shown). Subsequent immunocytochemical studies examined only BITC since it had a greater effect on α-tubulin levels and microtubule filament structure than PEITC.

3.2.5. Comparison of the effect of BITC on the actin and microtubule filament structure.

As shown in Figure 26, control A6 cells displayed actin stress fibers transversing the entire length of cells in mostly axial bundles, with the appearance of a few radial bundles located at the periphery. This pattern of actin cytoskeletal structure was also found in A6 cells that were exposed to 1, 2 and 4 h BITC at 22 °C. However, after 8 and 12 h of BITC treatment, membrane ruffling (yellow arrows) was present and localized to the periphery of cells. BITC exposure at 30 °C revealed membrane ruffling after only 2 h of treatment, and became more intense at 4 and 8 h (Fig. 27A and B). Additionally, cells exposed to BITC for 12 h at 30 °C displayed F-actin disorganization and collapse as well as larger F-actin structures present in the periphery of cells.

In contrast to the actin cytoskeleton, changes in microtubule filament morphology occurred after 1 h of BITC treatment at 22 °C (Fig. 26A and 26C). BITC-induced filament fragmentation was first detected after 2 h and was present after 4 and 8 h (white arrows; Fig. 26). However, after 12 h of BITC treatment at 22 °C, a coalescence of the microtubule filaments in the perinuclear region was apparent (white arrow). In comparison to BITC, treatment of cells with MG132 for 12 h resulted in some dysregulation of the actin cytoskeleton (yellow arrows), while the microtubule filament morphology was similar to control cells (Fig. 26B). Treatment of cells with BITC at 30 °C for 1 h induced microtubule filament fragmentation (white arrows Fig. 27A and C). After 2 and 4 h, microtubules were detected in the perinuclear regions of the cells as microtubule filament fragmentation increased while at 8 h microtubule filaments were

Figure 26. Time course examining the actin and microtubule filament structure in response to BITC treatment at 22 °C. In panels A and B, A6 cells were cultured on glass coverslips and then maintained at 22 °C (C) or treated with 7.5 μM BITC at 22 °C for 1-12 h. α-tubulin was detected with a mouse anti-α-tubulin antibody, and a secondary antibody conjugated to Alexa-488 (green). Actin and nuclei staining utilized phalloidin conjugated to TRITC (red) or DAPI (blue), respectively. The columns, from left to right, show the fluorescence detection channels for actin, α-tubulin, and merged images plus DAPI staining. In panel C, each of the previous α-tubulin images were enlarged for a better comparison of the change in microtubule structure with selected BITC treatment times. Yellow arrows indicate collapse or disorganization of the F-actin cytoskeleton while white arrows indicate microtubule fragmentation. The 20 μm scale bars are indicated at the bottom right corner of each panel. These images are representative of 3 different experiments.

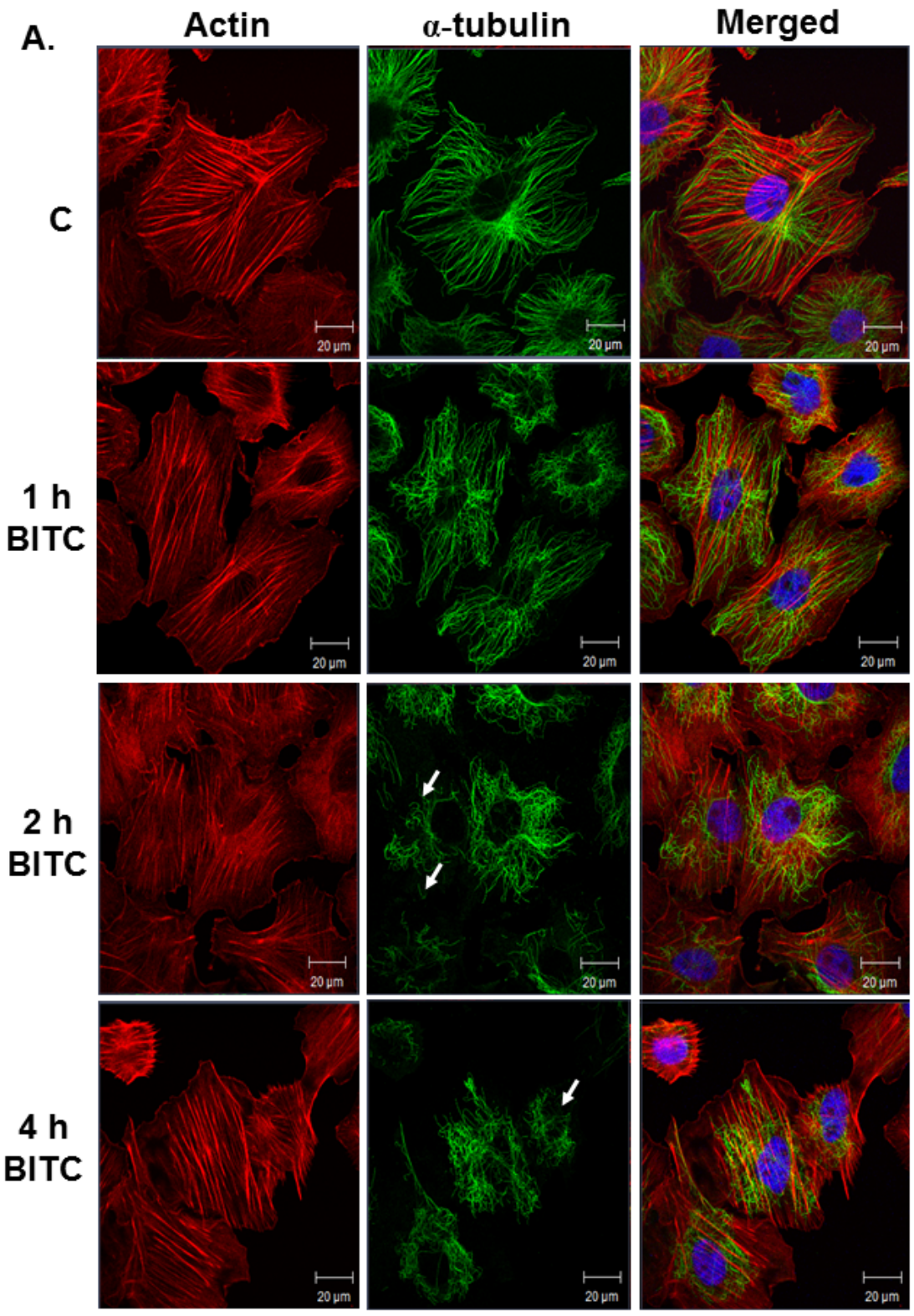
A.
Actin
α-tubulin
Merged
C
1 h BITC
2 h BITC
4 h BITC
20 μm

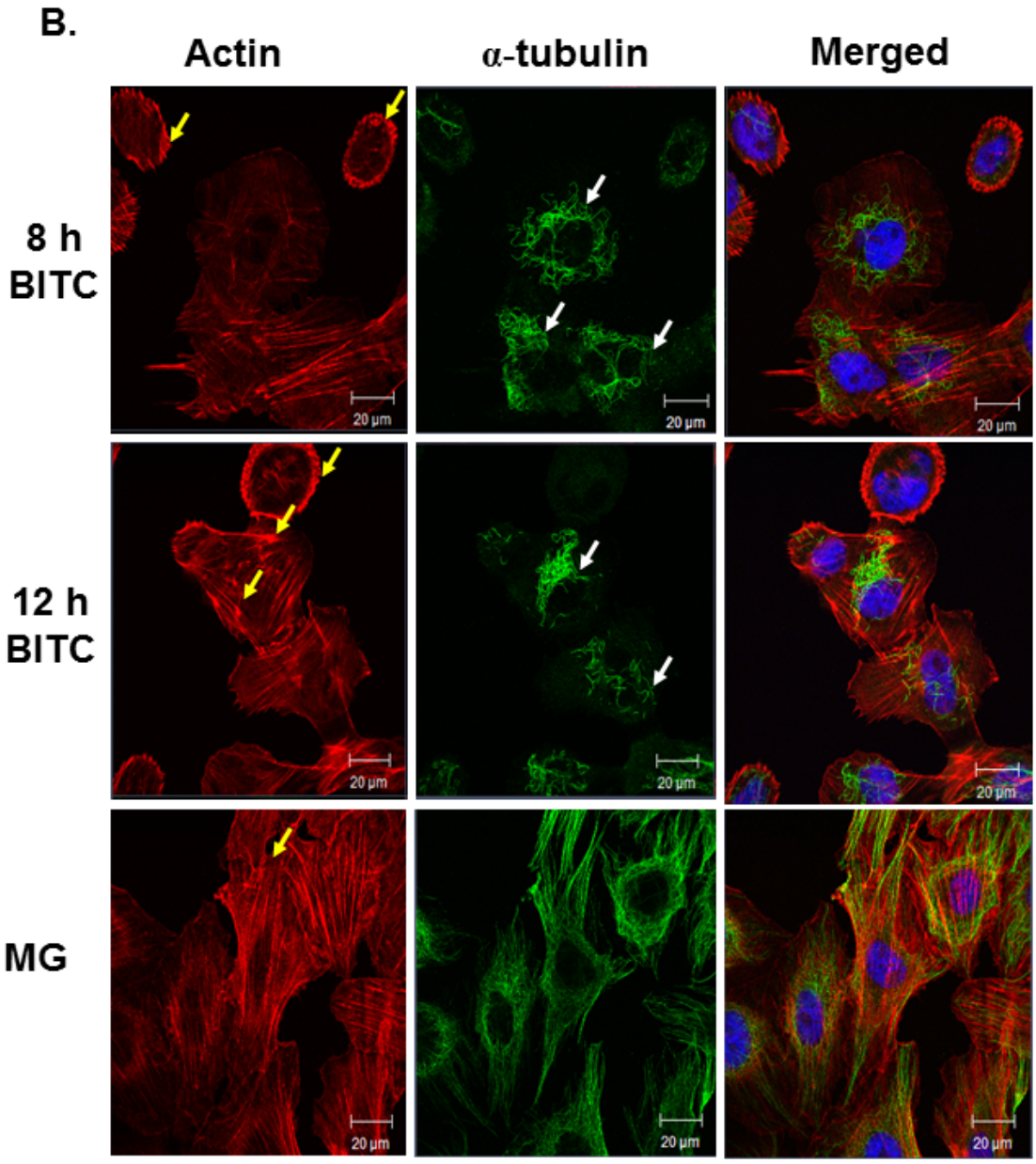
B.
Actin
α-tubulin
Merged
8 h BITC
12 h BITC
MG
20 µm

C.

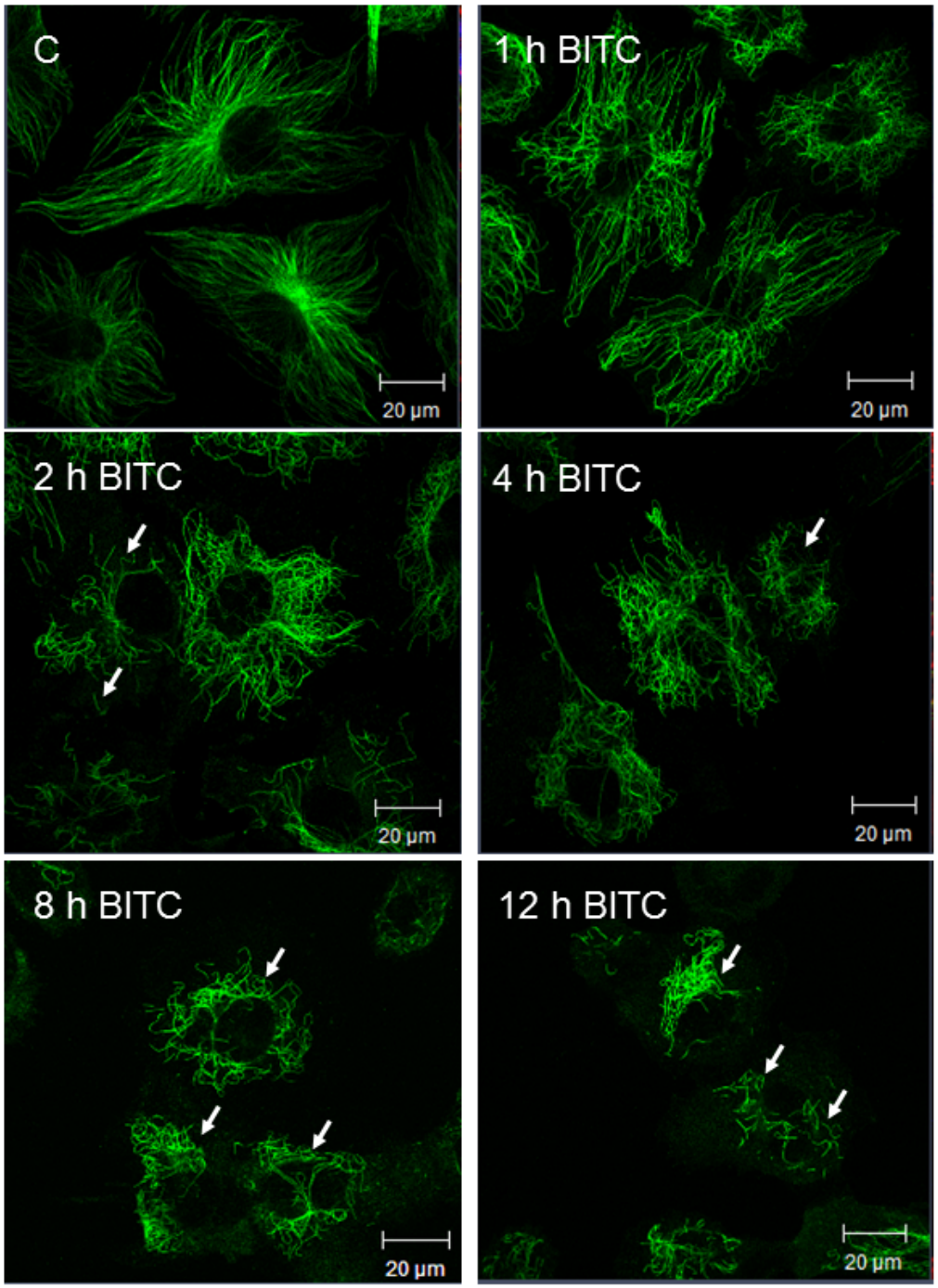
C
20 μm
1 h BITC
20 μm
2 h BITC
20 μm
4 h BITC
20 μm
8 h BITC
20 μm
12 h BITC
20 μm

Figure 27. Time course examining the actin and microtubule filament structure in A6 cells subjected to BITC treatment at 30 °C. In panels A and B, A6 cells were cultured on glass coverslips and then maintained at 22 °C (C), exposed to a higher temperature of 30 °C or treated with 30 μM MG132 (MG) for 12 h at 22 °C. Other cells were incubated with 7.5 μM BITC for 1-12 h at 30 °C. α-tubulin was detected with a mouse anti-α-tubulin antibody, and a secondary antibody conjugated to Alexa-488 (green). Actin and nuclei staining utilized phalloidin conjugated to TRITC (red) or DAPI (blue), respectively. The columns, from left to right, show the fluorescence detection channels for actin, α-tubulin, and merged images plus DAPI. C) Each of the previous α-tubulin images were enlarged for better comparison of the change in microtubule structure with selected BITC treatment times at 30 °C. Yellow arrows indicate membrane ruffling or disorganization of the F-actin cytoskeleton while white arrows indicate microtubule fragmentation. The 20 μm scale bars are indicated at the bottom right corner of each panel. These results are representative of 3 different experiments.

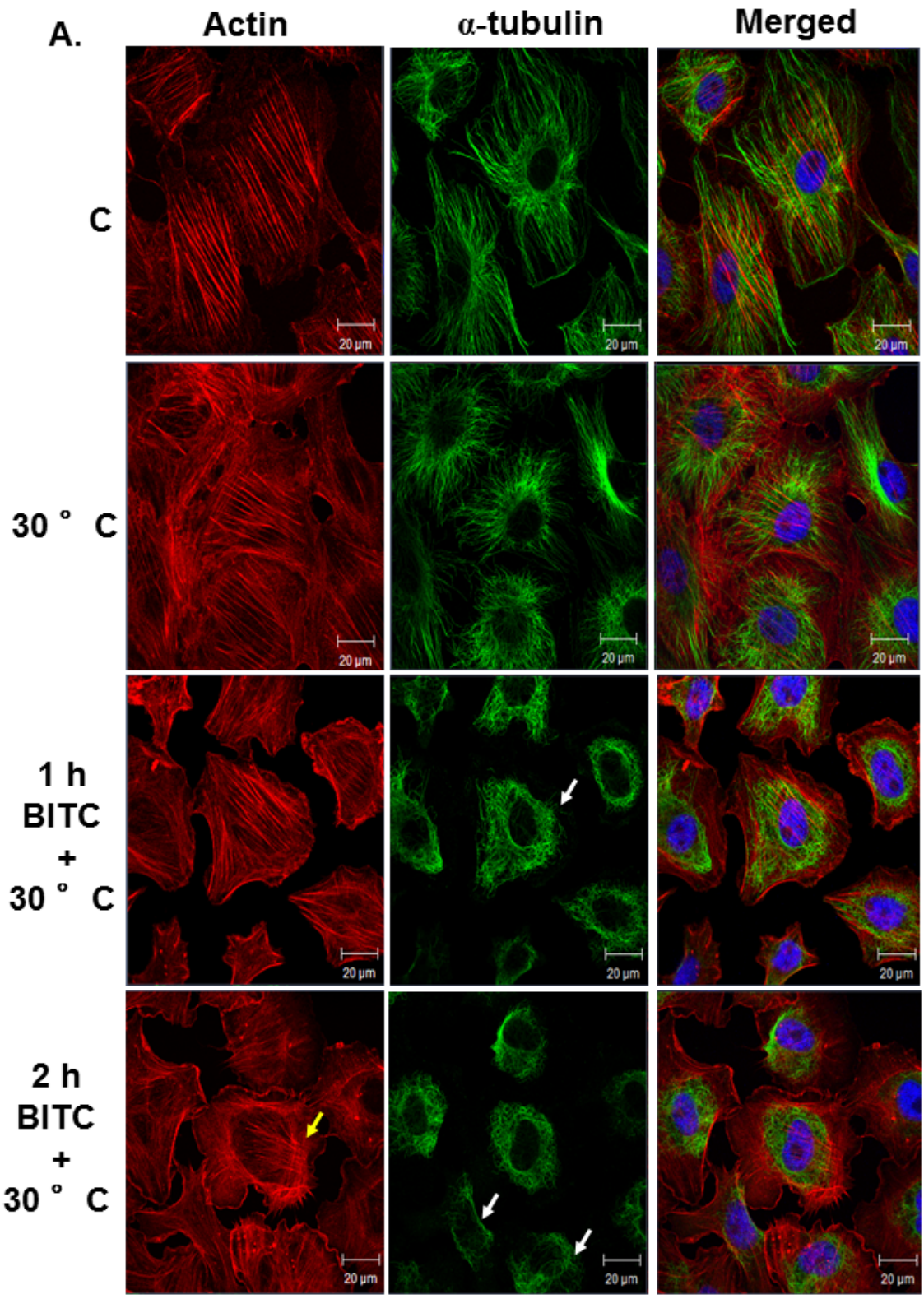
A.
Actin
α-tubulin
Merged
C
30 ° C
1 h BITC + 30 ° C
2 h BITC + 30 ° C
20 µm

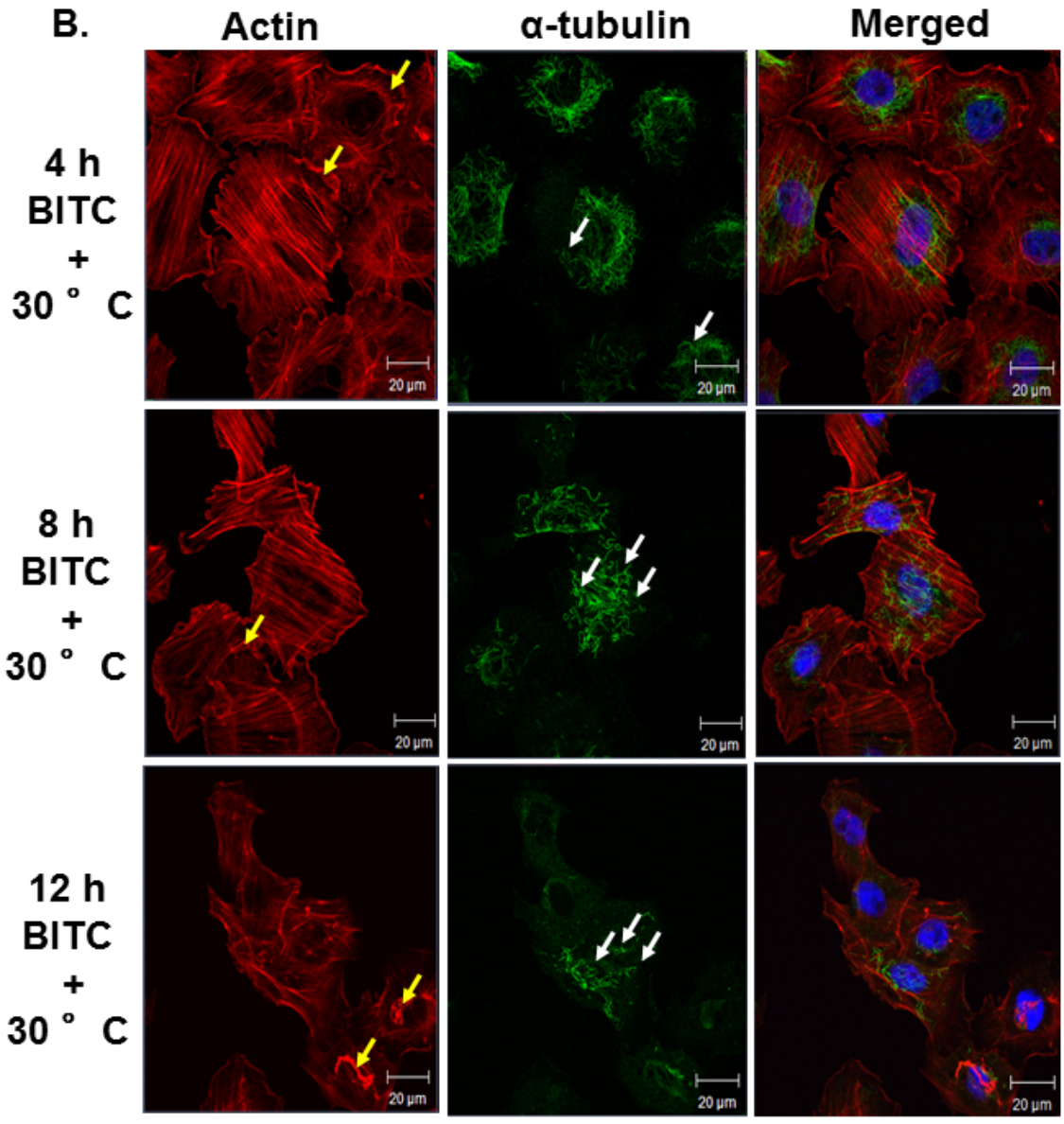
B.
Actin
α-tubulin
Merged
4 h BITC + 30 ° C
8 h BITC + 30 ° C
12 h BITC + 30 ° C
20 μm

C.

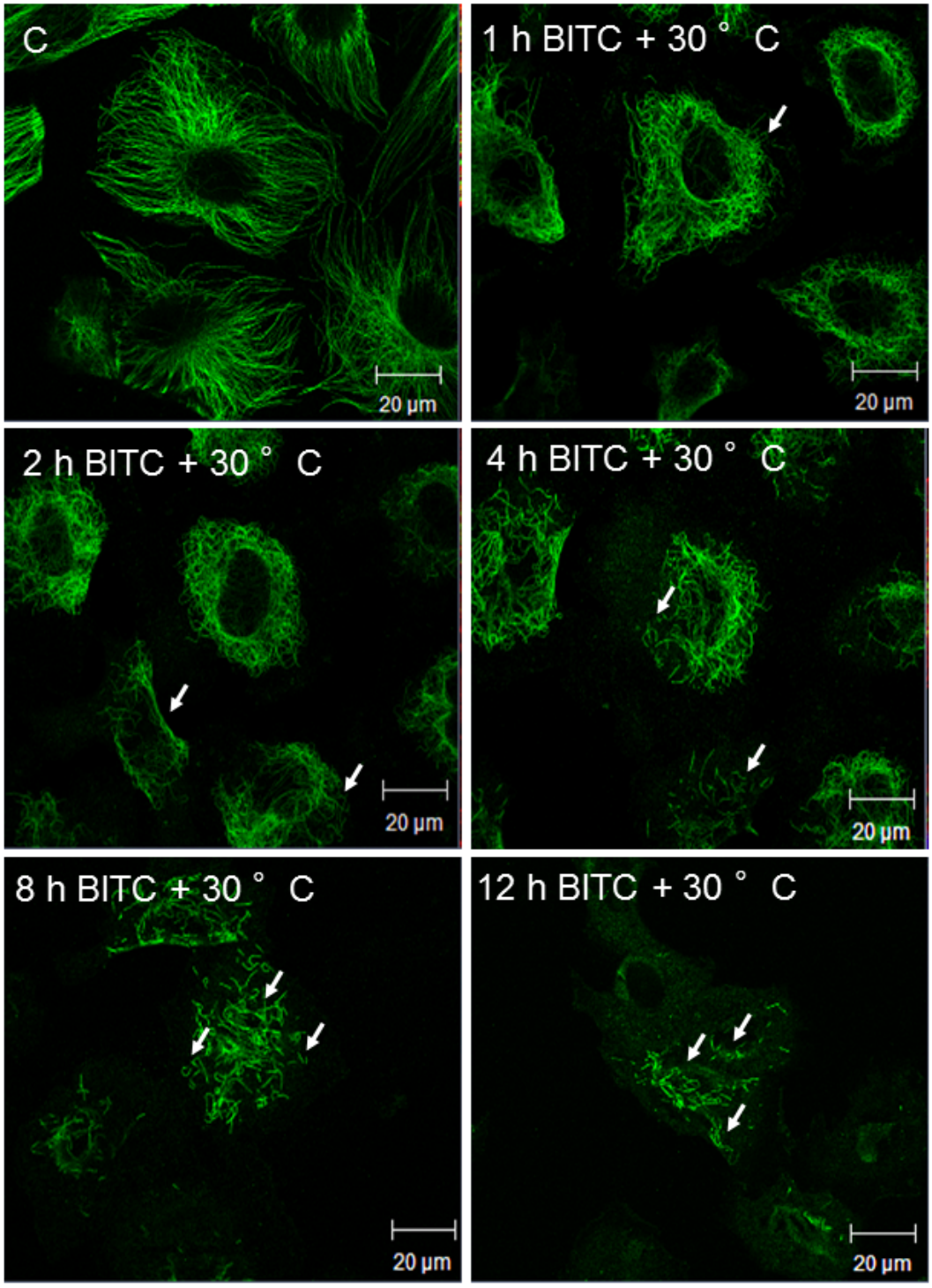
C
20 µm
1 h BITC + 30 ° C
20 µm
2 h BITC + 30 ° C
20 µm
4 h BITC + 30 ° C
20 µm
8 h BITC + 30 ° C
20 µm
12 h BITC + 30 ° C
20 µm

concentrated in the perinuclear region, as determined by Z-stacking. Furthermore, at 12 h of BITC at 30 °C, a substantial decrease in the number of fragmented filaments was observed relative to 4 and 8 h.

3.2.6. BITC pretreatment resulted in fewer MG132-induced aggresome-like structures in A6 cells.

Given the previous results, which revealed the presence of microtubule filament fragmentation in cells exposed to BITC for 12 h at 22 °C, it was possible that this phenomenon could potentially disrupt the movement of aggregated protein to the perinuclear region and the formation of aggresomes. In the following experiment, I examined whether pretreatment of cells with BITC could disrupt the formation of MG132-induced aggresome-like structures in the perinuclear region. As shown in Figure 28, treatment of cells with MG132 for 12 h at 22 °C resulted in intact microtubule filaments and the formation of large aggresome-like structures (white arrows) that localized primarily to the perinuclear region. Approximately 30-50 large aggresome-like structures were detected per cell in response to the MG132 treatment. However, a 2 h BITC pretreatment prior to the introduction of MG132 reduced the intensity, size and the number of aggresome-like structures (10-15 per cell) as well as inducing the fragmentation of microtubule filaments (white arrows). When the pretreatment time was lengthened to 4 h, the number of MG132-induced large aggresome-like structures became less than approximately 10 per cell, many of which were not located within the perinuclear region of A6 cells. Microtubule filament fragmentation was also more pronounced occurring in essentially every cell.

Figure 28. Effect of BITC pretreatment on the formation of MG132-induced aggresome-like structures in A6 cells. In panels A and B, A6 cells were cultured on glass coverslips and then maintained at 22 °C (C) or incubated with 30 μM MG132 (MG) for 12 h. Other cells were pre-treated with 7.5 μM BITC for 2 or 4 h at 22 °C before exposure to 30 μM MG132 for 12 h at 22 °C. A) To directly stain aggregated protein, the Proteostat aggresome detection kit was used. White arrows indicate aggresome-like structures in the perinuclear region. B) α-tubulin was detected with a mouse anti-α-tubulin antibody, and a secondary antibody conjugated to Alexa-488 (green). White arrows indicate aggresome-like structures in panel A and microtubule fragmentation in panel B. The 20 μm scale bars are indicated at the bottom right corner of each panel. These images are representative of 2 different experiments.

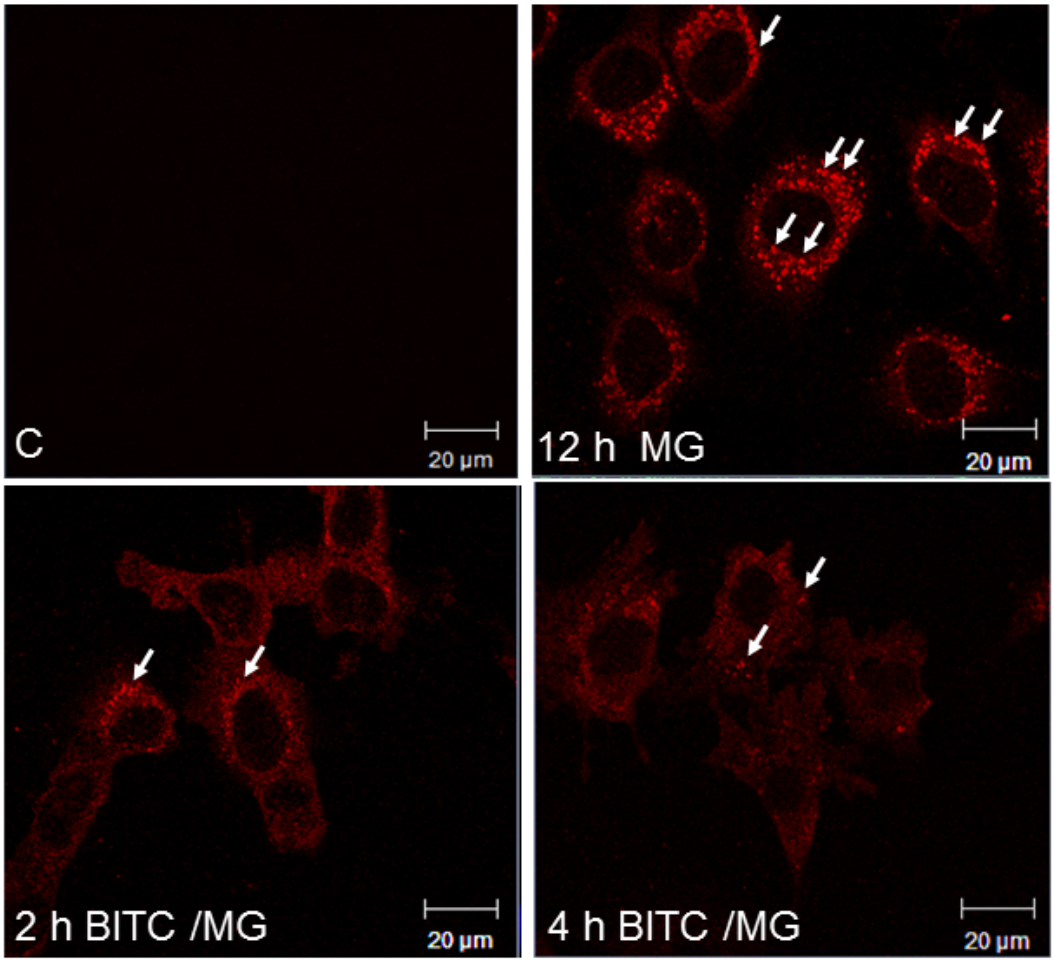
C
20 µm
12 h MG
20 µm
2 h BITC /MG
20 µm
4 h BITC /MG
20 µm

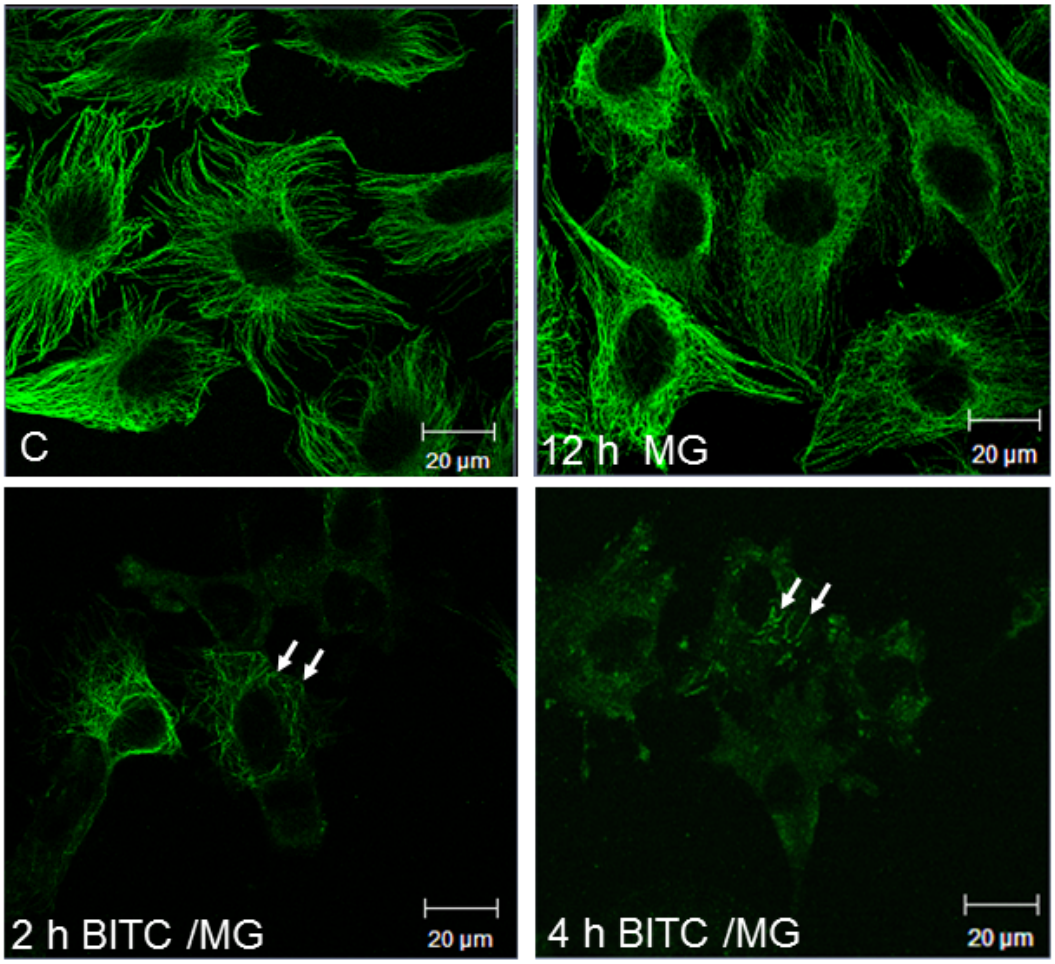
C
20 µm
12 h MG
20 µm
2 h BITC /MG
20 µm
4 h BITC /MG
20 µm

3.3. Analysis of HSPB6 structure and accumulation.

3.3.1. X. laevis hspB6 cDNA sequence analysis.

During the course of my doctoral research, I investigated the effect of ITCs on HSPB6 accumulation in A6 cells (Fig. 12). This work stemmed from the DNA sequence analysis of a putative *X. laevis hspB6* cDNA clone (GenBank Accession No. NM_001093010.1), which encoded a HSPB6 protein of 168 amino acids with an isoelectric point of 6.16 (Fig. 29). *X. laevis* HSPB6 has a predicted size of 18,831 Da, which was similar to values found with *X. tropicalis* (18,860 Da), the only other amphibian HSPB6 found in the GenBank database. The amphibian HSPB6 was slightly larger than human HSPB6 (17,151 Da).

The deduced *X. laevis* HSPB6 amino acid sequence (NP_001086479.1) was aligned with the well-characterized human, rat and mouse HSPB6 sequences to further confirm its identity (Fig. 30). A comparison of the 4 aligned sequences revealed a total of 78 identical amino acids, 26 conserved amino acid substitutions and 3 semi-conservative substitutions. Like the other members of the sHSP superfamily, *X. laevis* HSPB6 has an α-crystallin domain (E68-P149). The highest amount of amino acid conservation of the 4 HSPB6 sequences was found within the α-crystallin domains. Furthermore, comparable to other *X. laevis* sHSPs including HSP27 and HSP30C and D, HSPB6 has a C-terminal extension (T151 to K168). Interestingly, the *X. laevis* HSPB6 C-terminal extension had 13 amino acids out of 18 that were polar. Previous analyses of mouse, rat, swine, bovine and/or human HSPB6 have experimentally determined the presence of key phosphorylation sites at serines 16, 59 and 157 (Beall et al., 1999; Islamovic et al., 2007; Edwards et al., 2011; Mymrikov et al., 2011; Sin et al., 2015). Using the GPS 3.0 Kinase-Specific Phosphorylation Site Prediction software, multiple potential serine phosphorylation sites were detected in *X. laevis* HSPB6 (Xue et al., 2011). Of the 3 aforementioned mammalian

Figure 29. Nucleotide and putative amino acid sequence of a *Xenopus laevis hspB6* cDNA. Nucleotide and amino acid numbering is shown on the left and right hand side, respectively. The amino acids shown in bold comprise the α-crystallin domain while the underlined amino acids indicate the putative C-terminal extension.

```
1     cacgcgtccgttcagctttgcactcacacaatggatgttacaattcatcacccctggatg
                                      M  D  V  T  I  H  H  P  W  M   10
61    cgccgacccccactgtctccctcgttttttccctagccgaattctaggacagaggttcgga
      R  R  P  P  L  S  P  S  F  F  P  S  R  I  L  G  Q  R  F  G   30
121   gaaggggtcctggagtcggatctattccctgccatgcccatgccgatgacccttagcccg
      E  G  V  L  E  S  D  L  F  P  A  M  P  M  P  M  T  L  S  P   50
181   tactactatagttctcccagcatcccgcagccgagcgaagtcggactgtcagaggtgaag
      Y  Y  Y  S  S  P  S  I  P  Q  P  S  E  V  G  L  S  E  V  K   70
241   ttggataaggatcagttctcggttctcctggatgtgaaacatttctctccggaggagttg
      L  D  K  D  Q  F  S  V  L  L  D  V  K  H  F  S  P  E  E  L   90
301   aacgtcaaggttgtgggagattccgtggaagtccatgccaagcacgaggagcgcctggat
      N  V  K  V  V  G  D  S  V  E  V  H  A  K  H  E  E  R  L  D  110
361   gaacatggatttatatcccgagagttccacagaaggtacaagatccccccgactgtgaac
      E  H  G  F  I  S  R  E  F  H  R  R  Y  K  I  P  P  T  V  N  130
421   cccggggccatatcctcagctctgtctgcagaggggcttctgtctatccaggcccccgtc
      P  G  A  I  S  S  A  L  S  A  E  G  L  L  S  I  Q  A  P  V  150
481   actgccagtgggaaacaagaagagaggagcatccccatagccagaaaggacaagtaaagc
      T  A  S  G  K  Q  E  E  R  S  I  P  I  A  R  K  D  K       168
541   caaagccacccagtgtgtccctcctactgacaccaacacccacacatgggacctacccca

601   gcggctccaccaccaggatctcccaactcccttgtctggcttatgggtcacttatacacc

661   cacaggacccacccaatgcaactgtccactaacagcacccacaccccaatatagggcacc

721   cccagactacgtgcagcacctggaggcttctgtgtgtatcagccagtgcatctgccctaa

781   ataagcagcacccagagactcccctggatctgaatcttctctttcatgatgtttgcaata

841   aattcctttctaataaaaatagtctggtatcaaaaaaaaaaaaaaa
```

Figure 30. Comparison of the deduced amino acid sequence of *Xenopus laevis hspB6* cDNA to human, rat and mouse HSPB6. Multiple sequence alignment was performed using Clustal Omega as described in Materials and methods. Asterisks under the sequences indicate identical amino acids among all 4 species. Colons represent conservative amino acid substitutions, and periods represent semi-conservative substitutions. Deletions are indicated by dashes. The underlined amino acids indicate the α-crystallin domains. The *X. laevis* HSPB6 putative C-terminal extension composed of primarily polar residues is shown in bold. Serine residues that have been shown to be key points of phosphorylation in mammalian HSPB6 are indicated in bold and underlined.

```
X. laevis       --MDVTIHHPWMRRP--PLSPSFFPSRILGQRFGEGVLESDLFPAMPMPMTLSPYYYSSP    56
H. sapiens      MEIPVPVQPSWLRRASAPLLGLSAPGRLFDQRFGEGLLEAELAAL--CPTTLAPYYLRAP    58
R. norvegicus   MEIRVPVQPSWLRRASAPLPGFSTPGRLFDQRFGEGLLEAELASL--CPAAIAPYYLRAP    58
M. musculus     MEIPVPVQPSWLRRASAPLPGFSAPGRLFDQRFGEGLLEAELASL--CPAAIAPYYLRAP    58
                  : * ::  *:**   **     *.*:: ******:**::*      * :::***  :*

X. laevis       SIPQPSEVGLSEVKLDKDQFSVLLDVKHFSPEELNVKVVGDSVEVHAKHEERLDEHGFIS    116
H. sapiens      SVALPV----AQVPTDPGHFSVLLDVKHFSPEEIAVKVVGEHVEVHARHEERPDEHGFVA    114
R. norvegicus   SVALPT----AQVPTDPGYFSVLLDVKHFSPEEISVKVVGDHVEVHARHEERPDEHGFIA    114
M. musculus     SVALPT----AQVSTDSGYFSVLLDVKHFLPEEISVKVVDDHVEVHARHEERPDEHGFIA    114
                *:  *     ::*  *   ********** ***: **** : *****:**** *****::

X. laevis       REFHRRYKIPPTVNPGAISSALSAEGLLSIQAPVTASGKQEERSIPIARKDK      168
H. sapiens      REFHRRYRLPPGVDPAAVTSALSPEGVLSIQAAPASAQA----PPPAAAK--      160
R. norvegicus   REFHRRYRLPPGVDPAAVTSALSPEGVLSIQATPASAQA----SLPSPPAAK      162
M. musculus     REFHRRYRLPPGVDPAAVTSALSPEGVLSIQATPASAQA----QLPSPPAAK      162
                *******::** *.*.*::**** **:*****  ::.       *
```

HSPB6 serine phosphorylation sites, the only conserved site was at position 57, which corresponded to serine 59 in human, rat and mouse that was originally found to be phosphorylated *in vitro* by cAMP-dependent protein kinase (Beall et al., 1999; Mymrikov et al., 2011). The cAMP-dependent protein kinase motif associated with serine 57 in *Xenopus* HSPB6 has a low score for possible phosphorylation according to GPS 3.0. Nevertheless, it is possible that this site could be phosphorylated by other kinases.

Amino acid sequence comparison studies revealed that *X. laevis* HSPB6 shared a 94% identity with *X. tropicalis* putative HSPB6 but only 53% with *X. tropicalis* HSPB5 and 50, 49 and 43% with *X. laevis* HSPB1, HSPB4 and HSP30C, respectively. Additionally, *X. laevis* HSPB6 shared primary sequence identity with HSPB6 found in two reptiles (65% *P. sinensis* [turtle], 65% *A. carolinensis* [lizard]), two mammals (60% *M. davidii* [bat], 59% *H. sapiens*) and two fish HSPB6 (51% *P. mexicana* [Atlantic molly], 49% *D. rerio* [zebrafish]) (Table 1). Avian HSPB6 proteins were not detected in the GenBank gene or protein library. An amino acid comparison of the α-crystallin domains of *X. laevis* HSPB6 with *H. sapiens* HSPB6 and other *X. laevis* sHSPs is shown in Table 2. The percent identity of the α-crystallin domains of the various *X. laevis* sHSPs ranged from 36% to 56%. Also, there was greater identity between *X. laevis* HSPB6 and human HSPB6 (71%) than with the other *X. laevis* sHSPs.

Phylogenetic analysis of translated protein sequences employing a maximum-likelihood tree revealed that *X. laevis* and *X. tropicalis* HSPB6 sequences grouped more closely with mammalian and reptilian HSPB6s than with fish HSPB6 amino acid sequences (Fig. 31). Additionally, representative HSPB5s from different classes of vertebrates grouped together rather than with HSPB6 proteins. A similar phylogenetic tree was obtained when only the conserved α-crystallin domains of the various sHSPs were used in this analysis (data not shown).

A comparison of *X. laevis* HSPB6 with other sHSP amino acid sequences

	Percent identity with *Xenopus laevis* HSPB6 (NP_001086479.1)
Amphibians	
X. tropicalis HSPB6 (XP_002940672.2)	94
X. tropicalis αB-crystallin/HSPB5 (XP_002932964.1)	53
X. laevis HSPB1/HSP27 (NP_001087285.1)	50
X. laevis αA-crystallin/HSPB4 (NP_001079340.1)	49
X. laevis HSP30C (NP_001165977.1)	43
X. laevis HSP30D (NP_001165976.1)	39
Reptiles	
P. sinensis HSPB6 (XP_014426555.1)	65
A. carolinensis HSPB6 (XP_003224996.2)	65
P. mucrosquamatus HSPB6 (XP_015672057.1)	64
G. japonicus HSPB6 (XP_015264062.1)	63
C. picta bellii HSPB6 (XP_005311592.1)	62
Mammals	
M. davidii HSPB6 (XP_006761589.1)	60
H. sapiens HSPB6 (AAH68046.1)	59
M. musculus HSPB6 (NP_001012401.1)	53
R. norvegicus HSPB6 (NP_620242.1)	54
Fish	
P. mexicana HSPB6 (XP_014844531.1)	51
P. nyererei HSPB6 (XP_005738449.1)	50
C. semilaevis HSPB6 (XP_008321765.1)	50
D. rerio HSPB6 (NP_001094428.1)	49

An amino acid sequence comparison of *Xenopus laevis* HSPB6 with HSPB6 from amphibians, reptiles, mammals, fish and other sHSPs from *Xenopus laevis* and *Xenopus tropicalis*. Genbank accession numbers are indicated within the brackets.

A comparison of the α-crystallin domain of HSPB6 with human HSPB6 and sHSPs of *X. laevis*

Percent identity with the α-crystallin domain of HSPB6 (NP_001086479.1)	
sHSP	**%**
H. sapiens	
HSPB6 (NP_653218.1)	71
X. laevis	
HSPB5 (AAI70250.1)	56
HSPB1 (NP_001087285.1)	51
MGC85304 (NP_001087283.1)	49
HSPB8 (NP_001079782.1)	42
HSP30C (NP_001165977.1)	44
HSP30D (NP_001165976.1)	40
HSPB7 (NP_001086558.1)	36

An amino acid sequence comparison of the α-crystallin domains of *X. laevis* HSPB6 and other sHSPs was generated using the Blast program. Genbank accession numbers are indicated within the brackets.

Figure 31. Phylogenetic relationships among vertebrate HSPB6 proteins. The tree was constructed using MEGA7 maximum-likelihood analysis of amino acid sequences and rooted to the yeast sHSP *S. cerevisiae* HSP26 (GenBank accession no. NP_009396.2), as described in Materials and methods. The tree was drawn to scale, with branch lengths measured in the number of substitutions per site. Bootstrap values (percentage of 1000 replicates) are shown above each branch. The GenBank accession numbers for the HSPB6 amino acid sequences are shown in Table 1 except for the following HSPB5 sequences: *R. norvegicus* HSPB5 (NP_037067.1); *M. musculus* (AAH10768); *D. rerio* (AAI62206); *G. japonicus* (XP_015271074.1); *A. carolinensis* (XP_008119279.1).

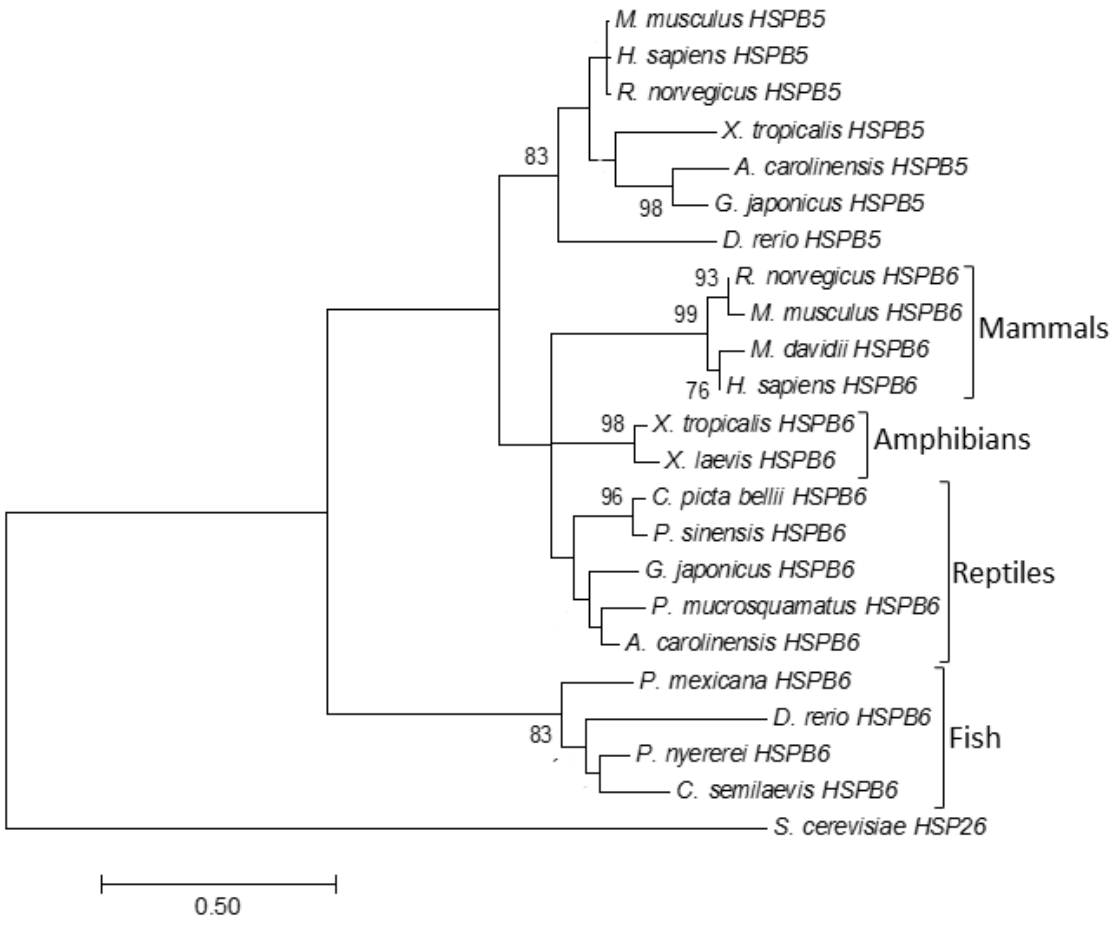
M. musculus HSPB5
H. sapiens HSPB5
R. norvegicus HSPB5
X. tropicalis HSPB5
A. carolinensis HSPB5
G. japonicus HSPB5
D. rerio HSPB5
R. norvegicus HSPB6
M. musculus HSPB6
M. davidii HSPB6
H. sapiens HSPB6
X. tropicalis HSPB6
X. laevis HSPB6
C. picta bellii HSPB6
P. sinensis HSPB6
G. japonicus HSPB6
P. mucrosquamatus HSPB6
A. carolinensis HSPB6
P. mexicana HSPB6
D. rerio HSPB6
P. nyererei HSPB6
C. semilaevis HSPB6
S. cerevisiae HSP26
83
98
93
99
76
98
96
83
Mammals
Amphibians
Reptiles
Fish
0.50

3.3.2. Immunoblot analysis of HSPB6 protein accumulation in Xenopus laevis A6 cells.

The next phase of this study examined the accumulation of HSPB6 in *X. laevis* A6 kidney epithelial cells subjected to various stressors including a 2 h 33 °C heat shock plus a 2 h recovery at 22 °C, treatment with the proteasomal inhibitor 30 μM MG132 or 100 μM cadmium chloride for 16 h at 22 °C (Fig. 32). The heat shock, MG132 and cadmium chloride treatments employed in this study were previously determined to induce the accumulation of HSP70 and HSP30 in A6 kidney epithelial cells (Gauley et al., 2008; Young and Heikkila, 2010; Khamis and Heikkila, 2013). Incubation of A6 cells at 33 °C did not significantly alter the relative level of HSPB6 above the level of untreated control cells. However, treatment of cells with 30 μM MG132 produced 2-fold increase in HSPB6 relative to control. Finally, incubation of A6 cells with 100 μM cadmium chloride induced a slight increase in HSPB6 levels compared to control that was only significant at $p < 0.1$. In other experiments, higher levels of cadmium chloride (200 or 400 μM) did not further enhance the relative levels of HSPB6 compared to 100 μM (data not shown). In contrast to HSPB6, all three stressors strongly induced the accumulation of HSP70. The relative levels of actin were not affected by these treatments.

3.3.3. Localization of HSPB6 in A6 cells.

An examination of HSPB6 localization in control A6 cells as well as after treatment with heat shock (HS), MG132 (MG) or cadmium chloride (Cd) was determined by immunocytochemistry and laser scanning confocal microscopy (Fig. 33). In control and heat shock treated cells, HSPB6 was localized primarily in the cytoplasm in a punctate or granular pattern at the periphery of the nucleus. I did not observe a detectable association of HSPB6 with actin stress fibers in control or stressor-treated cells. In some cells, a low level of HSPB6 was also detected within the nucleus. MG132 treatment resulted in an enhanced accumulation of

Figure 32. Relative levels of HSPB6 and HSP70 in cells subjected to heat shock or treated with MG132 or cadmium chloride. Cells were maintained at 22 °C (C) or incubated at 33 °C for 2 h followed by a recovery period at 22 °C for 2 h. Other flasks of cells were treated with 30 μM MG132 or 100 μM cadmium chloride for 16 h at 22 °C. A) Total protein was isolated and subjected to immunoblot analysis using an anti-HSPB6, anti-HSP70 or anti-actin antibody, with the representative immunoblot shown. ImageJ software was used to perform densitometric analysis of signal intensity for HSPB6 (panel B) and HSP70 (panel C) protein. The data for HSPB6 are expressed as a ratio to control levels while HSP70 is expressed as a percentage of the maximum band (30 μM MG132). Standard errors are represented by vertical bars. Statistical analysis was and the significant differences are indicated with an asterisk ($p < 0.05$) or a triangle ($p < 0.1$). These data are representative of at least 4 separate experiments.

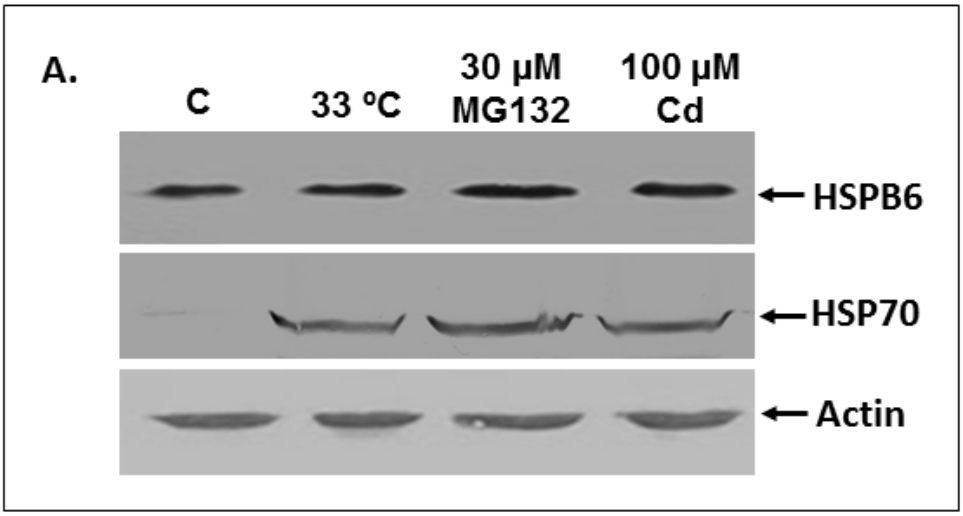
A.
C
33 ºC
30 µM MG132
100 µM Cd
HSPB6
HSP70
Actin

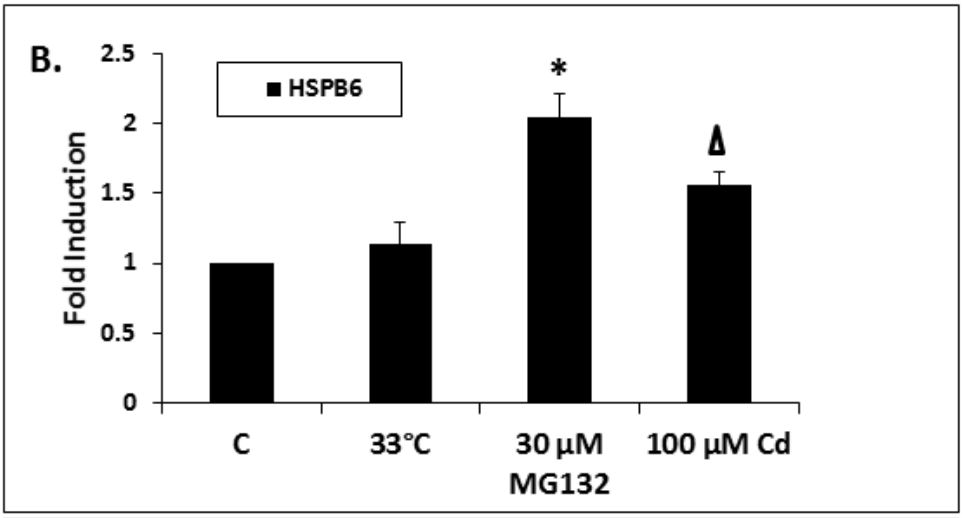
B.
HSPB6
Fold Induction
2.5
2
1.5
1
0.5
0
*
Δ
C
33°C
30 µM MG132
100 µM Cd

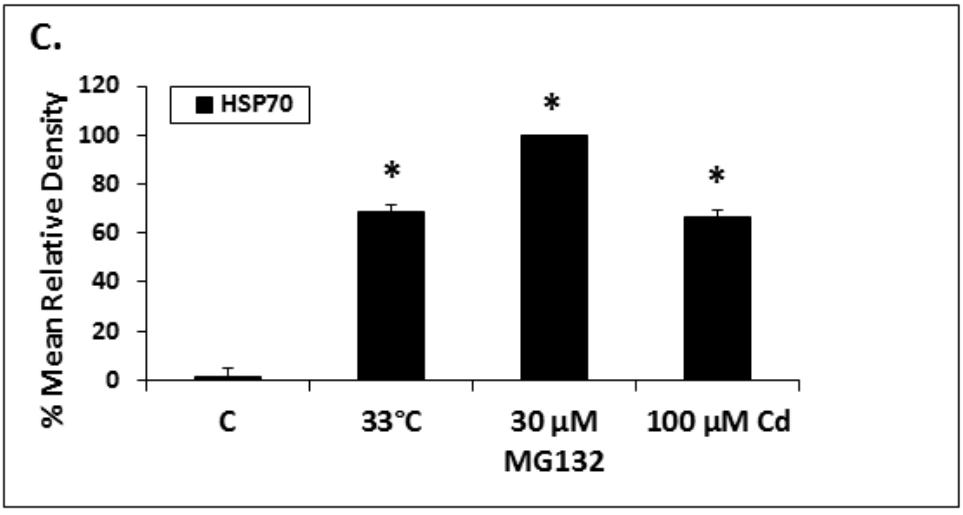
C.
HSP70
% Mean Relative Density
120
100
80
60
40
20
0
*
*
*
C
33°C
30 µM MG132
100 µM Cd

Figure 33. Localization of HSPB6 accumulation in A6 cells exposed to heat shock, MG132 or cadmium chloride. Cells were cultured on glass coverslips in L-15 media for 16 h at 22 °C (C) or incubated at 33 °C (HS) for 2 h followed by a 2 h recovery period at 22 °C. Other flasks of cells were treated with either 30 μM MG132 (MG) or 100 μM cadmium chloride (Cd) for 16 h at 22 °C. Actin and nuclei were stained directly with phalloidin conjugated to TRITC (red) and with DAPI (blue), respectively. HSPB6 was detected indirectly by an anti-HSPB6 antibody and Alexa-488 secondary antibody conjugate (green). From left to right, the columns display fluorescence detection channels for actin, HSPB6 and merged images which also contain DAPI staining. Yellow arrows indicate membrane ruffling of the F-actin cytoskeleton. The 20 μm white scale bar is shown. These images are representative of 4 different experiments.

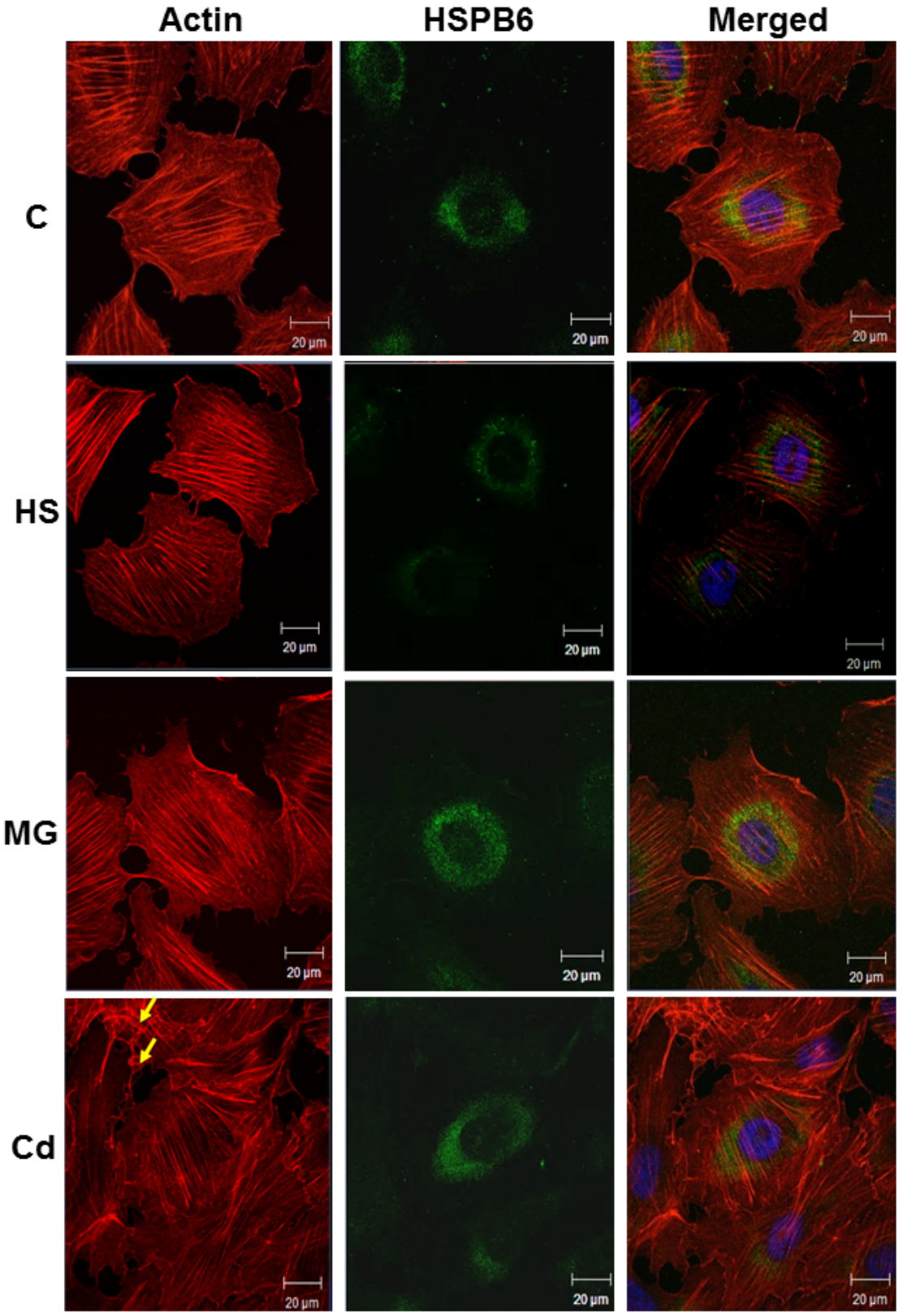
Actin
HSPB6
Merged
C
HS
MG
Cd
20 μm

HSPB6 in 90% of cells, in a granular pattern encircling the nucleus. Furthermore, cells treated with MG132 also displayed an increase in the relative amount of HSPB6 inside the nucleus. Cadmium chloride treatment slightly enhanced the relative level of HSPB6 in 40% of cells. This treatment also resulted in some cytoskeletal disorganization with increased membrane ruffling (yellow arrows).

Chapter 4: Discussion

The present study has investigated, for the first time in a poikilothermic model system, the effect of the ITCs, BITC, PEITC and SFN on the accumulation of the stress proteins HO-1, HSP70 and the sHSP, HSP30. In dose-response and/or time course studies performed with *X. laevis* A6 cells, it was determined that HO-1 accumulation was readily induced by each ITC. These findings with *Xenopus* HO-1 are in agreement with previous studies which observed ITC-induced HO-1 accumulation in human cell lines including prostate and liver cancer cells (Xu et al., 2006; Prawan et al., 2007). Also, pretreatment of A6 cells with a transcriptional or translational inhibitor repressed BITC-, PEITC or SFN-induced HO-1 accumulation suggesting that they were the result of *de novo* transcription and translation. Studies with mammalian cells have documented the transcriptional activation of *ho-1* gene expression in response to oxidative stress conditions involving the activation of Nrf2, the principal regulator of *ho-1* gene induction (Alam et al., 2000; Suzuki et al., 2003; Waisberg et al., 2003; Galazyn-Sidorczuk et al, 2009). Normally, Nrf2 is ubiquitinated and targeted for degradation by the UPS (Kobayashi, 2004; Choi et al., 2014). However, it was shown in mammalian cells that BITC- and PEITC-induced proteasomal inhibiton resulted in Nrf2 stabilization leading to the upregulation of *ho-1* gene expression (Stewart et al., 2003; Mi et al., 2008; 2011). In support of this mechanism, a study using rat adrenal pheochromocytoma cells found that an increase in Nrf2 stability was induced by treatment with the proteasomal inhibitor, MG132 (Martin et al., 2004). While BITC and PEITC likely induced HO-1 accumulation in A6 cells by means of this mechanism, it was possible that the mechanism associated with SFN was different since studies with murine and human cells found that SFN promoted proteasomal degradation activity (Parnaud et al., 2004; Kwak et al., 2007; Park et al., 2009). In agreement with these latter studies, I found that SFN did

not significantly alter the levels of ubiquitinated protein in A6 cells, which was indicative of a functional proteasome. It has been suggested that HO-1 accumulation in response to SFN treatment occurs by means of its rapid and prolonged binding and inactivation of glutathione, a key antioxidant, which then triggers the oxidative stress pathway (Mi et al., 2007). Finally, BITC-, PEITC- and SFN-induced HO-1 was inhibited by the HSF1 inhibitor, KNK437, in A6 cells. Although it is tenable that KNK437 could act on signalling proteins responsible for Nrf2 activation, my results indicate the potential involvement of HSF1 in *ho-1* gene expression. Previous studies employing KNK437 in our laboratory have consistently shown that this reagent inhibited HSP accumulation induced by a variety of stressors. In other studies, the effect of KNK437 on *hsp* mRNA or HSP accumulation was comparable to other means of inhibiting the HSF1 pathway including HSF1-targeted siRNA or generation of HSF1 knockout in somatic cells using CRISPR (Liu et al., 2012; Scheraga et al., 2016). As mentioned in the Introduction, an HSF1-binding DNA element, HSE, is present within the regulatory region of the *Xenopus ho-1* gene. Previously, our laboratory determined that heat shock did not induce HO-1 accumulaton, suggesting HSF1 activation is not sufficient for the expression of the *ho-1* gene (Music et al., 2014). However, it is possible HSF1 may play a role in stabilizing other transcription factors such as Nrf2, which is involved in ITC-induced *ho-1* gene expression (Alam and Cook, 2007; Koizumi et al., 2007).

Treatment of A6 cells with BITC, PEITC or SFN also induced an increase in HSP70. This finding was in agreement with studies examining the effect of ITCs on this molecular chaperone in mammalian cell lines (Gan et al., 2010; Sharma et al., 2010; Naidu et al., 2016). Gene expression inhibitor studies determined that the ITC-induced accumulation of *Xenopus* HSP70 in A6 cells was the result of *de novo* transcription and translation and involved the

transcription factor, HSF1. HSF1 activation, leading to *hsp* gene expression, is triggered by an increase in unfolded protein (Morimoto, 1998; Voellmy, 2004; Young and Heikkila, 2009). Since ITCs are electrophilic, it is possible that their interaction with cysteine thiol side chains found in hydrophobic pockets of targeted proteins resulted in conformational changes and/or protein unfolding, which lead to the initiation of the heat shock response (Mi et al., 2008). In contrast to HSP70, PEITC or SFN treatment of A6 cells did not induce HSP30 accumulation while BITC treatment resulted in relatively low levels of this sHSP. The reason for the differences in the ability to detect HSP70 and HSP30 accumulation following ITC treatments is not clear at this time. However, differences in the relative level of different HSPs or their mRNAs in response to various stressors such as heavy metals, metalloids, proteasomal inhibitors and heat shock in A6 cells have been reported (Gauley and Heikkila, 2007; Young et al., 2010; Khan et al., 2010; Walcott and Heikkila, 2010).

A6 cells treated with ITCs were also incubated at 30 °C to investigate whether an increase in incubation temperature affected the relative level of ITC-induced HO-1 and HSP accumulation. Exposure of cells to BITC, PEITC or SFN at 30 °C produced lower HO-1 accumulation levels than at 22 °C. This finding was in contrast to other stressors examined in our laboratory, which determined that treatment of A6 cells with low concentrations of either cadmium or arsenite at 30 °C enhanced the levels of HO-1 accumulation compared to 22 °C (Music et al., 2014). While the reason for the decrease in ITC-induced HO-1 accumulation at the higher incubation temperature is not known, it is possible that the reduced levels of HO-1 accumulation may be due to an inhibition of *ho-1* gene expression or decreased stability.

Treatment of A6 cells with BITC or SFN at 30 °C enhanced HSP70 accumulation relative to 22 °C but only enhanced HSP30 levels in cells exposed to BITC. Our laboratory has

observed a similar phenomenon in which various stressors (e.g. MG132, cadmium chloride, sodium arsenite or curcumin) plus a 30 °C incubation temperature acted synergistically in the induction of HSP70 and HSP30 accumulation (Woolfson and Heikkila, 2009; Young et al., 2009; Khan and Heikkila, 2011; Khamis and Heikkila, 2013). It is possible that the amount of ITC-induced unfolded and/or damaged protein which resulted from proteasomal inhibition or covalent interactions with thiol groups of cellular protein was enhanced at the higher incubation temperature. In contrast to individual stressors, it was suggested that the elevated levels of unfolded or damaged protein induced by multiple stressors can exceed a set point or threshold level, such that there is a strong activation of HSF1 leading to increased *hsp* gene expression (Young et al., 2009; Khamis and Heikkila, 2013; Heikkila, 2017). Studies with various model systems such as intertidal mussels, HeLa cells, mouse T-lymphocytes and testis and *Xenopus* heart have confirmed the existence of an HSF1 threshold level (Sarge, 1995; Lee et al., 1995; Ali et al., 1997; Buckley et al., 2001; Gothard et al., 2003).

Immunocytochemical analysis determined that BITC, PEITC or SFN induced the accumulation of HO-1 primarily in the perinuclear region in a punctate pattern with some HO-1 present in the nucleus. Mammalian studies reported the ability of HO-1 to translocate to the nucleus or mitochondria in response to stress conditions (Converso et al., 2006; Slebos et al., 2007; Lin et al., 2007; Gandini et al., 2012; Namba et al., 2014). Larger HO-1 structures were also detected in 30% of A6 cells treated with BITC at 30 °C. A previous study determined that NADPH cytochrome P450 reductase promoted the oligomerization of HO-1 into larger complexes, which also contained biliverdin reductase (Huber et al., 2009; Linnenbaum et al., 2012). It is possible that BITC treatment at 30 °C elicited a similar oligomerization of HO-1 into higher ordered complexes. In A6 cells treated with BITC at 30 °C, HSP30 occurred in a granular

pattern with occasional larger structures, which were reported previously in our laboratory in A6 cells in response to a variety of stressors (Gellalchew and Heikkila, 2005; Voyer and Heikkila, 2008; Woolfson and Heikkila, 2009; Young and Heikkila, 2010; Khan et al., 2015). The granular pattern of ITC-induced HSP30 was likely due to stress-induced multimeric complex formation, which is necessary for HSP30 molecular chaperone function (Ohan et al., 1998; MacRae, 2000; Fernando and Heikkila, 2000; Van Montfort et al., 2001; Fernando et al., 2003). The current study also determined that treatment of A6 cells with either BITC, PEITC or SFN caused F-actin cytoskeletal disorganization. Similar effects were noted after sodium arsenite or cadmium chloride treatment of amphibian and mammalian cultured cells (Li and Chou, 1992; Gellalchew and Heikkila, 2005; Woolfson and Heikkila, 2009; Khamis and Heikkila, 2013; Khan et al., 2015). Although minimal information is available on the effect of ITCs on the actin cytoskeleton, it was reported that two cysteine residues conserved within all actin isoforms were vulnerable to oxidative stress (Dalle-Donne et al., 2001). Therefore, it is conceivable that these two nucleophilic residues found within the actin molecule are targets for ITC modification, inducing actin cytoskeletal disorganization and membrane ruffling.

In this study, treatment of *X. laevis* A6 cells with BITC or PEITC significantly enhanced the relative levels of ubiquitinated protein. Studies with HeLa cells also reported an increase in ubiquitinated protein levels after exposure to either ITC (Mi et al., 2009). BITC and PEITC also inhibited the proteasome in multiple myeloma cells specifically repressing chymotrypsin-like, trypsin-like and caspase-like enzyme activities in a concentration-dependent manner (Mi et al., 2010). In this latter study, it was suggested that BITC and PEITC bound directly to susceptible cysteine residues within the proteasome B3 subunit, which protrudes into the active site of the B2 subunit. It is possible that ITC treatment inhibited the proteasome of A6 cells, which resulted

in the accumulation of ubiquitinated protein. BITC- and PEITC-induced ubiquitinated protein levels were greater in cells treated with ITCs at 22 °C than at 30 °C. This finding was not unexpected given that treatment of A6 cells at 30 °C alone reduced the relative level of ubiquitinated protein compared to control. Furthermore, it was possible that treatment of cells with ITCs at an elevated temperature may have an enhanced effect on the thiols associated with cysteine residues of enzymes that function in the addition of ubiquitin to proteins targeted for degradation. Alternatively, it was tenable that elevated levels of HSPs in ITC-treated cells at 30 °C bound to target proteins and prevented them from being targeted for degradation via ubiquitination. In support of this latter possibility, a potential relationship between an increase in HSP accumulation and a decrease in levels of ubiquitinated protein was reported in pear cells (Ferguson et al., 1994).

Immunocytochemical analysis employing the Proteostat aggresome detection assay determined that exposure of cells to BITC or PEITC increased the levels of aggregated protein structures relative to control. While ITC-induced proteasomal inhibition may have elevated the level of aggregated protein in A6 cells, studies with mammalian cell demonstrated the direct ability of ITCs to covalently bind and modify cysteine residues within proteins including α- and β-tubulin, resulting in conformational changes, exposure of hydrophobic regions and ultimately their aggregation (Mi et al., 2008; 2009; Xiao et al., 2012). Given that the tubulin family comprises 3-4% of the total protein in eukaryotic cells, the binding of ITCs to this protein alone could have accounted for a substantial portion of aggregated protein observed in A6 cells (Oakley, 2000). Other proteins that were found to be targeted by ITCs include proteasomal subunits, cytochrome P450s, HDAC6 and macrophage migration inhibitory factor (Fimognari et al., 2008; Gibbs et al., 2009; Ouertatani-Sakouhi et al., 2009). In comparison to BITC and

PEITC, treatment with the proteasomal inhibitor, MG132, resulted in aggregated protein and the formation of numerous aggresome-like structures in the perinuclear region of cells. This finding was in agreement with previous studies conducted in our laboratory as well as in mammalian cells including HeLa, embryonic kidney, glioma, neuroblastoma, adenocarcinoma, oligodendroglial neuronal and astrocyte cells (Ito et al., 2002; Bauer and Richter-Landsberg, 2006; Goldbaum et al., 2009; Bolhuis and Richter-Landsberg, 2010; Shen at al., 2011; Bang et al., 2014; Khan et al., 2015). As mentioned in the Introduction, these aggresome-like structures result from the coalescence of individual protein aggregates, which are then transported to the perinuclear region along microtubule filaments employing a dynein motor (Kopito, 2000; Ito et al., 2002; Rodriguez-Gonzalez et al., 2008; Driscoll and Chowdhury, 2012; Hao et al., 2013; Richter-Landsberg and Leyk, 2013). In contrast to MG132, very few large aggregated protein structures were present in cells exposed to BITC or PEITC.

Since soluble tubulin and microtubule filaments, as mentioned above, were determined to be the primary targets of BITC or PEITC, this phenomenon was investigated in A6 cells. Immunoblot analysis revealed that BITC decreased α-tubulin accumulation to a greater extent than PEITC in a concentration- and time-dependent manner. A similar phenomenon was reported in human non-small lung cancer, breast cancer, colon carcinoma, prostate cancer and HeLa cells (Mi et al., 2008; 2009). Since BITC is a smaller compound, containing a methyl group extending from its aromatic hydrocarbon compared to an ethyl group for PEITC, it has greater accessibility to cysteine residues buried within the tubulin molecule thus increasing its affinity for the protein (Mi et al., 2008).

Immunocytochemical analysis determined that exposure of A6 cells to BITC induced microtubule filament fragmentation in a time-dependent manner. Furthermore, the effect of

BITC was enhanced when cells were incubated at 30 °C. Disruption and degradation of the microtubule network by this ITC was also observed in immunocytochemical studies conducted in mammalian cells (Mi et al., 2008; 2009). Given that BITC and PEITC induced decreased levels of α-tubulin and caused the fragmentation of microtubule filaments in A6 cells, it was likely that these phenomena blocked the translocation of aggregated protein to the perinuclear region to form aggresome-like structures. The possibility that BITC could inhibit aggresome-like structure formation in A6 cells was supported by a series of experiments showing that a 2 or 4 h pretreatment of cells with BITC inhibited the accumulation of aggresome-like structures by MG132, a reversible proteasome inhibitor. A diagramatic comparison of the effect of BITC and MG132 on aggregated protein and aggresome formation is shown in Figure 34. It should be mentioned that factors other than microtubule filament fragmentation may be responsible for the lack of transport of aggregated protein in BITC-treated cells including the conformational change of dynein which is required for the movement of protein aggregates along filaments. These results are of significance, as they not only elucidated BITC's ability to induce aggregated protein, but in this work I have also shown how ITCs can potentially interfere with the translocation of aggregated protein to the perinuclear region, therefore inhibiting aggresome-like structure formation.

Finally, during the course of this study I determined that ITCs did not have a significant effect on the accumulation of a previously uncharacterized *Xenopus laevis* sHSP, namely, HSPB6 (HSP20). Given the lack of information on *Xenopus* HSPB6, I examined the properties of this protein encoded by a cDNA that had been sequenced in our laboratory. Alignment of the *X. laevis* HSPB6 amino acid sequence with HSPB6 proteins from various organisms indicated that it had 94% identity with *X. tropicalis* HSPB6, 62-65% with selected reptiles, 54-60% with

Figure 34. Movement of aggresome-like structures along microtubules. A) When the capacity of the UPS is exceeded or inhibited by agents like MG132, aggregated protein (red) is anchored to dynein motors and translocated (white arrows) along microtubule filaments to the perinuclear region of the cell to form aggresome-like structures (orange). The aggresome is ultimately degraded by autophagy. B) BITC pretreatment caused microtubule filament fragmentation, which inhibited MG132-induced protein aggregates from being transported along the microtubule filaments to the perinuclear region where they form aggresome-like structures. In these BITC-pretreated cells, potentially toxic aggregated protein remain dispersed throughout the cell.

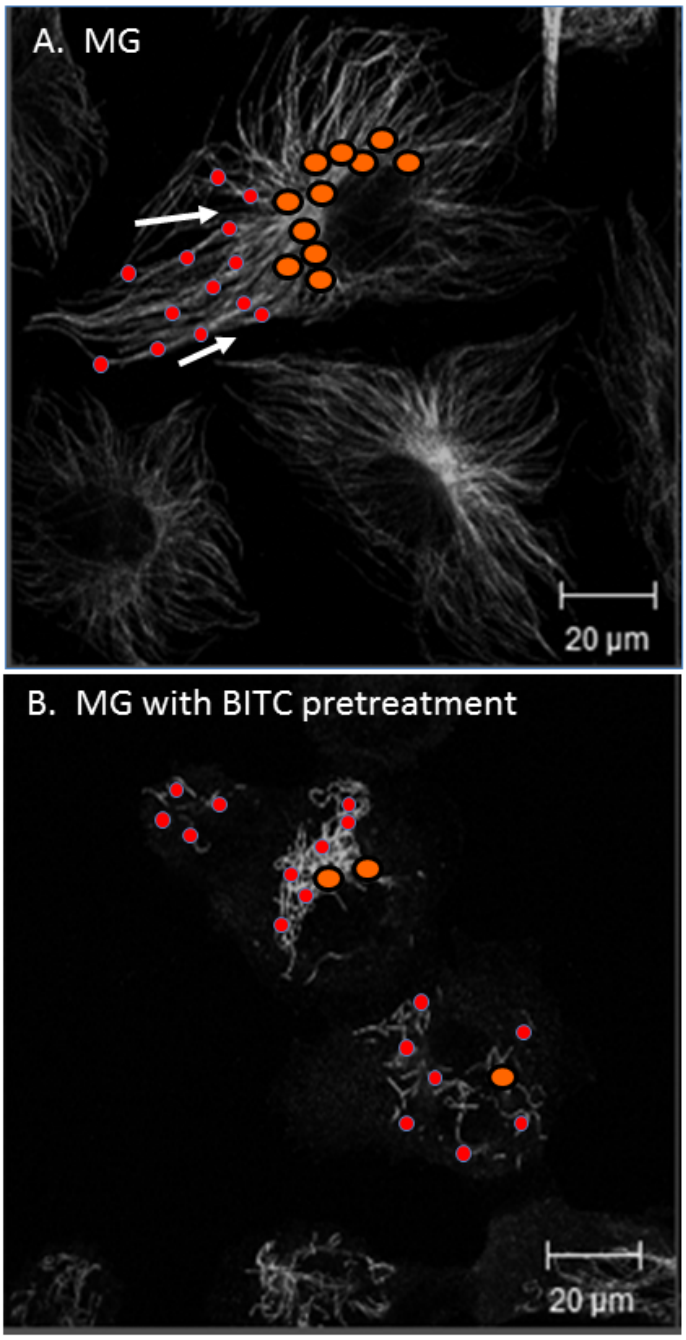
A. MG
20 µm
B. MG with BITC pretreatment
20 µm

mammalian HSPB6 proteins, and 49-51% with HSPB6 from various fish species. Also, *X. laevis* HSPB6 displayed 53% identity with *X. tropicalis* HSPB5 and 49% with *X. laevis* HSPB4 as well as 50, 43 and 39% identity with *X. laevis* HSPB1 (HSP27), HSP30C and HSP30D, respectively. Most of the identity shared among *X. laevis* HSPB6 and HSPB6's from other vertebrates was found in the α-crystallin domain. These findings support the results of previous studies showing the general lack of conservation of sHSPs between species except for the α-crystallin domain (Arrigo and Landry, 1994; Lindner et al., 1998; MacRae, 2000; Stromer et al., 2003).

Phylogenetic analysis indicated that *X. laevis* HSPB6 grouped with reptile and mammalian HSPB6 sequences but was distinct from amphibian, reptilian, mammalian and fish HSPB5 amino acid sequences. However, HSPB5 and HSPB6 sequences did share an older common ancestor. Additionally, fish HSPB6 amino acid sequences grouped together outside of the other HSPB6 and HSPB5 proteins mentioned above. Examination of the *X. laevis* HSPB6 amino acid sequence revealed that it has an 18 amino acid C-terminal extension containing approximately 13 polar residues. In contrast, the comparable regions of the human HSPB6 C-terminal regions had only 3 of 11 polar residues while rat and mouse both had 5 of 14. The high polarity of the C-terminal extension of *X. laevis* HSPB6 may be important for its molecular chaperone activity. Our previous results with *X. laevis* HSP30C determined that its C-terminal extension, which also had a high proportion of polar residues was essential for its solubility, maintenance of secondary structure and optimal chaperone activity (Fernando and Heikkila, 2000; Fernando et al., 2002). While the HSPB6 C-terminal extension in mammals contains fewer polar residues than *X. laevis* HSPB6, this region was important in the protection of mouse cardiomyocytes against simulated ischemia/reperfusion injury (Islamovic et al., 2007). Analysis of the *X. laevis* HSPB6 amino acid sequence with phosphorylation site prediction

software suggested the presence of multiple serine phosphorylation sites. Compared to human, rat and mouse HSPB6, the only conserved potential phosphorylation site in *X. laevis* HSPB6 is at serine 59. In rat, this site was phosphorylated in vitro by cAMP-dependent kinase but it is not known whether this serine is phosphorylated *in vivo* (Beall et al., 1999). Only future *in vivo* analysis will determine if this site and others are phosphorylated in *X. laevis* HSPB6.

Immunoblot and immunocytochemical analysis revealed that HSPB6 was detected constitutively in *X. laevis* A6 kidney epithelial cells. Most studies characterizing the properties of HSPB6 accumulation and function have been carried out in mammals, where HSPB6 was similarly detected constitutively at high levels, in different types of muscle tissue but also found in brain, stomach, liver, lung blood and kidney (Kato et al., 1994). While treatment of A6 cells with heat shock or ITCs did not induce a significant increase in the relative levels of HSPB6, treatment with cadmium chloride resulted in a minor increase whereas exposure to the proteasomal inhibitor, MG132 induced a 2-fold increase. In contrast, these stressors induced a 10-16-fold increase in HSP70 levels. The lack of an increase in HSPB6 levels in response to heat shock treatment of A6 cells agrees with previous results in fish and mammalian systems, which suggest that HSPB6 is not heat-inducible and likely does not depend on the action of HSF1 (Fan et al., 2005; Marvin et al., 2008; Kirbach and Golenhofen, 2011; Mymrikov et al., 2011). It was suggested that other signalling pathways may regulate the relative level of HSPB6 as well as its function (Mymrikov et al., 2011). For example, in a mouse model of glomerulonephritis, renal cortices of diseased mice demonstrated an enhanced accumulation of HSPB6 without an increase in HSP70, suggesting a lack of a generalized stress response (Guess et al., 2013). Also, increased levels of HSPB6 were reported in dog and rat heart due to congestive heart failure or exercise and also in rat bladder in response to partial urethral ligation (Batts et al., 2006; Boluyt et al.,

2006; Dohke et al., 2006). While the mechanism(s) associated with the increase in *X. laevis* HSPB6 levels in response to cadmium or MG132 is unclear, it is likely that their enhanced levels may be due at least in part, to a reduction in HSPB6 degradation since both cadmium and MG132 were found to inhibit the ubiquitin-proteasome system in *Xenopus* A6 cells (Young and Heikkila, 2010; Brunt et al., 2012; Khan et al., 2012; Khamis and Heikkila, 2013; Khan et al., 2015).

Immunocytochemical analysis of HSPB6 determined that it occurred as granular structures primarily in the cytoplasm in control and in heat shock-, MG132- and cadmium-treated A6 cells. A cytoplasmic localization of HSPB6 was also reported in swine carotid artery smooth muscle and in rat myocardial cells (Van de Klundert et al., 1998; Rembold and Zhang, 2001; Pipkin et al., 2003; Sin et al., 2015). In *Xenopus* A6 cells, HSPB6 was enriched in the cytoplasm at the nuclear periphery and in some cells low levels of HSPB6 were detected within the nucleus. The presence of *X. laevis* HSPB6 at the periphery of the nucleus is of interest since rat myocyte HSPB6 was shown to act as a nuclear import chaperone for protein kinase D1, which is important in the regulation of cardiac transcription during development (Sin et al., 2015).

Future Directions

In this thesis, I determined that treatment of A6 cells with ITCs enhanced the levels of HO-1. Further studies employing an Nrf2 inhibitor should be conducted to assess whether Nrf2 stability and/or activation contributed to ITC-induced HO-1 accumulation. Brusatol, a chemical compound known to sensitize cancer cells and increase efficacy of therapeutic agents, has the ability to supress the Nrf2 pathway through increased ubiquitination and subsequent degradation of this transcription factor (Ren at al., 2011). Therefore, it would be possible to inhibit the

synthesis of Nrf2 in A6 cells with a pretreatment of this compound for 6 h prior to ITC exposure. Subsequent immunoblot analysis revealing HO-1 protein levels could help to determine whether transcriptional activation of the *ho-1* gene involves Nrf2 activity.

Additionally, given that numerous mammalian studies have investigated and reported ITC-induced cell cycle arrest, it would be interesting to examine the effect of ITCs on the A6 cell cycle (Zhang et al, 2006; Mi et al., 2008; Mi et al., 2009). Specifically, this would involve an investigation of whether ITC-induced tubulin degradation is associated with cell cycle arrest in A6 cells employing flow cytometry. Immunofluorescence of both tubulin and DNA content would elucidate a potential correlation between ITC-induced degradation of tubulin and an increase in population of A6 cells in the G_2/M phase. Given the critical role of tubulin in the formation mitotic spindles to segregate replicated chromosomes, immunofluorescence of a mitotic biomarker such as histone 3 would indicate whether ITC-induced cell cycle arrest occurred specifically during the mitotic phase.

Finally, research conducted in *Xenopus laevis* A6 cells could be extended to eggs and embryos, which are large and amenable for injection of macromolecules such as DNA, mRNA, morpholino antisense oligonucleotides and protein (Krone and Heikkila, 1989; Heikkila, 1990; Kay and Peng, 1991; Gurdon, 2006; Liu, 2006). Given the large amount of information available on *Xenopus* embryogenesis, it would be an excellent system to monitor the effect of ITCs on early development. Since *hsp* gene expression in *Xenopus* embryos has been well characterized in response to heat and chemical stress, future studies could easily assess the effect of ITCs on *hsp* mRNA and protein levels in embryos employing Northern and Western blot analysis, respectively. Furthermore, the use of whole-mount in situ hybridization and immunocytochemistry could determine the spatial distribution of ITC-induced *hsp30* mRNA and

encoded protein in *Xenopus* embryos. In addition, it would be of interest to monitor the impact of ITCs on the expression of *ho-1* genes in embryos. Only the constitutive accumulation of *ho-1* mRNA has been examined during *Xenopus* development.

References

Abraham, N.G., Kappas, A., 2008. Pharmacological and clinical aspects of heme oxygenase. Pharmacol. Rev. 60, 79-127.

Acunzo, J., Katsogiannou, M., Rocchi, P., 2012. Small heat shock proteins HSP27 (HspB1) αB-crystallin (HspB5) and HSP22 (HspB8) as regulators of cell death. Int. J. Biochem. Cell Biol. 44, 1622-1631.

Alam, J., Wicks, C., Stewart, D., Gong, P., Touchard, C., Otterbein, S., Choi, A.M.K., Burow, M.E., Tou, J., 2000. Mechanism of heme oxygenase-1 gene activation by cadmium in MCF-7 mammary epithelial cells: role of p38 kinase and Nrf2 transcription factor. J. Biol. Chem. 275, 27694-27702.

Alam, J. and Cook, J., 2007. How many transcription factors does it take to turn on the heme oxygenase-1 gene? Am. J. Respir. Cell Mol. Biol. 36, 166-174.

Alberts, B., 2002. The Self-Assembly and Dynamic Structure of Cytoskeletal Filaments. Molecular Biology of the Cell. 4th Edition.

Ali, A., Fernando, P., Smoth, W.L., Ovsenek, N., Lepock, J.R., Heikkila, J.J., 1997. Preferential activation of HSF-binding activity and hsp70 gene expression in *Xenopus* heart after mild hyperthermia. Cell Stress Chaperones. 2, 229-237.

An, H., Statsyuk, A., 2015. An inhibitor of ubiquitin conjugation and aggresome formation. Chem. Sci. 6, 5235-5245.

Anckar, J., Sistonen, L., 2011. Regulation of HSF1 function in the heat stress response: implications in aging and disease. Annu. Rev. Biochem. 80, 1089-115.

Araujo, J.A., Zhang, M., Yin, F., 2012. Heme oxygenase-1 oxidation, inflammation, and atherosclerosis. Front Pharmacol. doi: 10.3389/fphar.2012.00119.

Arrigo, A.-P., Landry, J. 1994. Expression and function of the low-molecular weight heat shock proteins. In: R.I. Morimoto, A. Tissieres, and C. Georgopoulos (Eds.), The Biology of Heat Shock Proteins and Molecular Chaperones. Cold Spring Harbor Laboratory Press. Cold Spring Harbor, N.Y, pp. 335-373.

Backthisaran, R., Tangirala, R., Rao, Ch.M., 2015. Small heat shock proteins: Role in cellular functions and pathology. Biochim. Biophys. Acta. 1854, 291-319.

Balch, W.E., Morimoto, R.I., Dillin A., Kelly J.W., 2008. Adapting proteostasis for disease intervention. Science. 319, 916-919.

Bang, Y., Kang, B.Y., Choi, H.J., 2014. Preconditioning stimulus of proteasome inhibitor enhances aggresome formation and autophagy in differentiated SH-SY5Y cells. Neurosci. Lett. 566, 263-268.

Basha, E., O'Neill, H., Vierling, E., 2012. Small heat shock proteins and α-crystallins: dynamic proteins with flexible functions. Trends Biochem. Sci. 37, 106-17.

Bassermann, F., Eichner, R., Pagano, M., 2014. The ubiquitin proteasome system – implications for cell cycle control and the targeted treatment of cancer. Biochim. Biophys. Acta. 1843, 150-162.

Batts, T.W., Klausner, A.P., Jin, Z., Meeks, M.K., Ripley, M.L., Yang, S.K., Tuttle, J.B., Steers, W.D., Rembold, C.M., 2006. Increased expression of heat shock protein 20 and decreased contraction stress in obstructed rat bladder. J. Urol. 176, 1679-1684.

Bauer, N.G., Richter-Landsberg, C., 2006. The dynamic instability of microtubules is required for aggresome formation in oligodendroglial cells after proteolytic stress. J. Mol. Neurosci. 29, 153-168.

Beall, A., Bagwell, D., Woodrum, D., Stoming, T.A., Kato, K., Suzuki, A., Rasmussen, H., Brophy, C.M., 1999. The small heat shock-related protein, HSP20, is phosphorylated on serine 16 during cyclic nucleotide-dependent relaxation. J. Biol. Chem. 274, 11344-11351.

Beere, H.M., Wolf, B.B., Cain, K., Mosser, D.D., Mahboubi, A., Kuwana, T., Tailor, P., Morimoto, R.I., Cohen, G.M., Green, D.R., 2000. Heat-shock protein 70 inhibits apoptosis by preventing recruitment of procaspase-9 to the apaf-1 apoptosome. Nat. Cell Biol. 2, 469-475.

Bellaye, P.S., Burgy, O., Causse, S., Garrido, C., Bonniaud, P., 2014. Heat shock proteins in fibrosis and wound healing: good or evil? Pharmacol. Ther. 143, 119-32.

Bhattacharyya, S., Yu, H., Mim, C., Matouschek, A., 2014. Regulated protein turnover: snapshots of the proteasome in action. Nat. Rev. Mol. Cell Biol. 15, 122-133.

Bienz, M., 1984. Developmental control of the heat shock response in *Xenopus*. Proc. Natl. Acad. Sci. U. S. A. 81, 3138-3142.

Bolhuis, S., Richter-Landsberg, C., 2010. Effect of proteasome inhibition by MG-132 on HSP27 oligomerization, phosphorylation, and aggresome formation in the OLN-93 oligodendroglia cell line. J. Neurochem. 114, 960-971.

Boluyt, M.O., Brevick, J.L., Rogers, D.S., Randall, M.J., Scalia, A.F., Li, Z.B., 2006. Changes in the rat proteome induced by exercise training: increased abundance of heat shock protein, hsp20. Proteomics. 6, 3154-3169.

Briant, D., Ohan, N., Heikkila, J.J., 1997. Effect of herbimycin A on *hsp30* and *hsp70* heat shock protein gene expression in *Xenopus* cultured cells. Biochem. Cell Biol. 75, 777-782.

Brunt, J.J., Khan, S., Heikkila, J.J., 2011. Sodium arsenite and cadmium chloride induction of proteasome inhibition and HSP accumulation in *Xenopus laevis* A6 kidney epithelial cells. Comp. Biochem. Physiol. C Toxicol. Pharmacol. 155, 307-317.

Buckley, B.A., Owen, M.-E., Hofmann, G.E., 2001. Adjusting the thermostat: the threshold induction temperature for the heat-shock response in intertidal mussels (genus *Mytilus*) changes as a function of thermal history. J. Exp. Biol. 204, 3571-3579.

Bukach, O.V., Seit-Nebi, A.S., Marston, S.B., Gusev, N.B., 2004. Some properties of human small heat shock protein HSP20 (HspB6). Eur. J. Biochem. 271, 291-302.

Chang, M., Xue, J., Sharma, V., Habtezion, A., 2015. Protective role of hemeoxygenase-1 in gastrointestinal diseases. Cell Mol. Life Sci. 72, 1161-73.

Chau, L.Y., 2015. Heme oxygenase-1: emerging target of cancer therapy. J. Biomed. Sci. doi: 10.1186/s12929-015-0128-0.

Choi, A.M. and Alam, J., 1996. Heme oxygenase-1: function, regulation, and implication of a novel stress-inducible protein in oxidant-induced lung injury. Am. J. Respir. Cell Mol. Biol. 15, 9-19.

Choi, R.J., Cheng, M.S., Shik, K.Y., 2014. Desoxyrhapontigenin up-regulates Nrf2-mediated heme oxygenase-1 expression in macrophages and inflammatory lung injury. Redox Biol. 18, 504-512.

Converso, D.P., Taillé, C., Carreras, M.C., Jaitovich, A. Poderoso, J.J., Boczkowski, J., 2006. HO-1 is located in liver mitochondria and modulates mitochondrial heme content and metabolism. FASEB J. 20, 1236-1238.

Dalle-Donne, I., Rossi, R., Milzani, A., Di Simplicio, P., Colombo, R., 2001. The actin cytoskeleton response to oxidants: from small heat shock protein phosphorylation to changes in the redox state of actin itself. Free Radic. Biol. Med. 31, 1624-1632.

Darasch, S., Mosser, D.D., Bols, N.C., Heikkila, J.J., 1988. Heat shock gene expression in *Xenopus laevis* A6 cells in response to heat shock and sodium arsenite treatments. Biochem. Cell Biol. 66, 862-868.

Daugaard, M., Rohde, M., Jäättelä, M., 2007. The heat shock protein 70 family: Highly homologous proteins with overlapping and distinct functions. FEBS Lett. 581, 3702-3710.

Deshaies, R.J., 2014. Proteotoxic crisis, the ubiquitin-proteasome system, and cancer therapy. BMC Biol. doi: 10.1186/s12915-014-0094-0.

Dinkova-Kostova, A.T., 2012. The role of sulfhydryl reactivity of small molecules for the activation of the KEAP1/NRF2 pathway and the heat shock response. Scientifica. doi: 10.6064/2012/606104.

Dohke, T., Wada, A., Isono, T., Fuji, M., Yamamoto, T., Tsutamoto, T., Horie, M., 2006. Proteomic analysis reveals significant alternations of cardiac small heat shock protein expression in congestive heart failure. J. Card. Fail. 12, 77-84.

Dominguez, R., Holmes, K., 2011. Actin Structure and Function. Annu. Rev. Biophys. 40, 169-186.

Dou, Q.P., 2014. Resistance to proteasome inhibitors in cancer: molecular mechanisms and strategies to overcome resistance. Medical. 242-348.

Dreiza, C.M., Komalavilas, P., Furnish, E.J., Flynn, C.R., Sheller, M.R., Smoke, C.C., Lopes, L.B., Brophy, C.M., 2010. The small heat shock protein, HSPB6, in muscle function and disease. Cell Stress Chaperones. 15, 1-11.

Driscoll, J.J., Chowdhury, R.D., 2012. Molecular crosstalk between the proteasome, aggresomes and autophagy: translational potential and clinical implications. Cancer Lett. 325, 147-154.

Dufour, V., Alazzam, B., Ermel, G., Thepaut, M., Rossero, A., Tresse, O., Baysse, C., 2012. Antimicrobial activities of isothiocyanates against *Campylobacter jejuni* isolates. Front Cell Infect. Microbiol. doi: 10.3389/fcimb.2012.00053.

Dufour, V., Stahl, M., Rosenfeld, E., Stintzi, A., Baysse, C., 2013. Insights into the mode of action of benzyl isothiocyanate on *Campylobacter jejuni*. Appl. Environ. Microbiol. 79, 6958-68.

Edwards, H.V., Cameron, R.T., Baillie, G.S., 2011. The emerging role of HSP20 as a multifunctional protective agent. Cell Signal. 23, 1447-1454.

Eiserich, J.P., Estevez, A.G., Bamberg, T.V., Ye, Y.Z., Chumley, P.H., Beckman, J.S., Freeman, B.A., 1999. Microtubule dysfunction by posttranslational nitrotyrosination of alpha-tubulin: a nitric oxide-dependent mechanism of cellular injury. Proc. Natl. Acad. Sci. U. S. A. 96, 6365-6370.

Elicker, K.S., Hutson, L.D., 2007. Genome-wide analysis and expression profiling of the small heat shock proteins in zebrafish. Gene. 403, 60-69.

European Food Safety Authority, 2012. Perfluoroalkylated substances in food: occurrence and dietary exposure. EFSA Journal. 10, 2743.

Fan, G.C., Chu, G., Kranias, E.G., 2005. Hsp20 and its cardioprotection. Trends Cardiovasc. Med. 15, 138-141.

Ferguson, I.B., Lurie, S., Bowen, J.H., 1994. Protein Synthesis and Breakdown during Heat Shock of Cultured Pear (*Pyrus communis* L.) Cells. Plant Physiol. 104, 1429-1437.

Fernando, P., Heikkila, J.J., 2000. Functional characterization of *Xenopus* small heat shock protein, Hsp30C: The carboxyl end is required for stability and chaperone activity. Cell Stress Chaperones. 5, 148-159.

Fernando, P., Abdulle, R., Mohindra, A., Guillemette, J.G., Heikkila, J.J., 2002. Mutation or deletion of the C-terminal tail affects the function and structure of *Xenopus laevis* small heat shock protein, hsp30. Comp. Biochem. Physiol. B Biochem. Mol. Bol. 133, 95-103.

Fernando, P., Megeny, L.A., Heikkila, J.J., 2003. Phosphorylation-dependent structural alterations in the small hsp30 chaperone are associated with cellular recovery. Exp. Cell Res. 286, 175–185.

Fimognari, C., Lenzi, M., Hrelia, P., 2008. Interaction of the isothiocyanate sulforaphane with drug disposition and metabolism: pharmacological and toxicological implications. Curr. Drug Metab. 9, 668-678.

Franck, E., Madsen, O., van Rheede, T., Ricard, G., Huynen, M.A., de Jong, W.W., 2004. Evolutionary diversity of vertebrate small heat shock proteins. J. Mol. Evol. 59, 792-805.

Galazyn-Sidorczuk, M., Brzoska, M.M., Jurczuk, M., Moniuszko-Jakoniuk, J., 2009. Oxidative damage to proteins and DNA in rats exposed to cadmium and/or ethanol. Chem. Biol. Interac. 180, 31-38.

Gan, N., Wu, Y.C., Brunet, M., Garrido, C., Chung, F.L., Dai, C., Mi, L., 2010. Sulforaphane activates the heat shock response and enhances proteasome activity through up-regulation of Hsp27. J. Biol. Chem. 285, 35528-35536.

Gandini, N.A., Fermento, M.E., Salomón, D.G., Blasco, J., Patel, V., Gutkind, J.S., Molinolo, A.A., Facchinetti, M.M., Curino, A.C., 2012. Nuclear localization of heme oxygenase-1 is associated with tumor progression of head and neck squamous cell carcinomas. Exp. Mol. Pathol. 93, 237-245.

Ganea, E., 2001. Chaperone-like activity of α-crystallin and other small heat shock proteins. Curr Protein Pept. Sci. 2, 205-225.

Garcia de la serrana, D., Johnston, I.A., 2013. Expression of heat shock protein (Hsp90) paralogues is regulated by amino acids in skeletal muscle of Atlantic salmon. PLoS One. doi:10.1371/journal.pone.0074295.

Garcia-Mata, R., Bebok, Z., Sorscher, E.J., Sztul, E.S., 1999. Characterization and dynamics of aggresome formation by a cytosolic GFP-chimera. J. Cell. Biol. 146, 1239-1254.

Garrido, C., Paul, C., Seigneuric, R., Kampinga, H.H., 2012. The small heat shock proteins family: the long forgotten chaperones. Int. J. Biochem. Cell Biol. 44, 1588-1592.

Gauley, J., Young, J.T.F., Heikkila, J.J., 2008. Intracellular localization of the heat shock protein, HSP110, in *Xenopus laevis* A6 kidney epithelial cells. Comp. Biochem. Physiol. A Mol. Integr. Physiol. 151, 133-138.

Gellalchew, M., Heikkila, J.J., 2005. Intracellular localization of *Xenopus* small heat shock protein, hsp30, in A6 kidney epithelial cells. Cell Biol. Int. 29, 221-227.

Ghayour-Mobarhan, M., Saber, H., Ferns, G.A., 2012. The potential role of heat shock protein 27 in cardiovascular disease. Clin. Chim. Acta. 413, 15-24.

Giacoppo, S., Galuppo, M., Monttaut, S., Iori, R., Rollin, P., Bramanti, P., Mazzon, E., 2015. An overview on neuroprotective effects of isothiocyanates for the treatment of neurodegenerative diseases. Fitoterapia. 106, 12-21.

Gibbs, A., Schwartzman, J., Deng, V., Alumkal, J., 2009. Sulforaphane destabilizes the androgen receptor in prostate cancer cells by inactivating histone deacetylase 6. Proc. Natl. Acad. Sci. U. S. A. 106, 16663-16668.

Giuseppina, T., Gabriella, S., Fabiana, G., 2011. Hsp70 and its molecular role in nervous system diseases. Biochem. Res. Int. doi: 10.1155/2011/618127.

Goldbaum, O., Riedel, M., Stahnke, T., Richter-Landsberg, C., 2009. The small heat shock protein HSP25 protects astrocytes against stress induced by proteasomal inhibition. Glia. 57, 1566-1577.

Gorrochategui, E., Lacorte, S., Tauler, R., Martin, F.L., 2016. Perfluoroalkylated substance effects in *Xenopus laevis* A6 kidney epithelial cells determined by ATR-FTIR spectroscopy and chemometric analysis. Chem. Res. Toxicol. 29, 924-932.

Gothard, L.Q., Ruffner, M.E., Woodward, J.G., Park-Sarge, O.-K., Sarge, K.D., 2003. Lowered temperature set point for activation of the cellular stress response in T-lymphocytes. J. Biol. Chem. 278, 9322-9326.

Gottlieb, Y., Truman, M., Cohen, L.A., Leichtmann-Bardoogo, Y., Meyron-Holtz, E.G., 2012. Endoplasmic reticulum anchored heme-oxygenase 1 faces the cytosol. Haematologica. 97, 1489-1493.

Goyal, S., Patel, R.M., Sukhramani, P.S., Kamothi, K.A., 2010. Microtubule: A novel target for cancer therapy. IJPSR. Vol. 1, Issue 4.

Guerra, L., Favia, M., Fanelli, T., Calamita, G., Svetlo, M., Bagorda, A., Jacobson, K.A., Reshkin, S.J., Casavola, V., 2004. Stimulation of *Xenopus* P2Y1 receptor activates CFTR in A6 cells. Pflugers Arch. 449, 66-75.

Guess, A.J., Ayoob, R., Chanley, M., Manley, J., Cajaiba, M., Agrawal, S., Pengal., R., Pyle, A.L., Becknell, B., Kopp, J.B., Ronkina, N., Gaestel, M., Benndorf, R., Smoyer, W.E., 2013. Crucial Roles of the Protein Kinases MK2 and MK3 in a Mouse Model Glomerulonephritis. PLoS One. 10.1371/journal.pone.0054239.

Gurdon, J.B., 2006. Nuclear transplantation in *Xenopus*. Methods Mol. Biol. 325, 1-9.

Hanneken, A., Lin, F.F., Johnson, J., Maher, P., 2006. Flavonoids protect human retinal pigment epithelial cells from oxidative-stress-induced death. Invest. Opthalmol. Vis. Sci. 47, 3164-3177.

Hao, R., Nanduri, P., Rao, Y., Panichelli, R.S., Ito, A., Yoshida, M., Yaho, T.-P., 2013. Proteasomes activate aggresome disassembly and clearance by producing unanchored ubiquitin chains. Mol. Cell. 51, 819-828.

Haslbeck, M., Vierling, E., 2015. A first line of stress defense: small heat shock proteins and their function in protein homeostasis. J. Mol. Biol. 427, 1537-48.

Heikkila, J.J., 1990. Expression of cloned genes and translation of messenger RNA in microinjected *Xenopus* oocytes. Int. J. Biochem. 22, 1223-1228.

Heikkila, J.J., Krone, P.H., Ovsenek, N., 1991. Regulation of heat shock gene expression during *Xenopus* development. Heat Shock and Development. 17, 120-137.

Heikkila, J.J., 2004. Regulation and function of small heat shock protein genes during amphibian development. J. Cell Biochem. 93, 672-680.

Heikkila, J.J., 2010. Heat shock protein gene expression and function in amphibian model systems. Comp. Biochem. Physiol. A Mol. Integr. Physiol. 156, 19-33.

Heikkila, J.J., 2017. The expression and function of hsp30-like small heat shock protein genes in amphibians, birds, fish, and reptiles. Comp. Biochem. Physiol. A Mol. Integr. Physiol. 203, 179-192.

Heirbaut, M., Beelen, S., Strelkov, S.V., Weeks, S.D., 2014. Dissection of the functional role of the N-terminal domain of the human small heat shock protein HSPB6. PLoS One. doi:10.1371/journal.pone.0105892.

Helbing, C., Gallimore, C., Atkinson, B.G., 1996. Characterization of a *Rana catesbeiana* hsp30 gene and its expression in the liver of this amphibian during both spontaneous and thyroid hormone-induced metamorphosis. Dev. Genet. 18, 223-233.

Hentze, N., Le Breton, L., Wiesner, J., Kempf, G., Mayer, M.P., 2016. Molecular mechanism of thermosensory function of heat shock transcription factor Hsf1. Elife. doi: 10.7554/eLife.11576.

Hock, T.D., Nick, H.S., Agarwal, A., 2004. Upstream stimulatory factors, USF1 and USF2, bind to the human haem oxygenase-1 proximal promoter in vivo and regulate its transcription. Biochem. J. 383, 209-218.

Huber, III, W.J. Scruggs, B.A., Backes, W.L., 2009. C-terminal membrane spanning region of human heme oxygenase-1 mediates a time-dependent complex formation with cytochrome P450 reductase. Biochemistry. 48, 190-197.

Ikuzawa, M., Akiduki, S., Asashima, M., 2007. Gene expression profile of *Xenopus* A6 cells cultured under random positioning machine shows downregulation of ion transporter genes and inhibition of dome formation. Adv. Space Res. 40, 1694-1702.

Islamovic, E., Duncan, A., Bers, D.M., Gerthoffer, W.T., Mestril, R., 2007. Importance of small heat shock protein 20 (hsp20) C-terminal extension in cardioprotection. J. Mol. Cell Cardio. 42, 862-869.

Ito, H., Kamei, K., Iwamoto, I., Inaguma, Y., Garcia-Mata, R., Sztul, E., Kato, K., 2002. Inhibition of the proteasome induces accumulation, phosphorylation, and recruitment of HSP27 and alphaβ-crystallin to aggresomes. J. Biochem. 131, 593-603.

Ito, H., Iwamoto, I., Inaguma, Y., Takizawa, T., Nagata, K., Asano, T., Kato, K., 2005. Endoplasmic reticulum stress induces the phosphorylation of small heat shock protein, Hsp27. J. Cell Biochem. 95, 932-941.

Jaegar, A.M., Makley, L.N., Gestwicki, J.E., Thiele, D.J., 2014. Genomic heat shock element sequences drive cooperative human heat shock factor 1 DNA binding and selectivity. J. Biol. Chem. 289, 30459-30469.

Kato, K., Goto, S., Inaguma, Y., Haegawa, K., Morishita, R., Asano, T., 1994. Purification of a 20-kDa protein that is highly homologous to αB-crystallin. J. Biol. Chem. 269, 15302-15309.

Katoh, Y., Fujimoto, M., Nakamura, K., Inouye, S., Sugahara, K., Izu, H., Nakai, A., 2004. Hsp25, a member of the Hsp30 family, promotes inclusion formation in response to stress. FEBS Lett. 565, 28-32.

Katschinski, D.M., 2004. On heat and cells and proteins. News Physiol. Sci. 19, 11-15.

Kay, B.K., Peng, H.B., 1991. *Xenopus laevis*: practical uses in cell and molecular biology. Methods in cell biology, vol. 36. San Diego: Academic Press Inc.

Khamis, I., Heikkila, J.J., 2013. Enhanced HSP30 and HSP70 accumulation in *Xenopus* cells subjected to concurrent sodium arsenite and cadmium chloride stress. Comp. Biochem. Physiol. C Toxicol. Pharmacol. 158, 165-172.

Khamis, I., Chan, D.W., Shirriff, C.S., Campbell, J.H., Heikkila, J.J., 2016. Expression and localization of the *Xenopus laevis* small heat shock protein, HSPB6 (HSP20), in A6 kidney epithelial cells. Comp. Biochem. Physiol. A Mol. Integr. Physiol. 201, 12-21.

Khan, S., Heikkila, J.J., 2011. Curcumin-induced inhibition of proteasomal activity, enhanced HSP accumulation and the acquisition of thermotolerance in *Xenopus laevis* A6 cells. Comp. Biochem. Physiol. A Mol. Integr. Physiol. 158, 566-576.

Khan, S., Rammeloo, A.W., Heikkila, J.J., 2012. Withaferin A induces proteasome inhibition, endoplasmic reticulum stress, the heat shock response and acquisition of thermotolerance. PLoS One. doi: 10.1371/journal.pone.0050547.

Khan, S., Heikkila, J.J., 2014. Distinct patterns of HSPS30 and HSP70 degradation in *Xenopus laevis* A6 cells recovering from thermal stress. Comp. Biochem. Physiol. A Mol. Integr. Physiol. 168, 1-10.

Khan, S., Khamis, I., Heikkila, J.J., 2015. The small heat shock protein, HSP30, is associated with aggresome-like inclusion bodies in proteasomal inhibitor-, arsenite-, and cadmium-treated *Xenopus* kidney cells. Comp. Biochem. Physiol. A Mol. Integr. Physiol. 189, 30-40.

Kirbach, B.B., Golenhofen, N., 2011. Differential expression and induction of small heat shock proteins in rat brain and cultured hippocampal neurons. J. Neurosci. Res. 89, 162-175.

Kobayashi, A., Kang, M.I., Okawa, H., Ohtsuji, M., Zenke, Y., Chiba, T., Igarashi, K., Yamamoto, M., 2004. Oxidative stress sensor Keap1 functions as an adaptor for Cul3-based E3 ligase to regulate proteasomal degradation of Nrf2. Mol. Cell Biol. 24, 7130-7139.

Koizumi, S., Gong, P., Suzuki, K., Murata, M., 2007. Cadmium-responsive element of the human heme oxygenase-1 gene mediates heat shock factor 1-dependent transcriptional activation. J. Biol. Chem. 282, 8715-8723.

Komander, D., Rape, M., 2012. The ubiquitin code. Annu. Rev. Biochem. 81, 203-229.

Kondo, H., Harano, R., Nakaya, M., Watabe, S., 2004. Characterization of goldfish heat shock protein-30 induced upon severe heat shock in cultured cells. Cell Stress Chaperones. 9, 350-358.

Kononova, O., Kholodov, Y., Theisen, K.E., Marx, K.A., Dima, R.I., Ataullakhanov, F.I., Grishchuk, E.L., Barsegov, V., 2014. Tubulin bond energies and microtubule biomechanics determined from nanoindentation in silico. J. Am. Chem. Soc. 136, 17036-17045.

Kopito, R.R., 2000. Aggresomes, inclusion bodies and protein aggregation. Trends Cell Biol. 10, 524-530.

Kregel, K.C., 2002. Heat shock proteins: modifying factors in physiological stress responses and acquired thermotolerance. J. Appl. Physiol. 92, 2177-2186.

Krone, P.H., Heikkila, J.J., 1988. Analysis of hsp30, hsp70, and ubiquitin gene expression in *Xenopus laevis* tadpoles. Development. 103, 59-67.

Krone, P.H., Heikkila, J.J., 1989. Expression of microinjected *hsp 70*/CAT and *hsp 30*/CAT chimeric genes in development *Xenopus laevis* embryos. Development. 106, 271-281.

Krone, P.H., Snow, A., Ali, A., Pasternak, J.J., Heikkila, J.J., 1992. Comparison of regulatory and structural regions of the *Xenopus laevis* small heat-shock protein-encoding gene family. Gene. 110, 159-166.

Kwak, M.K., Cho, J.M., Huang, B., Shin, S., Kensler, T.W., 2007. Role of increased expression of the proteasome in the protective effects of sulforaphane against hydrogen peroxide-mediated cytotoxicity in murine neuroblastoma cells. Free Radic. Biol. Med. 43, 809-817.

Lambert, H., Charette, S.J., Bernier, A.F., Guimond, A., Landry, J., 1999. HSP27 multimerization mediated by phosphorylation-sensitive intermolecular interactions at the amino terminus. J. Biol. Chem. 274, 9378-9385.

Lang, L., Miskovic, D., Lo, M., Heikkila, J.J., 2000. Stress-induced, tissue-specific enrichment of hsp70 mRNA accumulation in *Xenopus laevis* embryos. Cell Stress Chaperones. 5, 36-44.

Lee, B.S., Chen, J., Angelidis, C., Jurivich, D.A., Morimoto, R.I., 1995. Pharmacological modulation of heat shock factor 1 by anti-inflammatory drugs results in protection against stress-induced cellular damage. Proc. Natl. Acad. Sci. U. S. A. 92, 7207-7211.

Lee, P.J., Alam, J., Wiegand, G.W., Choi, A.M.K., 1996. Overexpression of heme oygenase-1 in human pulmonary epithelial cells results in cell growth arrest and increased resistance to hyperoxia. Proc. Natl. Acad. Sci. U. S. A. 93, 10393-10398.

Lee, D.H., Goldberg, A.L., 1998. Proteasome inhibitors: valuable new tools for cell biologists. Trends Cell Biol. 8, 397-403.

Lehman, N.L., 2009. The ubiquitin proteasome system in neuropathology. Acta. Neuropathol. 118, 329-347.

Li, W., Chou, I.N., 1992. Effects of sodium arsenite on the cytoskeleton and cellular glutathione levels in cultured cells. Toxicol. Appl. Pharmacol. 114, 132-139.

Li, Y., Karagoz, G.E., Seo, Y.H., Zhang, T., Jiang, Y., Yu, Y., Duarte, A.M., Schwartz, S.J., Boelens, R., Carroll, K., Rudiger, S.G., Sun, D., 2012. Sulforaphane inhibits pancreatic cancer through disrupting Hsp90-p50 (Cdc37) complex and direct interactions with amino acids residues of Hsp90. J. Nutr. Biochem. 23, 1617-1626.

Lin, Q., Weis, S., Yang, G., Weng, Y.H., Helston, R., Rish, K., Smith, A., Bordner, J., Polte, T., Gaunitz, F., Dennery, P.A., 2007. Heme oxygenase-1 protein localizes to the nucleus and activates transcription factors important in oxidative stress. J. Biol. Chem. 282, 20621-20633.

Lindner, R.A., Carver, J.A., Erhnsperger, M., Buchner, J., Esposito, G., Behlke, J., Lutsch, G., Kotlyarov, A., Gaestel, M., 2000. Mouse Hsp25, a small heat shock protein, the role of its C-terminal extension in oligomerization and chaperone action. Eur. J. Biochem. 267, 1923-1932.

Lindquist, S., 1986. The heat-shock response. Annu. Rev. Biochem. 55, 1151-1191.

Linnenbaum, M., Busker, M., Kraehling, J.R., Behrends, S., 2012. Heme oxygenase isoforms differ in their subcellular trafficking during hypoxia and are differentially modulated by cytochrome P450 reductase. PLoS One. 7, e35483. doi: 10.1371/journal.pone.0035483.

Liu, X.J., 2006. *Xenopus* protocols: cell biology and signal transduction. Methods in molecular biology, vol. 322. Totowa, NJ: Humana Press.

Liu, Y., Zheng, T., Zhao, S., Liu, H., Han, D., Zhen, Y., Xu, D., Wang, Y., Yang, H., Zhang, G., Wang, C., Wu, J., Ye, Y. 2012. Inhibition of Heat Shock Protein Response Enhances PS-341-Mediated Glioma Cell Death. Ann. Surg. Oncol. 19, 421-429.

Ma, P., Zhao, S., Zeng, W., Yang, Q., Li, C., Lv, X., Zhou, Q., Mao, B., 2011. *Xenopus* Dbx2 is involved in primary neurogenesis and early neural plate patterning. Biochem. Biophys. Res. Commun. 412, 170-174.

MacRae, T.H., 2000. Structure and function of small heat shock/α-crystallin proteins: Established concepts and emerging ideas. Cell Mol. Life Sci. 57, 899-913.

Malik, B., Schlanger, L., Al-Khalili, O., Bao, H.F., Yue, G., Price, S.R., Mitch, W.E., Eaton, D.C., 2001. Enac degradation in A6 cells by the ubiquitin-proteasome proteolytic pathway. J. Biol. Chem. 276, 12903-12910.

Manwell, L.A., Heikkila, J.J., 2007. Examination of KNK437- and quercetin-mediated inhibition of heat shock-induced heat shock protein gene expression in *Xenopus laevis* cultured cells. Comp. Biochem. Physiol. A. 148, 521-530.

Martin, D., Rojo, A.I., Salinas, M., Diaz, R., Gallardo, G., Alam, J., Ruiz de Galarreta, C.M., Cuadrado, A., 2004. Regulation of heme oxygenase-1 expression through the phosphatidylinositol 3-kinase/Akt pathway and the Nrf2 transcription factor in response to the antioxidant phytochemical carnosol. J. Biol. Chem. 279, 8919-8929.

Marvin, M., O'Rourke, D., Kurihara, T., Juliano, C.E., Harrison, K.L., Hutson, L.D., 2008. Developmental expression patterns of the zebrafish small heat shock proteins. Dev. Dyn. 237, 454-463.

Mi, L., Wang, X., Govind, S., Hood, B.L., Veenstra, T.D., Conrads, T.P., Saha, D.T., Goldman, R., Chung, F.L., 2007. The role of protein binding in induction of apoptosis by phenethyl isothiocyanate and sulforaphane in human non-small lung cancer cells. Cancer Res. 67, 6409-6416.

Mi, L., Xiao, Z., Hood, B.L., Dakshanamurthy, S., Wang, X., Govind, S., Conrads, T.P., Veenstra, T.D., Chung, F.L., 2008. Covalent binding to tubulin by isothiocyanates. A mechanism of cell growth arrest and apoptosis. J. Biol. Chem. 283, 22136-22146.

Mi, L., Gan, N., Cheema, A., Dakshanamurthy, S., Wang, X., Yang, D.C., Chung, F.L., 2009. Cancer preventive isothiocyanates induce selective degradation of cellular alpha- and beta-tubulins by proteasomes. J. Biol. Chem. 284, 17039-17051.

Mi, L., Gan, N., Chung, F.L., 2010. Isothiocyanates inhibit proteasome activity and proliferation of multiple myeloma cells. Carcinogenesis. 32, 216-223.

Mi, L., Di Pasqua, A.J., Chung, F.L., 2011. Proteins as binding targets of isothiocyanates in cancer prevention. Carcinogenesis. 32, 1405-1413.

Micel, L.N., Tentler, J.J., Smith, P.G., Eckhardt, G.S., 2013. Role of ubiquitin ligases and the proteasome in oncogenesis: novel targets for anticancer therapies. J. Clin. Oncol. 31, 1231-1238.

Miller, K.M., Schulze, A.D., Ginther, N., Li, S., Patterson, D.A., Farrell, A.P., Hinch, S.G., 2009. Salmon spawning migration: metabolic shifts and environmental triggers. Comp. Biochem. Physiol. Part D Genomics Proteomics. 4, 75–89.

Molina-Vargas, L.F., 2013. Mechanism of action of isothiocyanates. A review. Agron. Colomb. 31, 1.

Morimoto, R.I., 1998. Regulation of the heat shock transcriptional response: Cross talk between a family of heat shock factors, molecular chaperones, and negative regulators. Genes Dev. 12, 3788-3796.

Morimoto, R.I., 2008. Proteotoxic stress and inducible chaperone networks in neurodegenerative disease and aging. Genes Dev. 22, 1427-1438.

Morris, A.M., Treweek, T.M., Aquilina, J.A., Carver, J.A., Walker, M.J., 2008. Glutamic acid residues in the C-terminal extension of small heat shock protein 25 are critical for structural and functional integrity. FEBS J. 275, 5885-5898.

Mukhtar, E., Adhami, V.M., Mukhtar, H., 2014. Targeting Microtubules by Natural Agents for Cancer Therapy. Mol. Cancer Ther. 13, 275-284.

Muller, M., Gauley, J., Heikkila, J.J., 2004. Hydrogen peroxide induces heat shock protein and proto-oncogene mRNA accumulation in *Xenopus laevis* A6 kidney epithelial cells. Can. J. Physiol. Pharmacol. 82, 523-529.

Mulligan-Tuttle, A., Heikkila, J.J., 2007. Expression of the small heat shock protein gene, hsp30, in *Rana catesbeiana* fibroblasts. Comp. Biochem. Physiol. 148, 308-316.

Munoz-Moreno, R., Barrado-Gil, L., Galindo, I., Alonso, C., 2015. Analysis of HDAC6 and BAG3-aggresome pathways in African swine fever viral factory formation. Viruses. 7, 1823-1831.

Murphy, M.E., 2013. The HSP70 family and cancer. Carcinogenesis. 34, 1181-1188.

Music, E., Khan, S., Khamis, I., Heikkila, J.J., 2014. Accumulation of heme oxygenase-1 (HSP32) in *Xenopus laevis* A6 kidney epithelial cells treated with sodium arsenite, cadmium chloride or proteasomal inhibitors. Comp. Biochem. Physiol. C Toxicol. Pharmacol. 166, 75-87.

Mymrikov, E.V., Seit-Nebi, A.S., Gusev, N.B., 2011. Large potential of small heat shock proteins. Physiol. Rev. 91, 1123-59.

Mymrikov, E.V., Haslbeck, M., 2015. Medical implications of understanding the functions of human small heat shock proteins. Expert Rev. Proteomics. 12, 295-308.

Nachamkin, I., Allos, B.M., Ho, T., 1998. *Campylobacter* species and Guillain-Barre syndrome. Clin. Microbiol. Rev. 11, 555-567.

Nagasawa, T., Matsushima-Nishiwaki, R., Toyoda, H., Matsuura, J., Kumada, T., Kozawa, O., 2014. Heat shock protein 20 (HSPB6) regulates apoptosis in human hepatocellular carcinoma cells: Direct association with Bax. Oncol. Rep. 32, 1291-1295.

Nahomi, R.B., DiMauro, M.A., Wang, B., Nagaraj, R.H., 2015. Identification of peptides in human Hsp20 and Hsp27 that possess molecular chaperone and anti-apoptotic activities. Biochem. J. 465, 115-125.

Naidu, S.D., Sutherland, C., Zhang, Y., Risco, A., de la Vega, L., Caunt, C.J., Hastie, C.J., Lamont, D.J., Torrente, L., Chowdhry, S., Benjamin, I.J., Keyse, S.M., Cuenda, A., Dinkova-Kostova, A.T., 2016. Heat Shock Factor 1 Is a Substrate for p38 Mitogen-Activated Protein Kinases. Mol. Cell Biol. 36, 2403-2417.

Naito, Y., Takagi, T., Uchiyama, K., and Yoshikawa, T., 2011. Heme oxygenase-1: a novel therapeutic target for gastrointestinal diseases. J. Clin. Biochem. Nutr. 48, 126-133.

Nakajima, Y., Suzuki, S., 2013. Environemental stresses induce misfolded protein aggregation in plant cells in a microtubule-dependent manner. Int. J. Mol. Sci. 14, 7771-7783.

Namba, F., Go, H., Murphy, J.A., La, P., Yang, G., Sengupta, S., Fernando, A.P., Yohannes, M., Biswas, C., Wehrli, S.L., Dennery, P.A., 2014. Expression level and subcellular localization of heme oxygenase-1 modulates its cytoprotective properties in response to lung injury: a mouse model. PLoS One. doi: 10.1371/journal.pone.0090936.

Niisato, N., Ohta, M., Eaton, D.C., Marunaka, Y., 2012. Hypotonic stress upregulates β- and γ-ENaC expression through suppression of ERK by inducing MKP-1. Am. J. Physiol. Renal Physiol. 303, 240-252.

Norris, C.E., Brown, M.A., Hickey, E., Weber, L.A., Hightower, L.E., 1997. Low-molecular weight heat shock proteins in a desert fish (*Poeciliopsis lucida*): homologs of human Hsp27 and *Xenopus* Hsp30. Mol. Biol. Evol. 14, 115–129.

Norris, C.E., Hightower, L.E., 2002. Discovery of two distinct small heat shock protein (HSP) families in the desert fish *Poecliopsis*. Prog. Mol. Subcell. Biol. 28, 19-35.

Ogawa, K., Sun, J., Taketani, S., Nakajima, O., Nishitani, C., Sassa, S., Hayashi, N., Yamamoto, M., Shibahara, S., Fujita, H., Igarashi, K., 2001. Heme mediates derepression of Maf recognition element through direct binding to transcription repressor Bach1. EMBO J. 20, 2835-2843.

Ohan, N.W., Tam, Y., Fernando, P., Heikkila, J.J., 1998. Characterization of a novel group of basic small heat shock proteins in *Xenopus laevis* A6 kidney epithelial cells. Biochem. Cell Biol. 76, 665-671.

Oksala, N.K., Ekmekci, F.G., Ozsoy, E., Kirankaya, S., Kokkola, T., Emecen, G., Lappalainen, J., Kaarniranta, K., Atalay, M., 2014. Natural thermal adaptation increases heat shock protein levels and decreases oxidative stress. Redox Biol. 3, 25-28.

Olzmann, J.A., Li, L., Chin, L.S., 2008. Aggresome formation and neurodegenerative diseases: therapeutic implications. Curr. Med. Chem. 15, 47-60.

Ouertatani-Sakouhi, H., El-Turk, F., Fauvet, B., Roger, T., Le Roy, D., Karpinar, D.P., Leng, L., Bucala, R., Zweckstetter, M., Calandra, T., Lashuel, H.A., 2009. A new class of isothiocyanate-based irreversible inhibitors of Macrophage Migration Inhibitory Factor (MIF). Biochemistry. 48, 9858-9870.

Ovsenek, N., Heikkila, J.J., 1990. DNA sequence-specific binding activity of the heat shock transcription factor is heat-inducible before midblastula transition of early *Xenopus* development. Development. 110, 427-433.

Pae, H.O., Chung, H.T., 2009. Heme oxygenase-1: its therapeutic roles in inflammatory diseases. Immune Netw. 9, 12-19.

Park, H.M., Kim, J.A., Kwak, M.K., 2009. Protection against amyloid beta cytotoxicity by sulforaphane: role of the proteasome. Arch. Pharm. Res. 32, 109-115.

Park, E.J., Kim, Y.M., Park, S.W., Kim, H.J., Lee, D.U., Chang, K.C., 2013. Induction of HO-1 through p38 MAPK/Nrf2 signaling pathway by ethanol extract of Inula helenium L. reduces inflammation in LPS-activated RAW 264.7 cells and CLP-induced septic mice. Food Chem. Toxicol. 55, 386-395.

Parker, A.L., Kavallaris, M., McCarroll, J.A., 2014. Microtubules and their role in cellular stress in cancer. Front Oncol. doi: 10.3389/fonc.2014.00153.

Parnaud, G., Li, P., Cassar, G., Rouimi, P., Tulliez, J., Combaret, L., Gamet-Payrastre, L., 2004. Mechanism of sulforaphane-induced cell arrest and apoptosis in human colon cancer cells. Nutr. Cancer. 48, 198-206.

Patra, R.C., Rautray, A.K., Swarup, D., 2011. Oxidative stress in lead and cadmium toxicity and its amelioration. Vet. Med. Int. doi: 10.4061/2011/457327.

Perez-De-Puig, I., Martin, A., Gorina, R., de la Rosa, X., Martinez, E., Planas, A.M., 2013. Induction of hemeoxygenase-1 expression after inhibition of hemeoxygenase activity promotes inflammation and worsens ischemic brain damage in mice. Neuroscience. 243, 22-32.

Pérez-Sala, D., Oeste, C., Martinez, A.E., Carrasco, M.J., Garzon, B., Canada, F.J. 2015. Vimentin filament organization and stress sensing depend on its single cysteine residue and zinc binding. Nat. Commun. doi: 10.1038/ncomms8287.

Pernet, L., Faure, V., Gilquin, B., Dufour-Guerin, S., Khochbin, S., Vourc'h, C., 2014. HDAC6-ubiquitin interaction controls the duration of HSF1 activation after heat shock. Mol. Biol. Cell. 25, 4187-4194.

Phang, D., Joyce, E.M., Heikkila, J.J., 1999. Heat shock-induced acquisition of thermotolerance at the levels of cell survival and translation in *Xenopus* A6 kidney epithelial cells. Biochem. Cell Biol. 77, 141-151.

Philpott, A., Yew, P.R., 2008. The *Xenopus* cell cycle: an overview. Mol. Biotechnol. 39, 9-19.

Pipkin, W., Johnson, J.A., Creazzo, T.L., Komalavilas, P., Brophy, C., 2003. Localization, macromolecular associations, and function of the small heat shock-related protein HSP20 in rat heart. Circulation. 107, 469-476.

Prawan, A., Keum, Y.S., Khor, T.O., Yu, S., Nair, S., Li, W., Hu, L., Kong, An.T., 2007. Structural influence of isothiocyanates on the antioxidant response element (ARE)-mediated heme oxygenase-1 (HO-1) expression. Pharm. Res. 25, 836-844.

Queiroga, C.S., Almeida, A.S., Vieira, H.L., 2012. Carbon monoxide targeting mitochondria. Biochem. Res. Int. doi: 10.1155/2012/749845.

Rafferty, K.A. Jr., 1968. Mass culture of amphibian cells: methods and observations concerning stability of cell type. In Biology of Amphibian Tumors (ed. M Mizzel), pp. 52-81. New York, NY, USA: Springer Verlag.

Rafferty, K.A. Jr., 1975. Epithelial cells: growth in culture of normal and neoplastic forms. Adv. Can. Res. 21, 249-272.

Rembold, C.M., Zhang, E., 2001. Localization of heat shock protein 20 in swine carotid artery. BMC Physiol. 1, 10.

Ren, D., Villeneuve, N.F., Jiang, T., Wu, T., Lau, A., Toppin, H.A., Zhang, D.D., 2011. Brusatol enhances the efficacy of chemotherapy by inhibiting the Nrf2-mediated defence mechanism. Proc. Natl. Acad. Sci. U. S. A. 108, 1433-1438.

Richter-Landsberg, C., Leyk, J., 2013. Inclusion body formation, macroautophagy, and the role of HDAC6 in neurodegeneration. Acta. Neuropath. 126, 793-807.

Ritossa, F., 1962. A new puffing pattern induced by temperature shock and DNP in *Drosophila*. Experienta. 13, 571-573.

Rodriguez-Gonzalez, A., Lin, T., Ikeda, A.K., Simms-Waldrip, T., Fu, C., Sakamoto, K.M., 2008. Role of the aggresome pathway in cancer: targeting histone deacetylase 6- dependent protein degradation. Cancer Res. 68, 2557-2560.

Ross, J.M., Olson, L., Coppotelli, G., 2015. Mitochondrial and the ubiquitin proteasome system dysfunction in ageing and disease: two sides of the same coin? Int. J. Mol. Sci. 16, 19458-19476.

Ryter, S., Kvam, E., Tyrrell, R.M., 1999. Heme oxygenase activity determination by high performance liquid chromatography. Methods Enzymol. 300, 322-336.

Ryter, S.W., Alam, J., Choi, A.M., 2006. Heme oxygenase-1/carbon monoxide: from basic science to therapeutic applications. Physiol. Rev. 86, 583-650.

Sakurai, H., Enoki, Y., 2010. Novel aspects of heat shock factors: DNA recognition, chromatin modulation and gene expression. FEBS J. 277, 4140-4149.

Sarge, K.D., 1995. Male germ cell-specific alteration in temperature set point of the cellular stress response. J. Biol. Chem. 270, 18745-18748.

Sarkars, R., Mukherjee, S., Roy, M., 2013. Targeting heat shock proteins by phenethyl isothiocyanate results in cell-cycle arrest and apoptosis of human breast cancer cells. Nutr. Cancer. 65, 480-493.

Scheraga, R.G., Thompson, C., Tulapurkar, M.E., Nagarsekar, A.C., Cowan, M., Potla, R., Sun, J., Cai, R., Logun, C., Shelhamer, J., Todd, N.W., Singh, I.S., Luzina, I.G., Atamas, S.P., Hasday, J.D., 2016. Activation of heat shock response augments fibroblast growth factor-1 expression in wounded lung epithelium. Am. J. Physiol. Lung Cell Mol. Physiol. 311, 941-955.

Schmitt, S.M., Gull, M., Brandli, A.W., 2014. Engineering *Xenopus* embryos for phenotypic drug discovery screening. Adv. Drug Deliv. Rev. 69-70, 225-246.

Segundo, L., Guimaraes, L., Fernandez, T.C., Beltran, E.M., Guilhermino, L., Pablos, M.V., 2016. Alterations in gene expression levels provide early indicators of chemical stress during *Xenopus laevis* embryo development: A case study with perfuorooctane sulfonate (PFOS). Ecotoxicol. Environ. Saf. 127, 51-60.

Sehrawat, A., Croix, C.S., Baty, C.J., Watkins, S., Tailor, D., Singh, R.P., Singh, S.V., 2016. Inhibition of mitochondrial fusion is an early and critical event in breast cancer cell apoptosis by dietary chemopreventative benzyl isothiocyanate. Mitochondrion. 30, 67-77.

Sevin, M., Girodon, F., Garrido, C., de Thonel, A., 2015. HSP90 and HSP70: Implication in inflammation processes and therapeutic approaches of myeloproliferative neoplasms. Mediators Inflamm. doi: 10.1155/2015/970242.

Shahid, M., Takamiya, M., Stegmaier, J., Middel, V., Gradl, M., Kluver, N., Mikut, R., Dickmeis, T., Scholz, S., Rastegar, S., Yang, L., Strahle, U., 2016. Zebrafish biosensor for toxicant induced muscle hyperactivity. Sci. Rep. 6, 23768. http://dx.doi.org/10.1038/srep23768.

Sharma, R., Sharma, A., Chaudhary, P., Pearce, V., Vatsyayan, R., Singh, S.V., Awasthi, S., Awasthi, Y.C., 2010. Role of Lipid Peroxidation in Cellular Responses to D, L-Sulforaphane, A Promising Cancer Chemopreventive Agent. Biochemistry. 49, 3191-3202.

Shen, D., Coleman, J., Chan, E., Nicholson, T.P., Sheppard, P.W., Patton, W.F., 2011. Novel cell- and tissue-based assays for detecting misfolded and aggregated protein accumulation within aggresomes and inclusion bodies. Cell Biochem. Biophys. 60, 173-185.

Shi, J., Mei, W., Yang, J., 2008. Heme metabolism enzymes are dynamically expressed during *Xenopus* embryonic development. Bio. Cell. 32, 259-263.

Shirriff, C.S., Heikkila, J.J., 2017. Characterization of cadmium chloride-induced BiP accumulation in *Xenopus laevis* A6 kidney epithelial cells. Comp. Biochem. Physiol. C Toxicol. Pharmacol. 191, 117-128.

Sikorski, E.M., Uo, T., Morrison, R.S., Agarwal, A., 2006. Pescadillo interacts with the cadmium response element of the human heme oxygenase-1 promoter in renal epithelial cells. J. Biol. Chem. 281, 24423-24430.

Sin, Y.Y., Martin, T.P., Wills, L., Currie, S., Baillie, G.S., 2015. Small heat shock protein (Hsp20) facilitates nuclear import of protein kinase D 1 (PKD1) during cardiac hypertrophy. Cell Commun. Signal. doi: 10.1186/s12964-015-0094-x.

Slebos, D.J., Ryter, S.W., van der Toorn, M., Liu, F., Guo, F., Baty, C.J., Karlsson, J.M., Watkins, S.C., Kim, H.P., Wang, X., Lee. J.S., Postma, D.S., Kauffman, H.F., Choi, A.M., 2007. Mitochondrial localization and function of heme oxygenase-1 in cigarette smoke-induced cell death. Am. J. Respir. Cell Mol. Biol. 36, 409-417.

Stewart, D., Killeen, E., Naquin, R., Alam, S., Alam, J., 2003. Degradation of transcription factor Nrf2 via the ubiquitin-proteasome pathway and stabilization by cadmium. J. Biol. Chem. 278, 2396-2302.

Stromer, T., Ehrnsperger, M., Gaestel, M., Buchner, J., 2003. Analysis of the interaction of small heat shock proteins with unfolding proteins. J. Biol. Chem. 278, 18015-18021.

Suzuki, H., Tashiro, S., Sun, J., Doi, H., Satomi, S., Igarashi, K., 2003. Cadmium induces nuclear export of Bach1, a transcriptional repressor of heme oxygenase-1 gene. J. Biol. Chem. 278, 49246-49253.

Tarozzi, A., Angeloni, C., Malaguti, M., Morroni, F., Hrelia, S., Hrelia, P., 2013. Sulforaphane as a potential protective phytochemical against neurodegenerative diseases. Oxid. Med. Cell Longev. doi: 10.1155/2013/415078.

Tenhunen, R., Marver, H.S., Schmid, R., 1968. The enzymatic conversion of heme to bilirubin by microsomal heme oxygenase. Proc. Natl. Acad. Sci. U. S. A. 61, 748-755.

Thit, A., Selck, H., Bjerregaard, H.F., 2013. Toxicity of CuO nanoparticles and Cu ions to tight epithelial cells from *Xenopus laevis* (A6): effects on proliferation, cell cycle progression and cell death. Toxicol. In Vitro. 27, 1596-1601.

Thit, A., Selck, H., Bjerregaard, H.F., 2015. Toxic mechanisms of copper oxide nanoparticles in epithelial kidney cells. Toxicol. In Vitro. 29, 1053-1059.

Tramutola, A., Di Domenico, F., Barone, E., Perluigi, M., Butterfield, D.A., 2016. It is all about (U)biquitin: role of altered ubiquitin-proteasome system and UCHL1 in Alzheimer Disease. Oxid. Med. Cell Longev. doi: 10.1155/2016/2756068.

Treweek, T.M., Meehan, S., Ecroyd, H., Carver, J.A., 2015. Small heat-shock proteins: important players in regulating cellular proteostasis. Cell Mol. Life Sci. 72, 429-451.

Uversky, V.N., Fink, A., 2007. Protein misfolding, aggregation, and conformational diseases. Molecular Mechanisms of Conformational Diseases. 6, 61-110.

Valastyan, J.S., Lindquist, S., 2014. Mechanisms of protein-folding diseases at a glance. Dis. Model Mech. 7, 9-14.

Van de Klundert, F.A.J.M., Smulders, R.H.P.H., Gusen, M.L.J., Lindner, R.A., Jaenicke, R., Carver, J.A., de Jong, W.W., 1998. The mammalian small heat-shock protein forms dimers and is a poor chaperone. Eur. J. Biochem. 258, 1014-1021.

Van Montfort, R., Slingsby, C., Vierling, E., 2001. Structure and function of the small heat shock protein/alpha-crystallin family of molecular chaperones. Adv. Protein Chem. 59, 105-156.

Verghese, J., Abrams, J., Wang, Y., Morano, K.A., 2012. Biology of the heat shock response and protein chaperones: budding yeast (*Saccharomyces cerevisiae*) as a model system. Microbiol. Mol. Biol. Rev. 76, 115-158.

Vidyasagar, A., Wilson, N.A., Djamali, A., 2012. Heat shock protein 27 (HSP27): biomarker of disease and therapeutic target. Fibrogenesis Tissue Repair. 5, 7.

Voellmy, R., 2004. On mechanisms that control heat shock transcription factor activity in metazoan cells. Cell Stress Chaperones. 9, 122-133.

Voyer, J., Heikkila, J.J., 2008. Comparison of the effect of heat shock factor inhibitor, KNK437, on heat shock- and chemical stress-induced *hsp30* gene expression in *Xenopus laevis* A6 cells. Comp. Biochem. Physiol A Mol. Integr. Physiol.

Waisberg, M., Pius, J., Hale, B., Beyersmann, D., 2003. Molecular and cellular mechanisms of cadmium carcinogenesis. Toxicology. 192, 95-117.

Walcott, S.E., Heikkila, J.J., 2010. Celastrol can inhibit proteasome activity and upregulate the expression of heat shock protein genes, *hsp30* and *hsp70*, in *Xenopus laevis* A6 cells. Comp. Biochem. Physiol. A Mol. Integr. Physiol. 156, 285-293.

Wang, Z., Chin, T.A., Templeton, D.M., 1996. Calcium-independent effects of cadmium on actin assembly in mesangial and vascular smooth muscle cells. Cell Motil. Cytoskeleton. 33, 208-222.

Wang, J., Wei, Y., Li, X., Cao, H., Xu, M., Dai, J., 2007. The identification of heat shock protein genes in goldfish (*Carassius auratus*) and their expression in a complex environment in Gaobeidian Lake, Beijing, China. Comp. Biochem. Physiol. C. 145, 350–362.

Wang, Y., Gu, Y., Qin, G., Zhong, L., Meng, Y., 2013. Curcumin ameliorates the permability of the blood-brain barrier during hypoxia by upregulating heme oxygenase-1 expression in brain microvascular endothelial cells. J. Mol. Neurosci. 51, 344-351.

Weathington, N.M., Mallampalli, R.K., 2014. Emerging therapies targeting the ubiquitin proteasome system in cancer. J. Clin. Invest. 124, 6-12.

Westerheide S.D., Morimoto, R.I., 2005. Heat shock response modulators as therapeutic tools for diseases of protein conformation. J. Biol. Chem. 280, 33097-33100.

Woolfson, J.P., Heikkila, J.J., 2009. Examination of cadmium-induced expression of the small heat shock protein gene, *hsp30*, in *Xenopus laevis* A6 kidney epithelial cells. Comp. Biochem. Physiol. A Mol. Integr. Physiol. 152, 91-99.

Wu, W.T., Chi, K.H., Ho, F.M., Tsao, W.C., Lin, W.W., 2004. Proteasome inhibitors up-regulate heme oxygenase-1 gene expression: requirement of p38 MAPK (mitogen-activated protein kinase) activation but not of NF-kappaB (nuclear factor kappaB) inhibition. Biochem. J. 379, 587-593.

Xiao, Z., Mi, L., Chung, F-.L., Veenstra, T.D., 2012. Proteomic Analysis of Covalent Modifications of Tubulins by Isothiocyanates. J. Nutr. 142, 1377-1381.

Xie, J., Tang, L., Lu, L., Zhang, L., Xi, L., Liu, H.C., Odle, J., Luo, X., 2014. Differential expression of heat shock transcription factors and heat shock proteins after acute and chronic heat stress in laying chickens (*Gallus gallus*). PLoS One. doi: 0.1371/journal.pone.0102204.

Xiong, R., Siegel, D., Ross, D., 2013. The activation sequence of cellular protein handling systems after proteasomal inhibition in dopaminergic cells. Chem. Biol. Interact. 204, 116-124.

Xu, C., Yuan, X., Pan, Z., Shen, G., Kim, J.H., Yu, S., Khor, T.O., Li, W., Ma, J., Kong, A.N., 2006. Mechanism of action of isothiocyanates: the induction of ARE-regulated genes is associated with activation of ERK and JNK and the phosphorylation and nuclear translocation of Nrf2. Mol. Cancer Ther. 5, 1918-1926.

Xue, Y., Liu, Z., Cao, J., Ma, Q., Gao, X., Wang, Q., Jin, C., Zhou, Y., Wen, L., Ren, J., 2011. GPS 2.1, enhanced prediction of kinase-specific phosphorylation sites with an algorithm of motif length selection. Protein Eng. Des. Sel. 24, 255-260.

Yachie, A., Niida, Y., Wada, T., Igarashi, N., Kaneda, H., Toma, T., Ohta, K., Kasahara, Y., Koizumi, S., 1999. Oxidative stress causes enhanced endothelial cell injury in human heme oxygenase-1 deficiency. J. Clin. Invest. 103, 129-135.

Yamamoto, N., Izumi, Y., Matsuo, T., Wakita, S., Kume, T., Takada-Takatori, Y., Sawada, H., Akaike, A., 2010. Elevation of heme oxygenase-1 by proteasome inhibition affords dopaminergic neuroprotection. J. Neurosci. Res. 88, 1934-1942.

Yeh, Y.T., Hsu, Y.N., Huang, S.Y., Lin, J.S., Chen, Z.F., Chow, N.H., Su, S.H., Shyu, H.W., Lin, C.C., Huang, W.T., Yeh, H., Chih, Y.C., Huang, Y.H., Su, S.J., 2016. Benzyl isothiocyanate promotes apoptosis of oral cancer cells via an acute redox stress-mediated DNA damage response. Food Chem. Toxicol. 97, 336-345.

Young, J.T.F., Gauley, J., Heikkila, J.J., 2009. Simultaneous exposure of *Xenopus* A6 kidney epithelial cells to concurrent mild sodium arsenite and heat stress results in enhanced *hsp30* and *hsp70* gene expression and the acquisition of thermotolerance. Comp. Biochem. Physiol. A Mol. Integr. Physiol. 153, 417-424.

Young, J.T.F., Heikkila, J.J., 2010. Proteasome inhibition induces *hsp30* and *hsp70* gene expression as well as the acquisition of thermotolerance in *Xenopus laevis* A6 cells. Cell Stress Chaperones. 15, 323-334.

Yu, A., Li, P., Tang, T., Wang, J., Chen, Y., Liu, L., 2015. Roles of Hsp70 in stress responses of microorganisms, plants and animals. Biomed. Res. Int. doi: 10.1155/2015/510319.

Yuan, J.M., Stepanov, I., Murphy, S.E., Wang, R., Allen, S., Jensen, J., Strayer, L., Adams-Haduch, J., Upadhyaya, P., Le, C., Kurzer, M.S., Nelson, H.H., Yu, M.C., Hatsukami, D., Hecht, S.S., 2016. Clinical trial of 2-phenethyl isothiocyanate as an inhibitor of metabolic activation of a tobacco-specific lung carcinogen in cigarette smokers. Cancer Prev. Res. (Phila). 9, 396-405.

Zaarur, N., Meriin, A.B., Gabai, V.L., Sherman, M.Y., 2008. Triggering aggresome formation. Dissecting aggresome-targeting and aggregation signals in synphilin 1. J. Biol. Chem. 283, 27575-27584.

Zarate, J., Bradley, T.M., 2003. Heat shock proteins are not sensitive indicators of hatchery stress in salmon. Aquaculture. 223, 175-187.

Zhang, R., Loganathan, S., Humphreys, I., Srivastava, S.K., 2006. Benzyl isothiocyanate-induced DNA damage causes G_2/M cell cycle arrest and apoptosis in human pancreatic cancer cells. J. Nutr. 136, 2728-2734.

Zhou, B., Gitschier, J., 1997. hCTR: a human gene for copper uptake identified by complementation in yeast. Proc. Natl. Acad. Sci. U. S. A. 94, 7481-7486.